Study on the Series resistance of Organic Dye based Devices

A thesis submitted for the Degree of Doctor of Philosophy (Science)

of

Jadavpur University

by

PALLAB KUMAR DAS

Condensed Matter Physics Research Centre

Department of Physics

Jadavpur University

Kolkata 700032

2023

Dedicated

to

my loving family

Declaration by the Author

This is to certify that this thesis, "Study on the Series resistance of Organic Dye based Devices," which is being submitted for the degree of Doctor of Philosophy (Science), contains only my original research and writing, and to the best of my knowledge and belief, neither the thesis nor any portion of it has been approved for the award of any other degree or certificate by the university or other institution of higher learning, with the exception of instances where appropriate credit has been given in the text.

(Pallab Kumar Das)

Date: 31.07.2023

JADAVPUR UNIVERSITY
KOLKATA - 700 032
INDIA
CONDENSED MATTER PHYSICS RESEARCH CENTRE
DEPARTMENT OF PHYSICS

Prof. N. B. MANIK
BOYSCAST FELLOW, DST, GOVT. INDIA
Professor
Department of Physics
Jadavpur University
Kolkata 700 032
Ph : 033 24138917 (O)
033 24831914 (R)
E-mail : nb_manik@yahoo.co.in

Certificate from the Supervisor

This is to certify that the thesis entitled "Study on the Series resistance of Organic Dye based Devices", submitted by Sri Pallab Kumar Das who got his name registered on 03.05.2016 for the award of Ph. D (Science) degree of Jadavpur University, is absolutely based upon his own work under the supervision of Prof. Nabin Baran Manik and that neither this thesis nor any part of it has been submitted for either any degree/diploma or any other academic award anywhere before.

25.07.2023

Date: 25.07.2023

Place: Kolkata

Prof. Nabin Baran Manik
Supervisor
Condensed Matter Physics Research Centre
Department of Physics
Jadavpur University
Kolkata-700032

Dr. NABIN BARAN MANIK
Professor
Department of Physics
Jadavpur University
Kolkata - 700 032

Telephone : 473-1484/4495/4643 Extn. : 22 Fax : 91 (33)-473-1484
Physics Dept (Head) & 413-8917

Acknowledgement

First and foremost, I want to express my sincere thanks to my supervisor Prof. Nabin Baran Manik for providing me with the chance to complete my Ph.D. in the Department of Physics, Jadavpur University. He provided continual advice, encouragement, and patience during my seven-year study period, and I will always be grateful for that. Without his mentoring, I could not have gotten to where I am now. He approaches research with a very extraordinary level of seriousness and comprehensive understanding of the equipment. Throughout my study project, I was able to stay on the right path because to Prof. Manik's clear directions and profound understanding. He also shared his perceptive knowledge beyond academics, and I am grateful for that since it helped me to develop my outlook and character in the field of research. Additionally, I would want to express my gratitude to Prof. A. N. Basu for his insightful comments that he provided during my study and that helped me improve how I viewed my thesis.

I am also thankful to the seniors and colleagues of my laboratory who have helped me a lot during my work. I would particularly like to thank Dr. A. Haldar, Dr. S. Maity, Dr. Md. R. Islam, Dr. S. Saha, Dr. P. Dalapati, Mr. S. Bhunia, Mr. S. Sen, Mr. D. Sahoo, Mr. A.K Karan and Miss S. Rakshit for their valuable cooperation and encouragement in my work. Further, I would like to convey my gratitude to all the members of the CMPRC group, Department of Physics, Jadavpur University, for their help and cooperation.

Most of the measurements were carried out using equipment that was purchased with funds from research projects supported by the UGC and CSIR, which were conducted in our lab. I want to thank the CSIR in India and the UGC for their financial support, without which it would not have been able to purchase the instruments.

Last but not the least, I would want to acknowledge and thank my loving parents, who made it possible for me to be where I am today. They have always been incredibly supportive and encouraging to me. I want to express my gratitude to my wife for her assistance and support during my work. The task could not have been satisfactorily finished without their assistance. They have consistently been my pillar of support.

List of Figures

Chapter 1

Chapter 2

Chapter 3

Chapter 4

Chapter 5

Chapter 6

List of Tables

Chapter 3

Chapter 4

Chapter 5

Chapter 6

Chapter 7

List of Abbreviations

Ag	Silver
Al	Aluminium
Al-M	Aluminium coated Mylar
CB	Conduction Band
CNT	Carbon nanotubes
COOH	Carboxylic Acid functionalized
CU	Copper
CV	Crystal Violet
DSSC	Dye-sensitized solar cell
EC	Ethylene carbonate
E_c	Trap energy
E_m	Photon Energy
FF	Fill Factor
HOMO	Highest occupied molecular orbital
H_n	Trap density
IPV	Inorganic photovoltaics
I-V	Current-Voltage
I-t	Current-Time
I_{ph}	Photocurrent
ITO	Indium tin oxide
J_{sc}	Short-circuit current density
LUMO	Lowest unoccupied molecular orbital

MG	Malachite Green
MR	Methyl Red
MWCNT	Multi-walled carbon nanotubes
NP	Nanoparticle
N_c	Effective density of states
OD	Optical diameter
OPV	Organic photovoltaic
PC	Propylene carbonate
PCE	Power conversion efficiency
PEC	Photo electrochemical cell
PEO	Polyethylene oxide
PMMA	Poly (methyl methacrylate)
PSF	Phenosafranine
PVA	Polyvinyl alcohol
PV	Photovoltaics
R_s	Series resistance
TH	Thionin
SCLC	Space charge limited current
Si	Silicon
SWCNT	Single-walled carbon nanotubes
T_c	Characteristic temperature
VB	Valence Band
V_{oc}	Open circuit voltage

Contents

Chapter 3

Effect of dye concentration on Series resistance (Rs) of Thionin dye based electrochemical cell (PEC)

Chapter 4

Effect of nanoparticles on Series resistance of Phenosafranine (PSF) and Methyl Red (MR) dye based organic devices

Chapter 5

Effect of temperature on Series resistance and trap energy of Methyl Red (MR) dye based organic device

Chapter 6

Study on the Series Resistance of Crystal Violet (CV) and Malachite Green (MG) Dye Based Organic Photovoltaic Device in Presence of Single Walled Carbon Nanotubes

Chapter 7

Conclusion and Future Scope of the work

Preface

The major objective of this work is to study on the Series resistance (R_s) of organic dye based devices. In order to complete this study, it has been proposed to create different organic dye based devices and studied the current-voltage (I-V) characteristics in order to analyze various electrical parameters using the most appropriate theory.

The finding of electrical conductivity in organic materials has recently given these materials a prominent position in the field of materials science research. Different organic and polymer materials are being widely used to develop different electronic and optoelectronic devices such as diode, photodiode, solar cell and etc. Due to their cheap cost, simple fabrication methods, and easy tuning of their electrical and optical characteristics, devices based on these organic materials have an advantage over those based on inorganic materials. It is also simple to dope organic materials to change their electrical and optical characteristics over a wide range. However, there are also certain restrictions, because of its poor mobility, the existence of traps, the effects of moisture, etc. Low efficiency in organic devices is a big issue because of these restrictions.

Although organic semiconductors have several desirable properties, the performance and conductivity of the devices made from these materials are poor. The total value of current in organic devices has been found to be significantly less than that of inorganic devices, and to understand why, it is crucial to have the information of many electronic parameters obtained from current voltage characteristics. Out of many electronic parameters one of the important parameters is series resistance (R_s). So the study of the current-voltage (I-V) characteristics is essential for understanding the effect of R_s in organic dye based devices. The present work has been begun with the objective of resolving some of these problems.

It is well known that the dark I-V characteristics of any organic device show linearity in the semi logarithm scale at low voltage. However, the characteristic deviates from linearity as the bias voltage increases. The fundamental cause of this variation is the existence of series resistance. This series resistance affects the functionality of several devices, including diodes, photodiodes, solar cells, etc. This series resistance may be measured using a variety of methods.

The value of this series resistance of any organic diode is quite high, according to several literary sources. Organic diodes' high series resistance values are not well known, and the impact of traps at the metal–organic semiconductor interface is also not well understood. It is possible to state that by lowering the value of R_s, entire performance of the device will improve. In order to improve overall performance, research on the calibration of R_s by inclusion of other guest materials, such as nanoparticles and CNTs, is also essential.

In this context to study the Dark I-V characteristics of organic dye based devices. The dyes like Thionin (TH), Phenosafranin (PSF), Crystal Violet (CV), Methyl Red (MR), Malachite Green (MG) etc. are selected for this work. The effects on the parameters of the devices due to the introduction of the nanoparticles, carbon nanotubes, have also been studied in this work. We have also searched the relationship between trap energy and R_s since organic devices are prone to have electronic traps at the interface and in the bulk. Moreover we also studied the effect of temperature on R_s. In addition, we have also studied and compared the electrical and photoelectric properties with the incorporation of Single Walled Carbon nanotubes (SWCNTs).

In the last section of this study, a summary of the entire work is provided. The findings of the research have also been discussed. Additionally, future scope of the work has also been mentioned.

For those who are working in this field, we believe the findings of the current study may be helpful. The measurement's accuracy has been examined several times for a variety of systems. We also give a list of our publications at the end.

Chapter 1

Motivation and Outline

1.1 Introduction

Inorganic semiconductors such as Silicon, Germanium, Gallium Arsenide etc. and other metals such as Copper, Aluminum etc. are basically the backbone of the semiconductor industry [1-4] for last few decades. However from the middle of the last century researchers have started to discover the semiconducting properties in organic compounds [5-6]. In 1977, with the discovery of the first highly conducting polymer, chemically doped Polyacetylene, it has been exhibited that polymers could be used as electrically active materials. Since then, various types of organic devices such as organic diodes, solar cells, organic photovoltaic devices, organic thin film transistors etc. have been prepared and studied as well [7-9].

1.2 Organic electronic devices: advantages and limitations

These organic electronics have received huge attention for their advantages compared to inorganic electronics like low manufacturing cost, easy fabrication process, flexibility, easy tunability of electrical and optical properties etc [10-11]. Fig 1.1 shows the varieties of applications from the versatility of organic electronics technology. Compared to traditional inorganic semiconductors, organic semiconductors offer several advantages for research and development in this field. One key property of organic semiconductors is their tunability [12-13]. To attain particular electrical and optoelectronic properties, organic molecules can be simply modified. Researchers can adjust the energy levels, mobility of charge carriers, and absorption properties of organic materials by altering their chemical structures. This level of modification makes it possible to create high-performance devices with improved usefulness and efficiency. In contrast, inorganic semiconductors typically have fixed features that restrict their ability to be modified. Another advantage of organic semiconductors is their flexibility and versatility [14-17], which are difficult to achieve with inorganic materials.

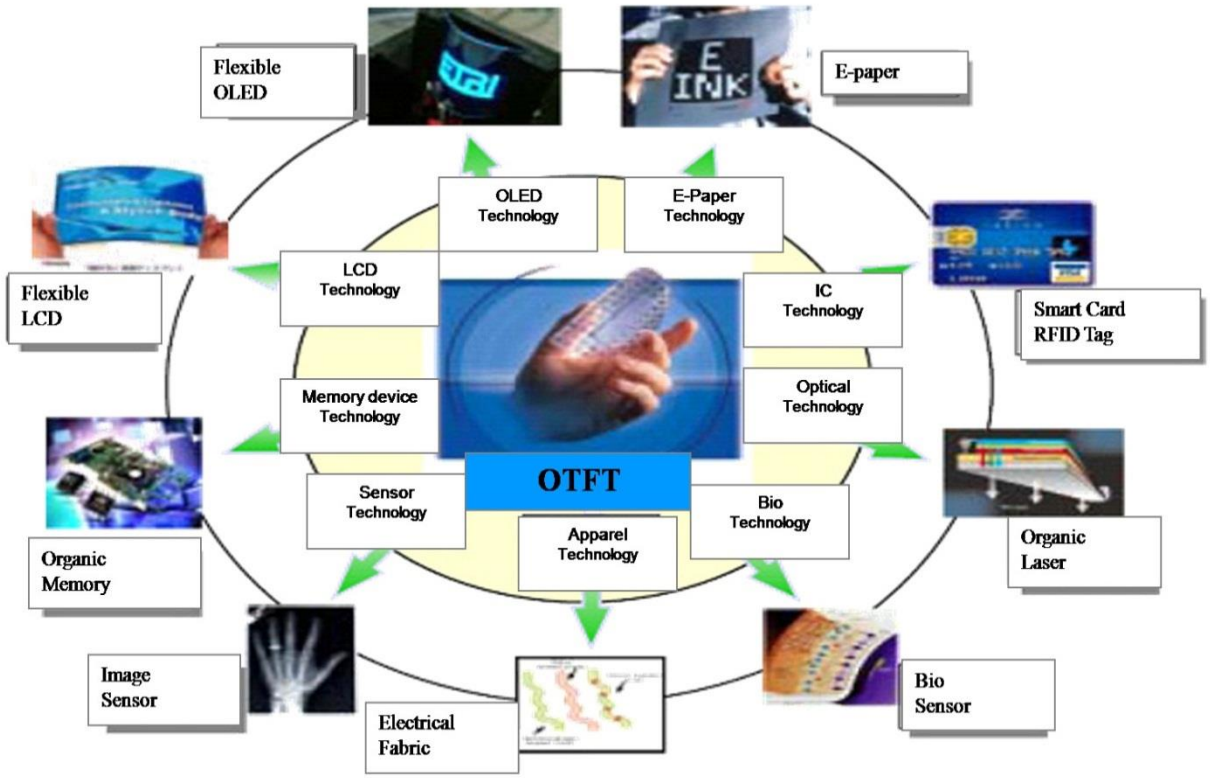

Fig. 1.1 A variety of applications where the versatility of organic electronics technology might be useful [18]

Organic devices can be bent or folded due to their flexibility and compatibility with flexible substrates. This flexibility expands their application areas, including flexible displays, smart textiles, and conformable sensors. Another significant advantage of organic semiconductor-based devices is their low-cost fabrication [19-21]. Basically inorganic devices require complex and expensive manufacturing processes like lithography. Whereas in organic devices can be made using solution-based methods. These methods include techniques like inkjet printing, roll-to-roll printing, and spray coating, which are compatible with large-area and flexible substrates. This cost-effective fabrication approach makes organic devices more accessible and opens up opportunities for their integration into everyday objects. Additionally, organic semiconductor-based devices have a significantly lower environmental impact compared to inorganic devices [22-24]. As organic materials usually have light components like carbon and hydrogen, they are

more environmentally friendly. The manufacture of organic devices also uses low-temperature processing methods that require less energy and emit fewer greenhouse gases.

Another major application of organic materials are related to develop non-conventional or renewable energy source. Basically the conventional energy sources such as coal, natural gas, oil etc. are the major sources of energy and due to huge demand there will be a serious crisis of these energy sources [25-26]. Fig 1.2 shows the start of abatement of the conventional energy source after 2070.

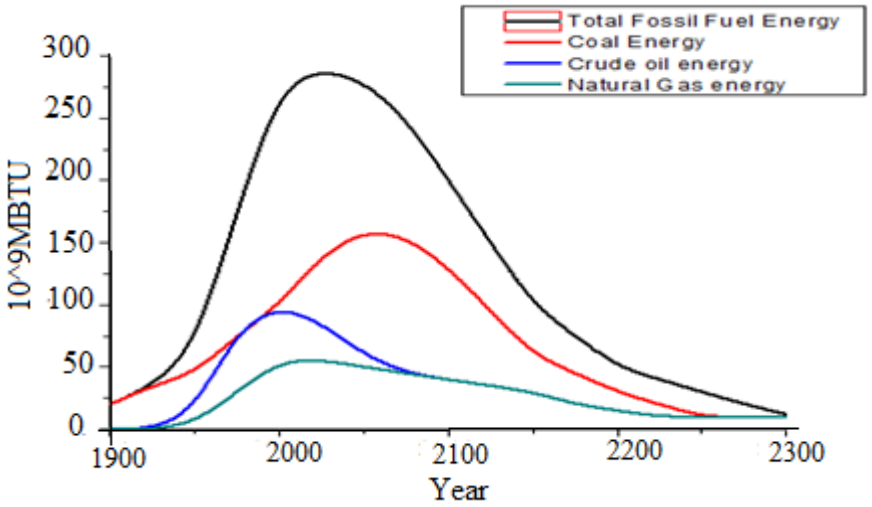

Fig 1.2 The crisis of fossil fuels is causing a problem in meeting the demand for energy in the near future

Apart from that the uses of these energies enhance the emission of CO_2 and raise the greenhouse effect which again will result in global warming [27-28]. So searching for alternative renewable energy sources which are acquired from naturally replenished sources or processes of earth such as bio energy, geothermal energy, solar energy, wind energy, ocean energy etc. are very essential to overcome these problems [29-30]. Out of these renewable energy sources solar energy is one of the important sources as the energy from the sun can be used directly for electricity generation and heating applications [31-33]. Moreover, as organic semiconductors are mainly based on carbon and hydrogen atoms; with semiconducting properties also other elements such as heteroatoms are also included such as sulfur, nitrogen and oxygen. The assistance of mechanical and chemical organic compounds with the electronic and optical properties makes organic semiconductor one of the most interesting materials [34]. So the emergence of organic

semiconductors is also one of the main reasons for the alternation of renewable energy sources from conventional energy sources.

Overall, the unique properties of organic semiconductors, including their tunability, flexibility, excellent charge transport, and potential for low-cost production, make them highly attractive for researchers studying various organic semiconductor-based devices. Continued research and development in this field have the potential to unlock new applications and advancements in electronics, optoelectronics, and energy conversion technologies.

The various attractive properties of organic semiconductor have drawn the interest of the academic and industrial world and create an intriguing platform to explore new science. Nevertheless there are still many limitations and unanswered questions that need to be explained in order to improve this field [35]. Basically organic semiconductor is disordered due to structural defects and chemical impurities, which can be attributed to trap states. These trap state restrict the charge transport process. The charge carriers are recombined at the trap centers. Presence of traps also influences the interface and bulk properties. So overall technologies are dependent on the formation of the interface, movement of charge carriers within the material and the diffusivity of charges which govern the performance of the organic semiconductor based devices. In this regard, from so many years the nature of the charge transport process through these materials has puzzled the researchers. Moreover it is also observed that the conductivity of the organic semiconductor based materials is very poor which degrades the efficiency and overall performance. So it is very crucial to understand the charge transport process and address the reasons for poor performance of those devices and in addition some way to enhance their performance. In this context researchers in this field are attempting to fabricate devices using different device architectures and apply different techniques as well as incorporating new guest materials such as different Nanoparticles, Carbon Nanotubes (CNT) to make them even more effective.

1.3 Objective of our work

The existence of high value series resistance (R_s) is one of the primary causes of the poor charge transport process of organic dye based devices. There is not much study on the series resistance

of organic devices and its correlation with the trap energy. The objective of the present work is to study and estimate the series resistance of different organic dye based devices considering the effect of traps. For this purpose, we have prepared several organic devices using Thionin (TH), Phenosafranin (PSF), Crystal Violet (CV), Methyl Red (MR) and Malachite Green (MG) dyes and study the series resistance of these devices. The current voltage characteristics of the devices have been analyzed by using different techniques to measure the R_s. The correlation between trap energy and R_s has also been studied. Different NPs such as TiO_2, ZnO and CNT have been incorporated to study their effects on R_s. The effect of temperature on R_s is also been investigated in this work. With the experimental works, attempts have been made to understand the charge transport mechanism of these devices with suitable theoretical model.

We employed spin coating techniques to prepare the organic dye-based cells. It is possible to fabricate large area devices using these techniques. The results of this investigation will be helpful for future research in this field. The findings will also be helpful to understand R_s of organic devices and also its relation with trap energy.

1.4 Outline of the work

The outline of our work is covered in the next section. The entire work is organized into seven chapters.

The **Chapter 1** discussed the advantages and disadvantages of organic semiconductors as an intriguing substitute for inorganic semiconductors. Different electronics and opto electronics devices are being fabricated with organic materials. Particularly researches for renewable photovoltaic devices with organic materials are going on all over the world. Significant crisis in conventional energy sources will emerge due to the world's rapid technological progress. Therefore, it is crucial to switch from conventional to renewable energy sources. Organic semiconductor based devices can be used to generate renewable energy sources. Along with different advantages, we have also outlined the associated limitations of organic devices. The organic semiconductor based devices suffer from low efficiency and stability. There are several reasons for this poor performance. One of the main reasons is the presence of high R_s in organic devices. There are different methods to estimate the R_s by analyzing the current-voltage

characteristics of organic dye-based devices. Charge trapping mechanism is a major issue in organic devices. The relation of traps and R_s is also very important to understand the device performance. Effect of different NPs and CNTs will also be studied on R_s. Keeping all these, we have mentioned the objectives of our work in abridged manner in this **Chapter 1**.

In **Chapter 2**, we discussed the basic properties of electrical conductivities in conjugated organic semiconductors. The role of series resistance in organic devices is discussed. Generally the R_s is quite high in organic devices and one of the major reasons is the presence of traps in organic semiconductor. Brief idea about the nature of tarps and the charge injection mechanism at the metal organic semiconductor has been discussed. Charge injection at the MS contact and its expression has been mentioned. The charge transport at the bulk of the devices has been discussed. During transport the charges are being accumulated at the traps. The SCLC models are used to explain the charge transport mechanism and estimate the tarps energy. Different methods to estimate the value of R_s is discussed. At the end of this chapter the role of different NP like ZnO, TiO_2 and SWCNT and MWCNT that has been used in this work has been mentioned. In this chapter we have reviewed the necessary background for our work.

In the following four chapters, from **Chapter 3 to Chapter 7**, experimental works of our thesis been described.

In **Chapter 3**, we have examined the I-V properties of an ITO/Thionin/Al electrochemical system. We have discussed the cell preparation technique and also the experimental procedure has been discussed. We have measured the dark I-V data. The data was fitted using the thermionic emission theory as well as the Cheung Cheung function, which is essentially a version of the thermionic emission theory that incorporates the influence of series resistance. The high values of R_s and n of the device arises due to the trapping of charge carriers. By raising the dye concentration, it has been found that the value of R_s decreases. It is expected that the trap charge also reduced with increasing the dye concentration.

In **Chapter 4**, we have prepared devices containing PSF dye and MR dyes respectively without and with TiO_2 and ZnO nanoparticles. In this study, by analyzing the I –V characteristics, R_s, n,

and trap energy have been estimated in presence and in absence of TiO_2 and ZnO nanoparticles. It has been observed that these nanoparticles reduce the above mentioned electrical parameters significantly. It has been attempted to provide an explanation for the potential cause of these alterations.

In **Chapter 5**, we investigated the R_s of Methyl Red (MR) dye-based organic device at various temperatures in this work. The preparation techniques for devices, as well as the experimental methods, have been discussed. Studies have been done on steady state dark current - voltage (I-V) measurements. The effect of temperature change on R_s, n, and trap energy has been seen, and an effort has been made to properly explain the findings.

In **Chapter 6**, we examined how single-walled carbon nanotubes (SWCNTs) impacted OPV devices based on the Malachite Green (MG) and Crystal Violet dyes (CV). We have analyzed the devices' dark and light I-V characteristics. The incident photon energy (E_m), which is absorbed by the OPV device, controls the charge transfer under illumination. We have also deduced the E_m from the light I-V characteristics. We have studied the effect of SWCNTs on R_s and E_c. Furthermore, we investigated R_s using the area method in both the absence and presence of SWCNTs under illumination.

In **Chapter 7**, overall findings of the work are mentioned in a systematic manner. Due to presence of traps, the value of series resistance is high. By using different nanoparticles and CNTs, the trap energy is reduced which results in a lowering of the value of series resistance. This is one of the major findings of our work. Different methods are employed to estimate the series resistance and the value obtained from these methods are consistent with each other.

1.5 References

1. G. Nama, Semiconductors and Its Application, Journal of Emerging Technologies and Innovative Research, (2018), 5: 217-221
2. Md. A. Rahman, A Review on Semiconductors Including Applications and Temperature Effects in Semiconductors, American Scientific Research Journal for Engineering, Technology, and Sciences, (2014), 7: 50-70

3. C. Y. Lung, C. Y. Lee, and Y. L. Huang, Copper metal for semiconductor interconnects, Noble and Precious Metals-Properties, Nanoscale Effects and Applications (2018): 220-221.
4. J. K. Jhothiraman, R. Balachandran, Electroplating: Applications in the Semiconductor Industry, Advances in Chemical Engineering and Science, (2019), .9: 239-261
5. C. Kunkel, J. T. Margraf, K. Chen, et al., Active discovery of organic semiconductors. Nat Communications, (2021), 12: 2422.
6. M. Pope and C. E. Swenberg, Electronic processes in organic crystals and polymers. University Press, (1999), Oxford
7. C. W. Lee, O. Y. Kim, J. Y. Lee, Organic materials for organic electronic devices. Journal of Industrial and Engineering Chemistry, (2014), 20: 1198–1208.
8. A. K. Chauhan, P. Jha, D. K. Aswal, et al., Organic Devices: Fabrication, Applications, and Challenges, Journal of Electronics Materials, (2022), 51: 447–485.
9. A. K. Jan, Solar cells based on dyes, Journal of Photochemistry and Photobiology A: Chemistry, (2000), 132: 1–17
10. M. Eslamian, Inorganic and Organic Solution- Processed Thin Film Devices, Nano – Micro Letters, (2017), 9: 1-23
11. S. E. Root, S. Savagatrup, A. D. Printz, D. Rodriquez, and D. J. Lipomi, Mechanical Properties of Organic Semiconductors for Stretchable, Highly Flexible, and Mechanically Robust Electronics, Chemical Reviews, (2017), 117: 6467-6499
12. B. Wegner, Molecular doping of organic semiconductors-contribution to its basic understanding and application, (2019)
13. I. Salzmann, G. Heimal, M. Oehzelt, S. Winkler, N. Koch, Molecular electrical doping of organic semiconductors: Fundamental mechanisms and emerging dopant design rules, (2016), 49: 370-378
14. J. A. Rivera, A. C. Castillom M. L. M. Gonzalez, Organic semiconductors: synthesis, properties and applications, ISBN: 9783030021696, (2019): 547-573
15. C. Yumusak, N. S. Sariciftci, M. I. Vladu, Purity of organic semiconductors as a key factor for the performance of organic electronic devices, Materials chemistry frontiers, (2020), 4: 3678-3689

16. D. Corzo, G. T. Biazquez, D. Baran, Flexible electronics: status, challenges and opportunities, Frontier in electronics, (2020), 1: 1-13
17. C. Kunkel, J. T. Margraf, K. Chen, H. Oberhofer, K. Reuter, Active discovery of organic semiconductors, Nature Communications,(2021), 12:1-11
18. S. Saxena, Exploring Electronics, http://interactshradha.blogspot.com/2012/02/organic-semiconductor-technology.html
19. A. Dey, A. Singh, D. Das, P. K. Iyer, Organic semiconductors: A new future of nanodevices and applications, (2015), ISBN: 978-3-319-14773-4: 97-128
20. Y. Wei, Y. Geng, K. Wang, H. Gao, Y. Wu, L. Jiang, Organic ultrathin nanostructure arrays: materials, methods and applications, (2022), 4: 2399-2411
21. M. Payne, D. Redinger, Organic TFTs: Solution-Processable Small-Molecule Semiconductors, (2015), ISBN: 978-3-642-35947-7: 1-12
22. E. K. Lee, M. Y. Lee, C. H. Park, H. R. Lee, J. H. Oh, Toward environmentally robust organic electronics: Approaches and applications, Advanced materials, (2017), 29: 1-29
23. A. S. Mahdi, L. M. Shaker, A. Alamiery, Recent advances in organic solar cells: materials, design, and performance, Journal of optics, (2023), https://doi.org/10.1007/s12596-023-01262-2
24. S. Ahmad, Organic semiconductors for device applications: current trends and future prospects, Journal of polymer engineering, (2014), 34 : 279-338
25. M. Kamran, M. R. Fazal, Fundamentals of renewable energy systems, Renewable Energy Conversion Systems, ISBN 978-0-12-823538-6, (2021): 1-19
26. P. A. Owusu & S. A. Sarkodie, A review of renewable energy sources, sustainability issues and climate change mitigation, Cogent Engineering,(2016), 3:1167990
27. P. Latake, P. Pawar, A. C. Ranveer, The greenhouse effect and its impacts on environment, Internal Journal of Innovative Research and Creative Technology, (2016), 1 : 333-337
28. A. L. E. Zein, N. A. Chehayeb, The effect of greenhouse gases on earth's temperature, International Journal of Environmental Monitoring and Analysis, (2015), 3(2) : 74-79
29. O. Ellabban, H. A. Rub, F. Blaabjerg, Renewable energy resources: Current status, future prospects and their enabling technology, Renewable and Sustainable Energy Reviews, (2014), 39 : 748–764

30. B. Mustafa, Usage of energy sources and environmental problems, Energy Exploration & Exploitation, (2005), 23: 141-168
31. Y. Hubenova, M. Mitov, Conversion of solar energy into electricity by using duckweed in direct photosynthetic plant fuel cell, Bioelectrochemistry, (2012), 87 : 185-191
32. N. P. Lokhande, , N. G. Maraskolhe, S. S. Lokhande, B. S. Rakhonde, Solar energy conversion and its utilization, International Research Journal of Engineering and Technology, (2017), 4(1) : 1737-1739
33. A. M. Baghir, et.al, Types of solar cells and applications, American Journal of Optics and Photonics, (2015), 3(5) : 94-1113
34. S. E. Root, S. Savagatrup, A. D. Printz, D. Rodriquez, and D. J. Lipomi, Mechanical Properties of Organic Semiconductors for Stretchable, Highly Flexible, and Mechanically Robust Electronics, Chemical Reviews (2017), 117 (9): 6467-6499
35. L. Li, G. Meller, H. Kosina, Influence of traps on charge transport in organic semiconductors. Solid-state Electronics - Solid State Electron, (2007) 51: 445-448

Chapter 2

Study on properties of organic semiconductors, the impact of series resistance in organic devices, the presence of nanoparticles and SWCNTs in the devices

2.1 Introduction

2.2 Electrical conductivity in organic/ polymer materials

2.3 Conjugated Polymers

2.4 Series resistance in organic devices

2.5 Traps and its influence on charge transport in organic devices

2.6 Metal Organic Interface: Barrier potential and current transport process at the interface

2.7 Current transport across the metal semiconductor interface: Thermionic emission theory

2.8 Current-Voltage equation at the metal organic interface in presence of R_s

2.9 Bulk limited current flow in organic devices

2.10 Estimation of trap energy from Space charge limited current (SCLC)

2.11 Different methods to determine series resistance (R_s) from dark I-V characteristics

2.11.1 $\frac{dV}{dI}$ Vs. I Method

2.11.2 Cheung Cheung Method, ($\frac{dV}{dlnI}$ Vs. I Method and H(I) Vs. I Method)

2.12 Light I-V characteristics

2.13 Different methods to determine series resistance (R_s) from light I-V characteristics

2.13.1 The two characteristics method
2.13.2 Area method
2.13.3 Maximum power point method

2.14 Carbon Nano Tubes (CNTs) in organic device

2.14.1 Single Walled Carbon Nanotubes (SWCNTs)
2.14.2 Multi Walled Carbon Nanotubes (MWCNTs)

2.15 Nanoparticles in organic devices

2.15.1 Titanium Dioxide (TiO_2) nanoparticles
2.15.2 Zinc Oxide (ZnO) nanoparticles

2.16 Effect of Carbon nanotubes and nanoparticles

2.17 Conclusion

2.18 References

2.1 Introduction

In the last chapter, we discussed about why organic semiconductors have become an interesting alternative in comparison to inorganic semiconductors. In this context, we have underlined the significance of organic devices along with its limitations. The preceding chapter provided an overview of the present study and also the organization of the thesis. This chapter will provide a brief review of the organic semiconductor. We will go through the basic properties of conductivities in conjugated organic semiconductors. The role of traps in organic devices has been discussed. The impact of series resistance (R_s) on the performance of organic device has a major role. We have discussed various methods to estimate R_s using the dark and light I-V characteristics. A brief review is also given to understand how these organic devices behave, when incorporation of nanoparticles or SWCNTs [1-2] are performed. This brief overview will assist to support the objective of our work.

2.2 Electrical conductivity in organic/ polymer materials

Organic electronics has added a new dimension in material science due to the discovery of conductivity in organic polymers in 1977. The conductivity of Polyacetelene film was enhanced by many orders of magnitude when it is doped with the halogens like bromine, iodine, or chlorine by Alan J. Hegger, A. G. Mac Diamrid, and H. Shirakawa [3-5]. Later, several investigations were conducted on various organic materials. Analysing atomic orbitals will be crucial for a better understanding of the semiconducting characteristics of organic materials.

The properties of organic semiconductor are relying on the formation of the carbon atoms. The electronic configuration of the C atom is $1s^2 2s^2 2p^2$, where two electrons reside in 1s level denoted by $1s^2$ and another four electrons are in 2s and 2p levels represented by $2s^2$ and $2p^2$ respectively. In the C atom one of the s electrons from $2s^2$ is promoted to the p orbital and forms four single valence orbitals as shown in the Fig. 2.1. By combining these four orbitals, new hybridised orbitals are created. Three different hybridization types are available, and they are denoted by the letters sp^3, sp^2, and sp, where the superscript indicates how many p orbitals are participating in the hybridization [6].

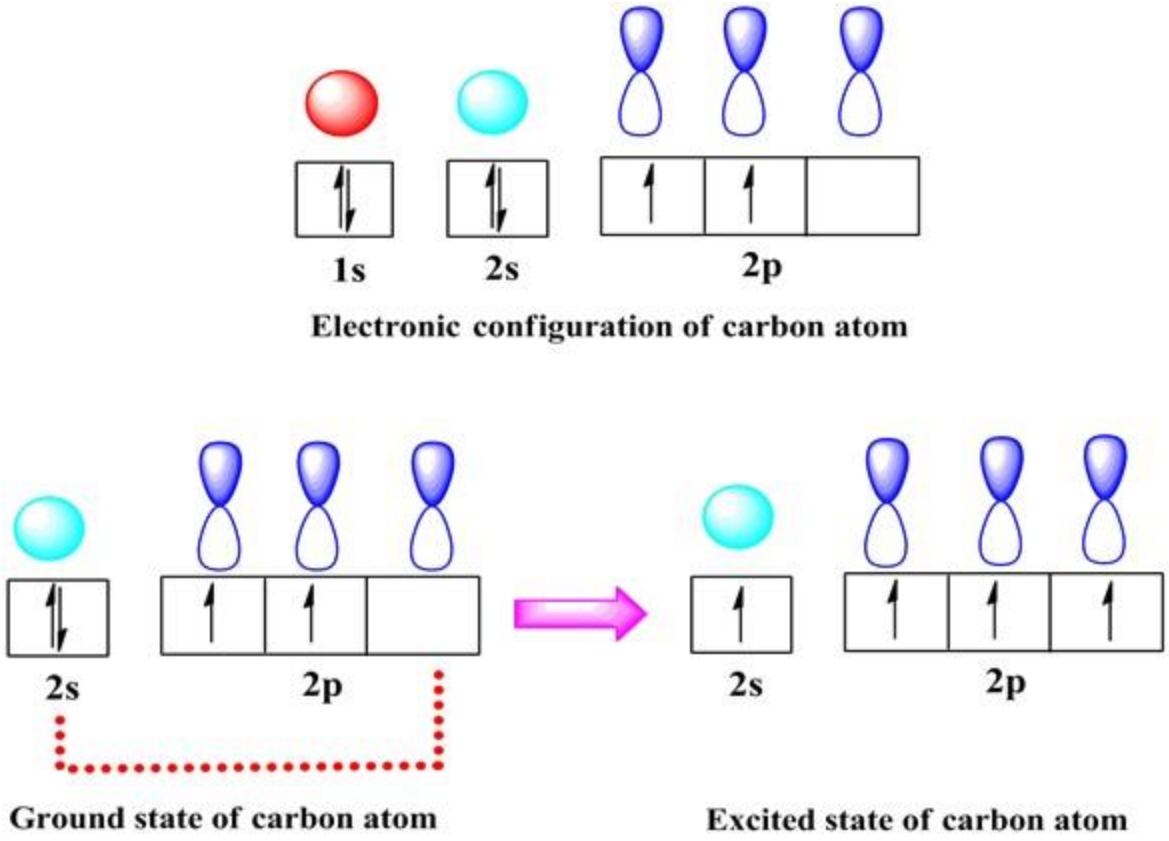

Fig 2.1 Hybridization of C atom

Four hybridised orbitals are created in the sp^3 hybridization process from the combination of one s and three p orbitals. Each sp^3 orbital has two lobes of varying sizes, with the four bigger lobes being aligned at an angle of 109.5° to one another and having a tetrahedral form as seen in Fig.2.2. In the backbone of sp^3-based polymers, there are only single bonds. As a result, the polymers belonging to this group have wider band gaps and display insulating characteristics.

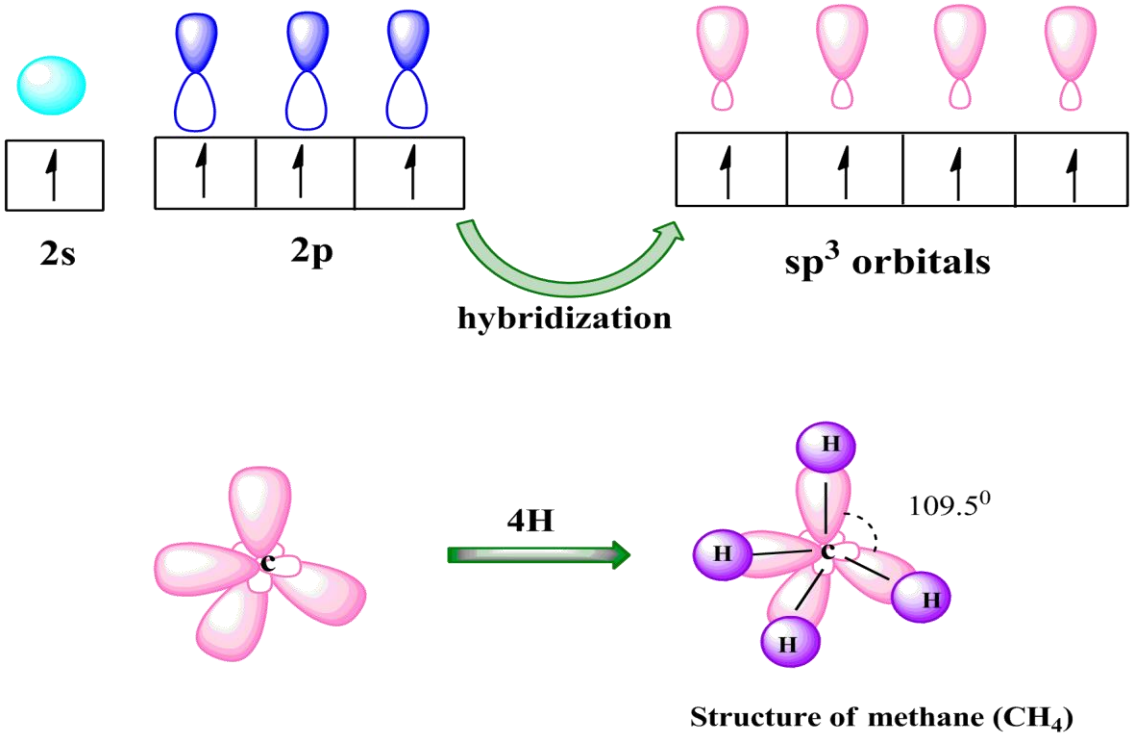

Fig. 2.2 sp^3 hybridization of C atom

One s orbital and two p orbitals ($2p_x$ and $2p_y$) are combined in the sp^2 hybridization to create three hybridised orbitals. The three sp^2 orbitals' bigger lobes are triangular in form and orientated to one another at 120˚ angle. As illustrated in Fig.2.3, the $2p_z$ orbital is still unhybridized and parallel to the sp^2 orbitals. The $3p_z$ orbitals overlap and establish a connection with the sp^2 orbitals when they engage with nearby atoms. Hence, an alternatingconnection is produced. Due to the presence of alternate single and double bonds, sp^2 hybridised organic semiconductors are also known as conjugated semiconductors. These sp^2 hybridization-based polymers show semiconductor-like characteristics.

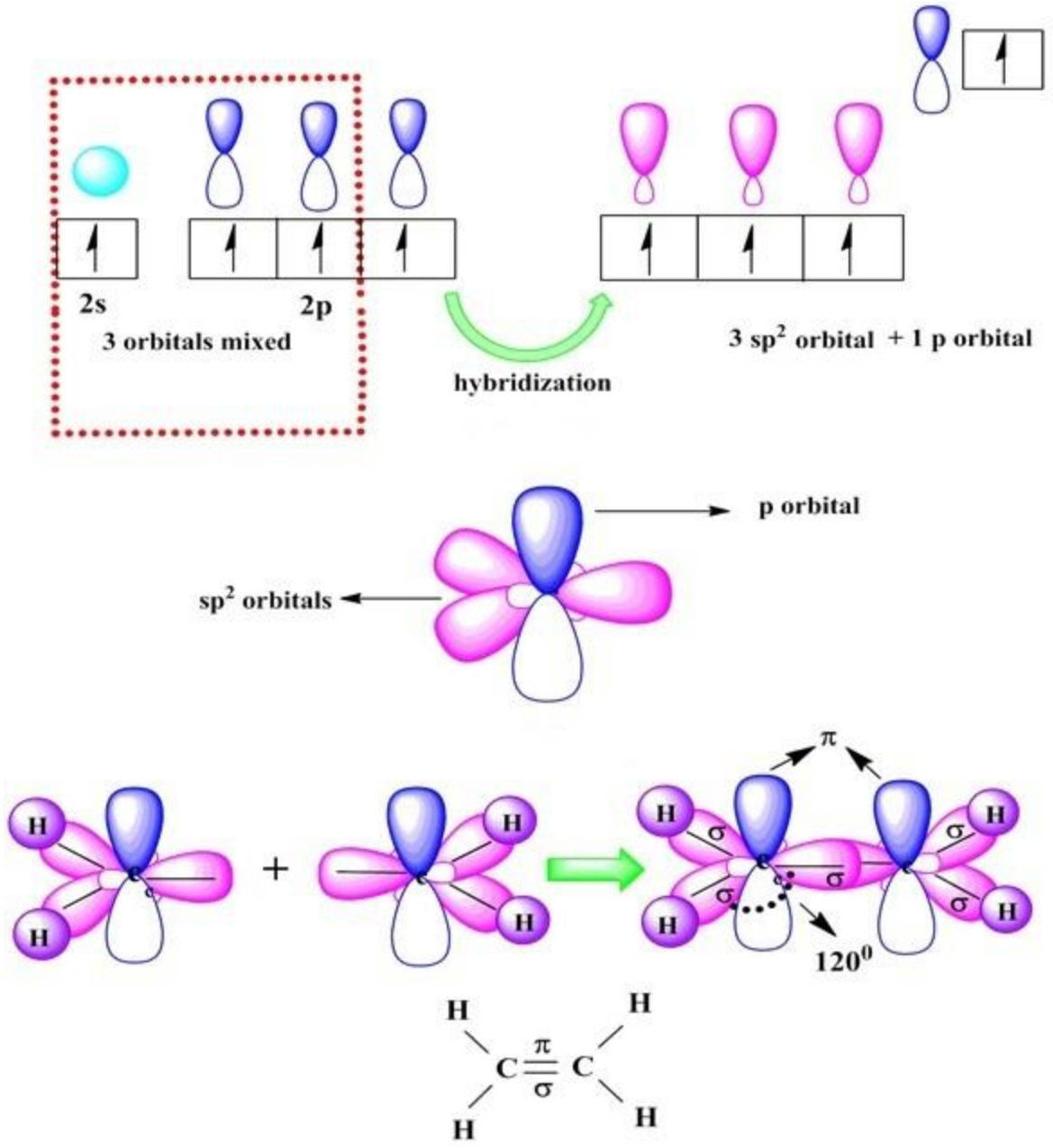

Fig 2.3 sp^2 hybridization of C atom

Similarly a combination of one s orbital and one p orbital (p_x) of C atom formed two sp orbitals in sp hybridization. In this hybridization p_y and p_z orbitals remain unhybridized and the sp orbitals make an angle of 180˚ to one another as shown in Fig. 2.4 below. During interaction

with other atoms the sp orbital will form a sigma bond whereas the unhybridized orbitals will form π bond. So two π bonds and one σ bond will be formed in this configuration.

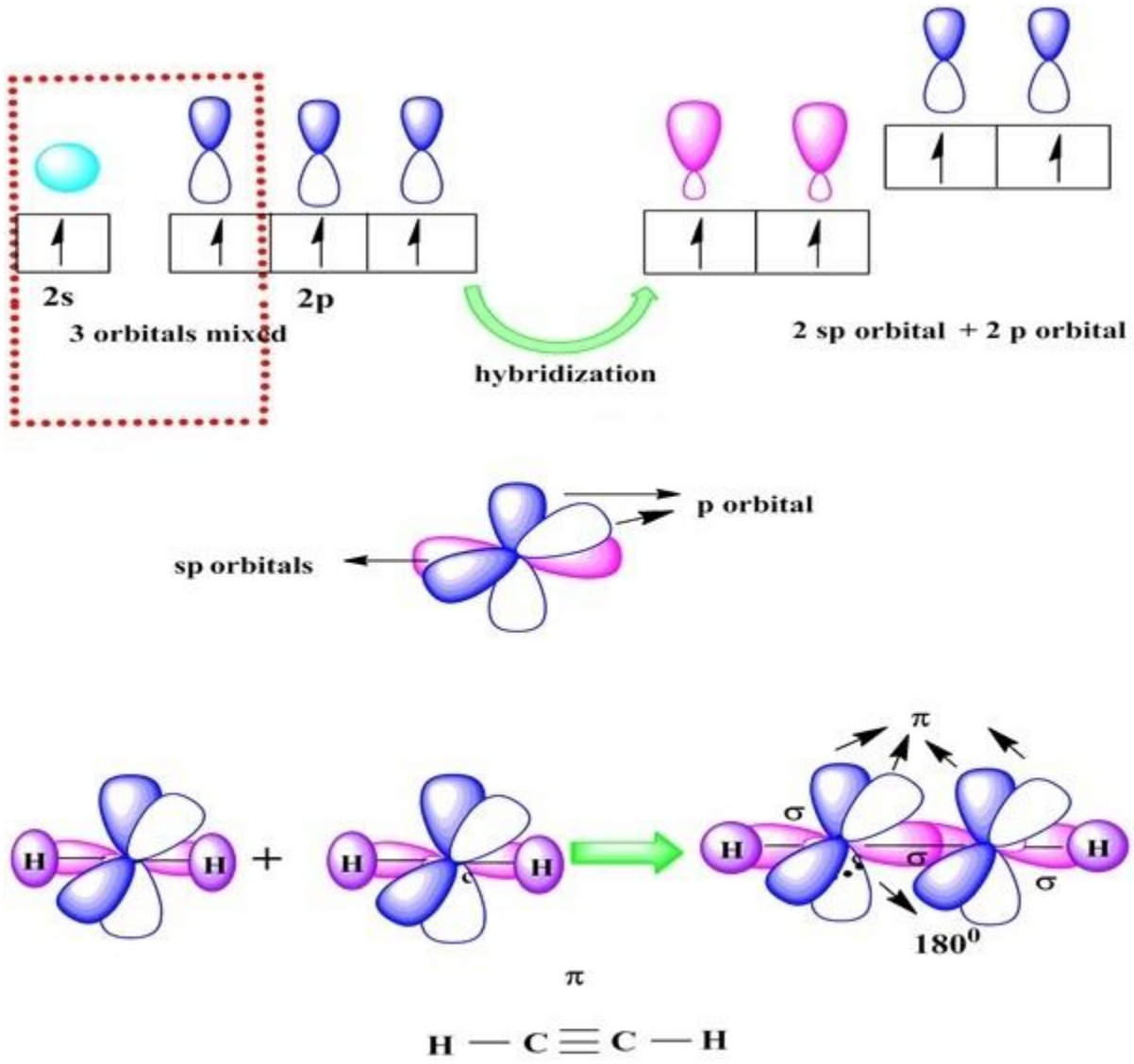

Fig 2.4 sp hybridization of C atom

2.3 Conjugated Polymers

Discovery of conductivity in conjugated polymers has drawn the attention of scientists in the field of materials science. Numerous investigations have been done to improve the electrical conductivity of conjugated polymers [7-8]. Fig. 2.5 shows variety of conjugated polymer types.

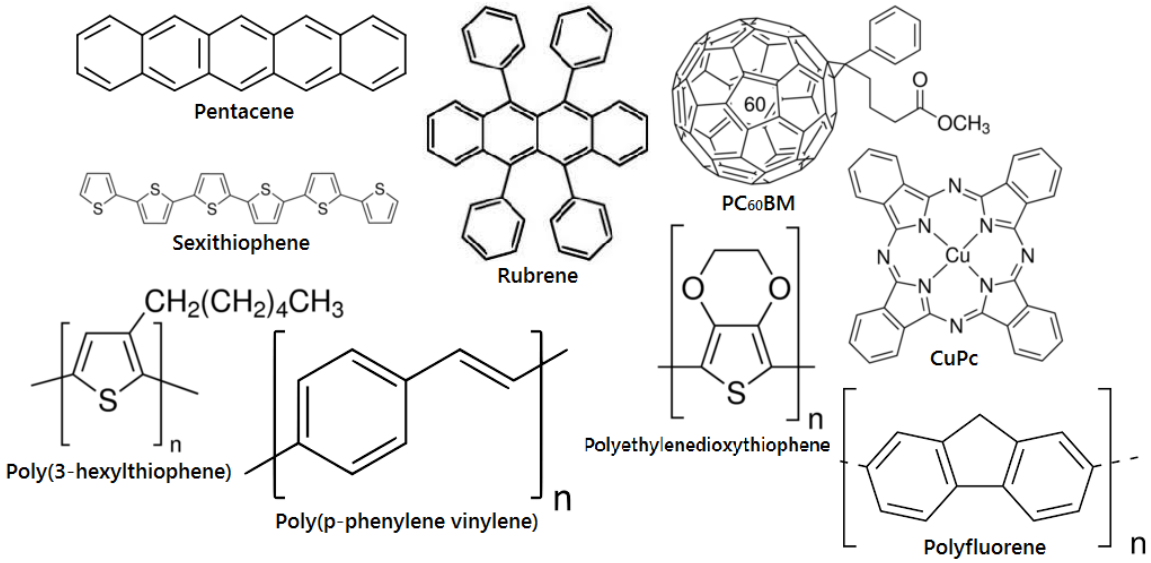

Fig. 2.5 Structures of different organic semiconducting materials

These sp^2 hybridised polymers are known as conjugated polymers because the backbone of their structure contains alternate single and double bonds. As was previously mentioned, each carbon atom in conjugated polymers has three sp^2 hybrid orbitals and one unhybridized orbital p_z. Sigma bonds are formed between the electrons in the sp^2 orbitals of C atoms and the atoms next to them. The unhybridized p_z orbitals, on the other hand, are perpendicular and use the pi bond for creating covalent bonds with nearby atoms. This formation of π bonds enables delocalization of π electrons throughout the polymer chain [9-10]. The charge transport process within the conjugated polymer is aided by the delocalization of electrons throughout the whole system. The structure of conjugated polymers is shown in Fig. 2.6.

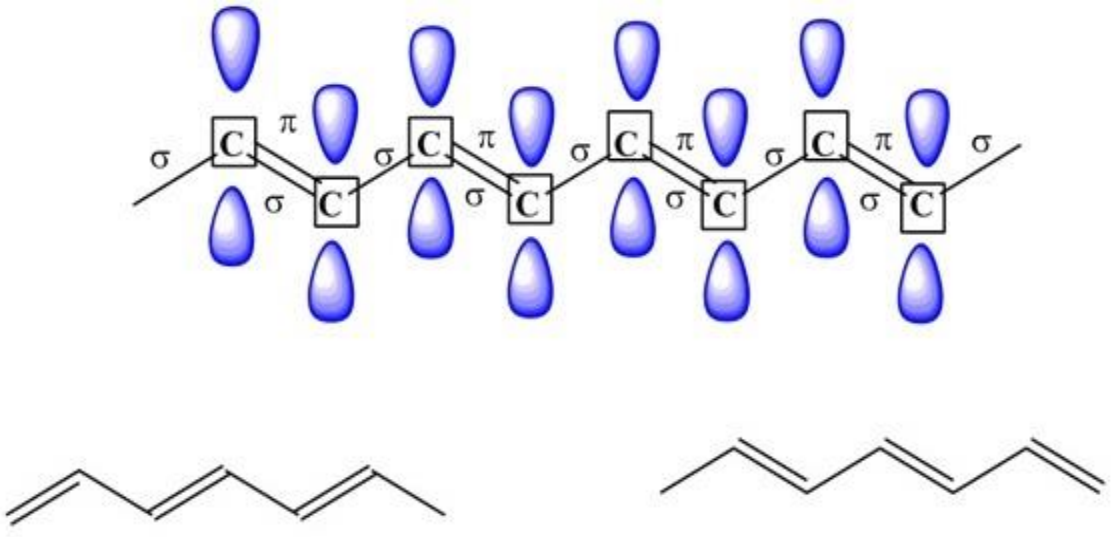

Fig. 2.6 Structure of conjugated semiconductor

The electronic structure of the polymer can be described in terms of energy bands, shown in the Fig. 2.7.As indicated in Fig. 2.7, the bonding orbitals (π) located lower in energy, form a valence band, with the name highest occupied molecular orbital (HOMO) and the conduction bond is formed by the molecular orbitals with higher energy, the anti-bonding orbitals (π*), with the lowest state named lowest unoccupied molecular orbital (LUMO) [11]. The distance between the conjugated polymer's HOMO and LUMO is roughly about 1-4 eV in this arrangement.

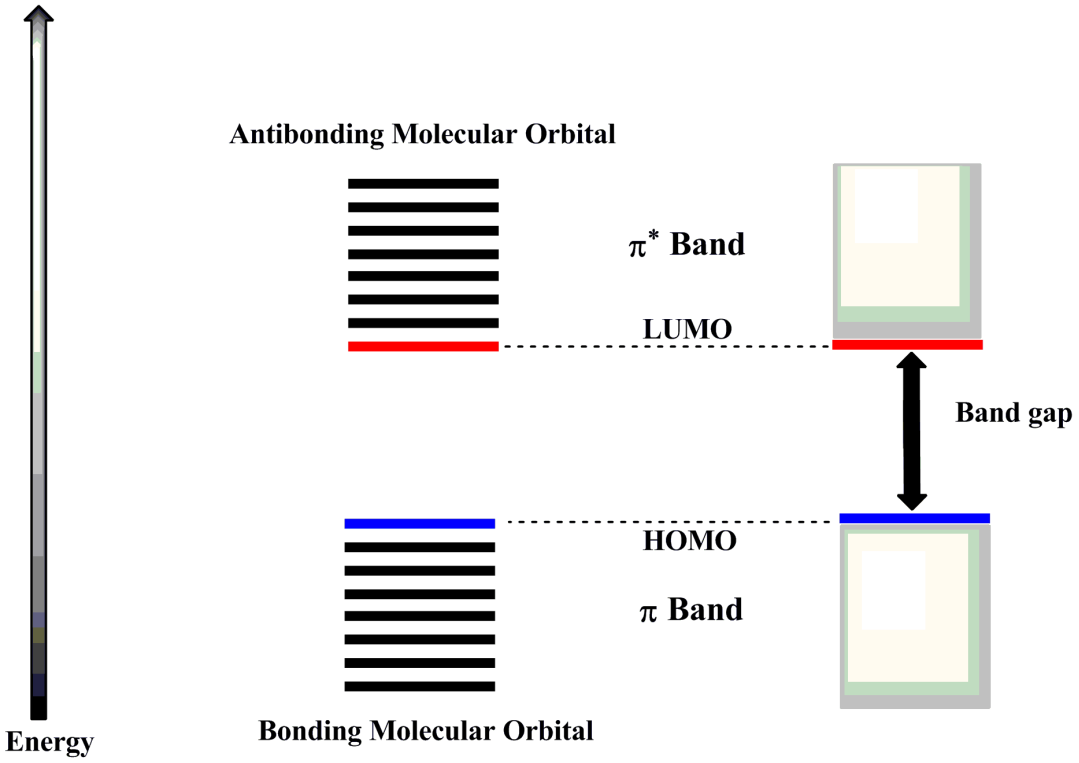

Fig 2.7 The diagram displaying the Energy band of an organic semiconductor

2.4 Series resistance in Organic devices

Organic semiconductor devices are showing interest in the field of electronics from the last few decades. The researchers study the device performance made by these organic materials because of their numerous prospective applications, including their low cost, flexibility, and ease of manufacturing [12–13]. However, low efficiency is a serious problem for organic devices. The low stability and efficiency of these devices have a number of causes [14–15]. One of the main reasons which we have considered is the effect of series resistance. It has been observed that the value of series resistance of the organic devices is very high [16-19]. It is observed that the value of current in organic devices is very low and also at high voltage regions the dark I-V characteristics deviates from linearity in semi logarithmic scale. This deviation of I-V curve is due to the presence of series resistance. So study of the physics behind the series resistance of organic devices and its effect on the performance is very crucial for the enhancement of the device efficiency. Reduction of series resistance will improve device performance. Recently some literatures described about some techniques on how to reduce series resistance [20]. But

the impact of series resistance on charge transport mechanism of devices is still not properly elaborated. Therefore in this work, we have studied the reasons for high value of series resistance and how it can be reduced to improve the performance of organic devices.

There are various factors which contributes R_s in organic devices. One of the major reasons of high series resistance arises due to the presence of traps. These traps introduce energy states in between HOMO and LUMO. These traps captured the charge carriers during the charge transport process. Also when the organic dye comes in contact with a metal, localized energy states introduce at the interface which increase the barrier potential of the device. This increased barrier potential reduces charge injection and flow of charge carriers which in turn create an impact on R_s of organic devices.

So it can be said that the trapping of charge carriers significantly contribute to series resistance in organic devices. As a result, it is very essential to understand the origin of traps, the formation of metal semiconductor interfaces, and current transport mechanisms in the presence of traps. In the following sections, we will go through these factors of organic devices.

2.5 Traps and its influence on charge transport in organic devices

In any organic device the presence of imperfection in the organic semiconductor introduces structural defects called traps in the energy space [21-22]. Electronic traps are introduced in organic semiconductors basically from two types of sources. One is an intrinsic source of traps and another one is extrinsic sources of traps. The term "intrinsic sources of traps" refers to traps caused by defects in structure and chemical impurities. When compared to intrinsic sources of traps, extrinsic sources are introduced by electromagnetic radiation, temperature gradients, interacting organic semiconductor with other materials, etc.[23]. Presence of traps shows localized energy states between the HOMO and LUMO energy band gaps. By trapping and releasing charge carriers, these localised energy states limit the process of charge transmission. As a result, these localised energy states prevent charge carriers from taking part in the charge transport process, which lowers the efficiency of organic semiconductor devices. According to the different literature in organic devices the distribution of traps are explained in three different ways [24-26]. These three different types of trap distributions are discrete energy level,

Exponential and Gaussian trap distribution. Gaussian and Exponential trap distributions are widely used to describe the traps at metal – organic interface. These the distribution of traps are shown in Fig. 2.8.

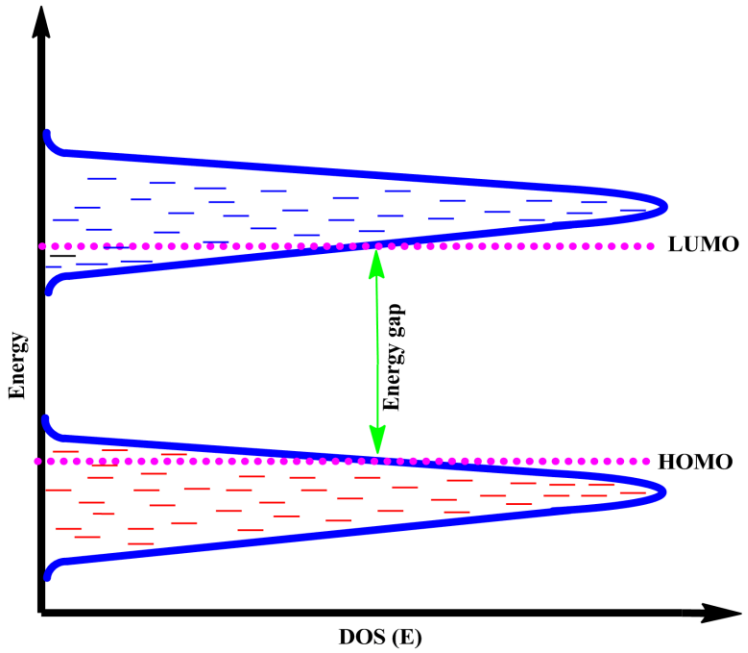

(a)

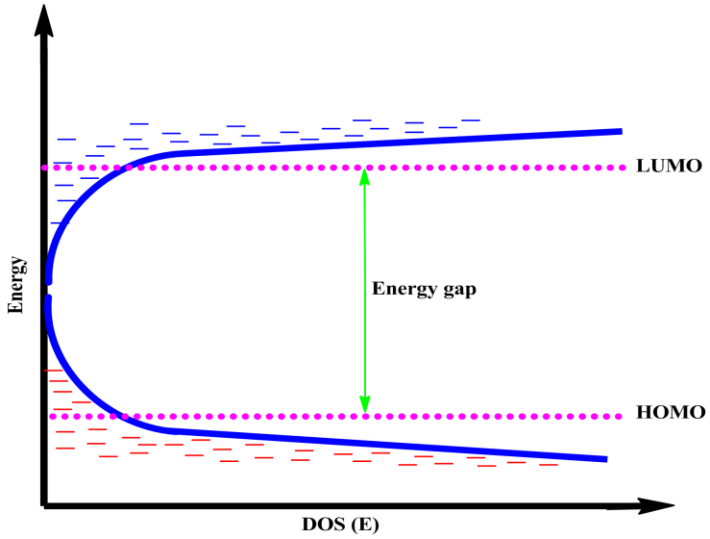

(b)

Fig. 2.8 (a) Gaussian trap distribution and (b) Exponential trap distribution

Traps can be classified as shallow traps and deep traps based on the energy of the trap.According to Fig. 2.9, shallow level traps are found close to band edges, whereas deep level traps are found farther inside the band gap [23,27].

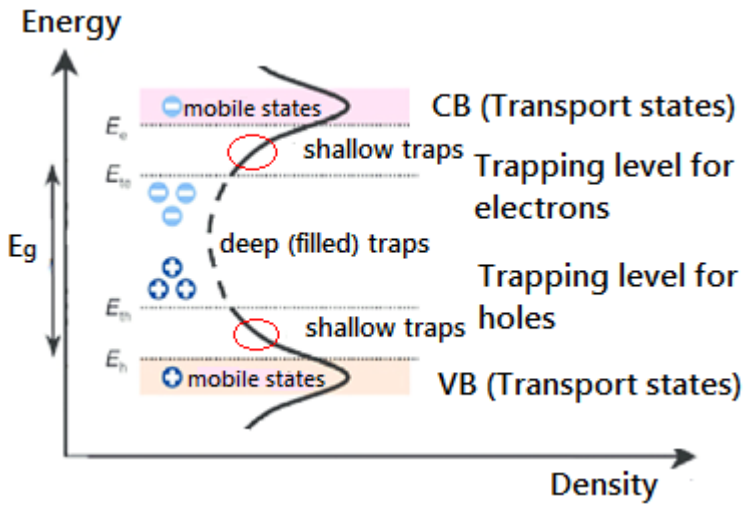

Fig. 2.9 Shallow and deep traps in organic semiconductors

Presence of shallow level traps captures the free charge carriers. These captured charge carriers can be released by an external incitation such as electric field, thermal energy or photon energy. So in organic semiconductor during charge transport process due to these shallow traps charge carriers are trapped within delocalized states. These trapped charges are again released by external thermal energy. This continuous trapping and detrapping of charge carriers is defined as multiple trapping and detrapping model shown in Fig. 2.10. Moreover thermally activated hopping or tunneling processes of charge carriers from one localized state to another localized states are governed for the higher density of traps. Releasing of charge carriers from the trap states is possible if the traps are shallow level traps. The possibility of releasing from deep level traps is negligible at room temperature. Fig. 2.10 shows the various possible transport processes of trapped charge carriers.

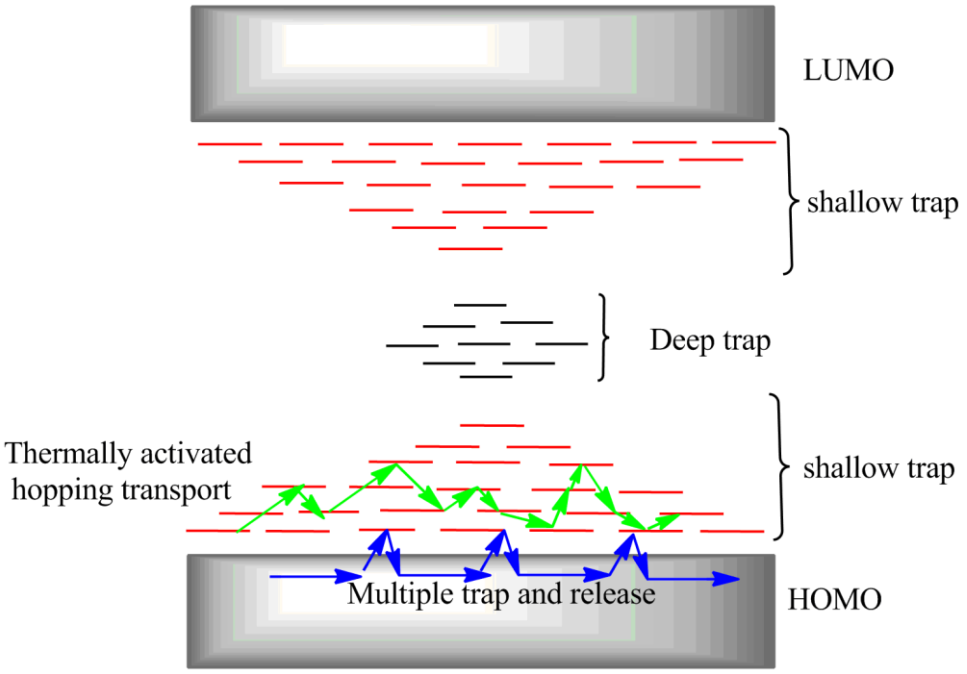

Fig. 2.10 Different transport regimes, including thermally-activated hopping transport between localized states (Green) and multiple trap and release Mechanisms (Blue)

So localized energy states are taking an important role on the charge transport process and overall current transport mechanism of the device.

2.6 Metal Organic Interface: Barrier potential and current transport process at the interface

The performance of any organic device depends significantly on the metal organic semiconductor interface [28]. The metal–organic interface has a significant role in the electrical conduction process. The work function, which is the separation between the Fermi levels and the vacuum level, is defined as the minimal energy needed to evict an electron from the surface of a solid into the vacuum. In this context when metal comes in contact with organic semiconductor depending on the work function charge carriers will defuse until the Fermi levels are aligned. Due to this transfer of charge carriers, a band bending effect occurs at the metal semiconductor interface. There are two types of contact formation at the interface that can be formed as a result of band bending effect. These contacts are Ohmic contact and Schottky contact which are shown in the Fig. 2.11.

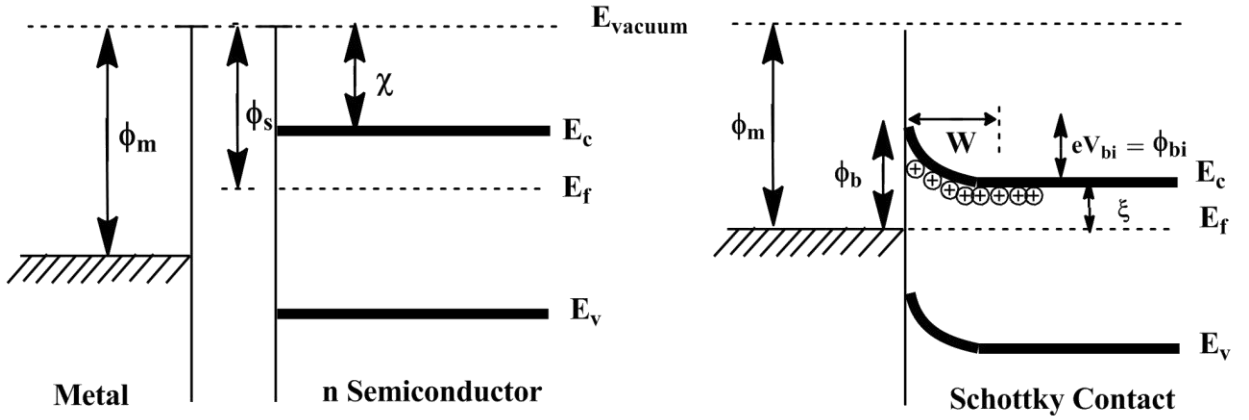

(a)

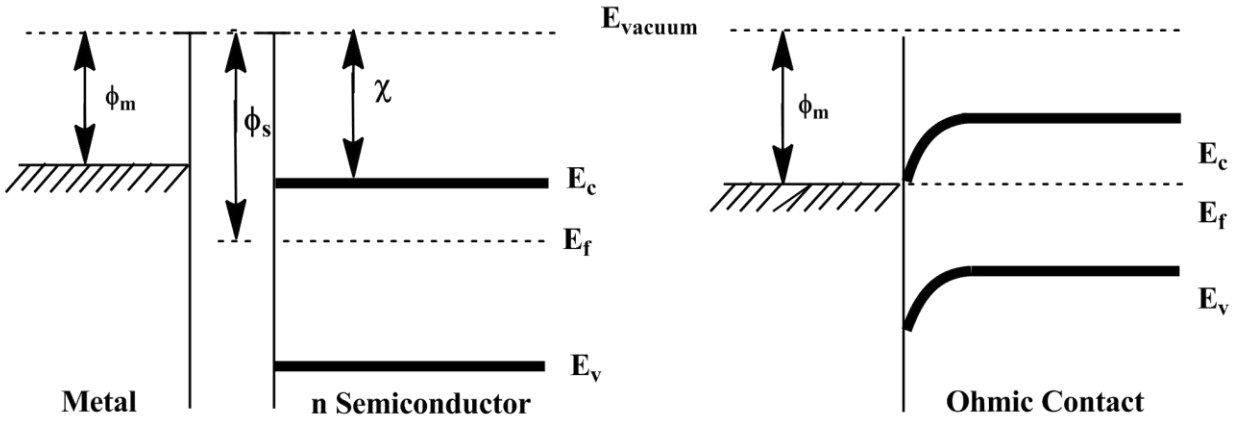

(b)

Fig 2.11 Energy barriers at the metal/n organic semiconductor interface both before and after contact. Charge transfer takes place after contact, causing the organic semiconductor's "band bending" and the formation of Ohmic or Schottky contact

The energy band diagram before contact is shown in Fig. 2.11, where ϕ_m denotes the metal work function and ϕ_s denotes the semiconductor work function. If $\phi_m > \phi_s$, electrons will go from the n type semiconductor to the metal in the case of an n type semiconductor. This transfer of electrons will happen until the alignment of the Fermi levels of metal and semiconductor reaches to same energy level. As a result of transfer of electrons to the metal, a depletion layer of positive charges with a thickness (W) will be formed near this interface. For an ideal contact between a metal and an n-type semiconductor, the barrier height is expressed as,

$$\phi_b = \phi_m - \chi \tag{2.1}$$

Where ϕ_b can also be expressed as,

$$\phi_b = eV_{bi} + \xi \tag{2.2}$$

$$= \phi_{bi} + \xi \tag{2.3}$$

Where χ is the electron affinity of the semiconductor, e is the electronic charge, ξ is the energy difference between the conduction band and the fermi energy level of the semiconductor and eV_{bi} is the band bending at zero bias which can also be defined as built in potential ϕ_{bi} formed between metal and semiconductor[29].

The built in potential can be expressed as,

$$\phi_{bi} = eV_{bi} = \frac{eN_D W^2}{2\varepsilon} \tag{2.3}$$

Where W is the thickness of the depletion layer, ε is the permittivity of the semiconductor materials and N_d is the ionized donor density.

Therefore, a Schottky barrier will form at equilibrium for an n-type semiconductor when $\phi_m > \phi_s$ because of the effects of electron transport from semiconductor to metal, shown in Fig. 2.11 (a). Reverse bias refers to the application of positive voltage across the semiconductor, which increases the band bending. Forward bias refers to the application of negative voltage across the semiconductor, which lowers the band bending and increases the passage of electrons from semiconductor to metal. In contrast, if $\phi_m < \phi_s$, electrons will go from the metal to the n type semiconductor. At the metal semiconductor interface seen in Fig. 2.11 (b) under this situation, an ohmic contact will be created. Similar to this, Fig. 2.12 also illustrates the contact formation for a p type semiconductor. From this figure it can be said that in $\phi_m > \phi_s$ due to the transfer of charge carriers, ohmic contact will be formed at the interface, whereas for $\Phi_m < \Phi_s$ Schottky barrier will be formed at the interface.

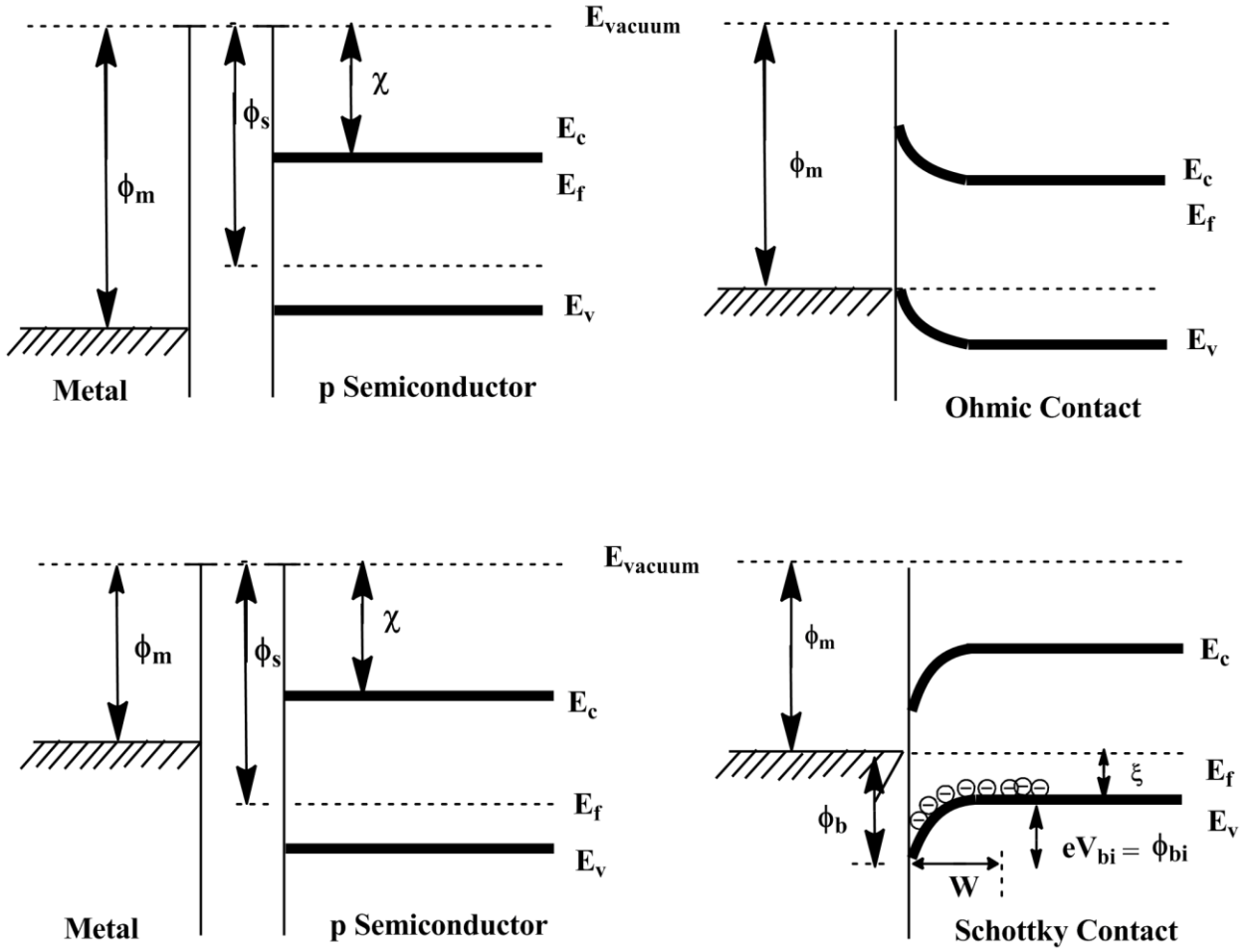

Fig 2.12 Energy barriers at the metal/p type organic semiconductor interface both before and after contact. Charge transfer takes place after contact, causing the organic semiconductor's "band bending" and the formation of Ohmic or Schottky contact

2.7 Current transport across the metal semiconductor interface: Thermionic emission theory

At the metal–organic interface different charge transport mechanism occurs. The most important mechanism is the thermionic emission theory [30]. Thermionic emission theory assumes that the barrier height ϕ_b is significantly more than kT and the electrons with energies greater than the top of the barrier will pass through the barrier. According to the Richardson formula the current density of the thermionic emission is given by [31],

$$J_{Rs} = AT^2 \exp\left(-\frac{\phi_b}{kT}\right) \tag{2.4}$$

Where $A = 4\pi em^* \left(\frac{k^2}{h^3}\right)$ (Richardson constant) T is the absolute temperature.

Therefore by considering this Thermionic emission theory, in any Schottky barrier the current density is described by the Shockley formula expressed as [32],

$$J = A^* T^2 \exp\left(-\frac{\phi_b}{kT}\right)\left[\exp\left(\frac{eV}{nKT}\right) - 1\right] \quad (2.5)$$

$$= J_0\left[\exp\left(\frac{eV}{nkT}\right) - 1\right] \quad (2.6)$$

Where A^* is the effective Richardson constant, T is the absolute temperature, k is the Boltzmann constant, V is the applied voltage, and J_0 is the reverse saturation current.

$$J_0 = A^* T^2 \exp\left(-\frac{\phi_b}{kT}\right) \quad (2.7)$$

2.8 Current-Voltage equation at the metal organic interface in presence of R_s

As organic semiconductors are prone to traps, they operate as recombination centers or as defects in organic materials, influencing the interface state and so increasing the Schottky barrier. As a result, charge injection is low at the metal organic interface because of which the overall current of the device is also very low. So for the evaluation of the organic devices performance it is very essential to study the current voltage characteristics. In dark I-V characteristics voltage is applied to the cell for the flowing of charge carriers. The importance of dark I-V characteristics is to analyze the junction formation, the grid and contact resistance. Moreover from this dark I-V characteristic we can extract various parameters which provide essential information about the device. It is well known that the dark I-V characteristics of the cell produce an exponential curve and exhibits diode-like behavior. Also it is observed that at the high voltage the current-voltage characteristics in semi logarithm scale deviates from linearity. The deviation occurs due to presence of R_s. As a result, the current density equation provided by the Shockley formula has been modified using the Cheung-Cheung method by including the influence of R_s. The mathematical relation of the I-V curve is given by [33-35],

$$I = I_0\left[\exp\left(\frac{q(V - IR_s)}{nkT}\right) - 1\right] \quad (2.8)$$

and,

$$I_0 = AA^* T^2 \exp(-\frac{q\phi_b}{kT})$$

2.9 Bulk limited current flow in organic devices

As discussed before, in any organic devices, charges are being trapped at the trap centers and a space charge region is found. So the current transport mechanism of organic system differs from inorganic system. Our discussion of the Cheung-Cheung method in the previous section has not taken into account the impact of charge carrier trapping. So in presence of traps the transport mechanism is modified which we will discuss in the subsequent section.

In any organic device the current flow is mainly restricted by two methods (i) injection-limited or (ii) bulk-limited. The injection limited current mainly occurs at low voltage or below the threshold voltage and in injunction limited, the non-ohmic metal-polymer contacts restrict the current through the polymer. At above the threshold voltage, the charge transport may be considered as bulk transport, known as bulk limited current. Basically, when conducting polymer is sandwiched in between two electrodes one of the interfaces creates an ohmic barrier with a low barrier height from which charge carriers will be injected. These injected charge carriers and the equilibrium free charge carriers inside polymer generate a space charge region. When an external voltage is applied, additional charge carriers will be injected from low barrier electrode to the polymer. These traps capture free carriers during the charge transport process, reducing the electrical characteristics of the organic polymer and hence its performance. In this circumstance the current flow is known as space charge restricted current in presence of traps [36]. The trapped space charge limited current is affected by the distribution of trap states at the energy band gap. In the following section, we have calculated the total current in presence of an exponential trap distribution.

2.10 Estimation of trap energy from Space charge limited current (SCLC)

The space charge limited current will be modified according to trap distribution [37-38]. We could state that in organic semiconductor devices with high trap charge density compared to free charge carrier density ($n_t >> n$),

$$\frac{dE}{dx} = \frac{e}{\varepsilon} n_t \qquad (2.9)$$

Now for exponential trap density the concentration of trap energy is expressed as,

$$n_t = H_n \exp\left(\frac{F_n}{kT_c}\right) \tag{2.10}$$

H_n is the trap density, F_n is the Fermi energy of electron, T_c is the characteristics temperature $T_c = \frac{E_c}{K}$, and k is the Boltzmann constant.

The expression of free charge carrier density is,

$$n = N_c \exp\left(\frac{F_n}{kT}\right) \tag{2.11}$$

So n_t can be written as,

$$n_t = H_n \exp\left(\frac{F_n}{kT} \times \frac{T}{T_c}\right) \tag{2.12}$$

$$n_t = H_n \left(\frac{n}{N_c}\right)^{\frac{1}{m}} \tag{2.13}$$

$$= C n^{\frac{1}{m}} \tag{2.14}$$

Where, $m = \frac{T_c}{T}$ and $C = \frac{H_n}{N_c^{\frac{1}{m}}}$

So the equation 2.9 can be written as,

$$\frac{dE}{dx} = \frac{e}{\varepsilon} c n^{\frac{1}{m}} \tag{2.15}$$

By representing E in terms of V,

$$\frac{d^2V}{dx^2} \times \left(\frac{dV}{dx}\right)^{\frac{1}{m}} = \frac{e}{\varepsilon} c \left(\frac{1}{q\mu}\right)^{\frac{1}{m}} \tag{2.16}$$

By integrating the equation with respect to x,

$$\left(\frac{dV}{dx}\right)^{\frac{1+m}{m}} \times \frac{m}{1+m} = \frac{e}{\varepsilon} c \left(\frac{1}{q\mu}\right)^{\frac{1}{mx}} + C \tag{2.17}$$

At x=0, $\frac{dV}{dX}$ will be zero,

So,

$$\frac{dV}{dx} = \left(\frac{m+1}{m}\right)^{\frac{m}{m+1}} \times q^{\frac{m-1}{m+1}} \times \left(\frac{J}{\mu}\right)^{\frac{m}{m+1}} \times x^{\frac{m}{m+1}} \tag{2.18}$$

Again by integrating with respect to x between x=0 to x=L, the equation will be,

$$\int_0^V dV = \left(\frac{m+1}{m}\right)^{\frac{m}{m+1}} \times \left(\frac{C}{\varepsilon}\right)^{\frac{m}{m+1}} \times q^{\frac{m-1}{m+1}} \times \left(\frac{J}{\mu}\right)^{\frac{m}{m+1}} \int_0^L x^{\frac{m}{m+1}} dx \quad (2.19)$$

$$V = \left(\frac{m+1}{m}\right)^{\frac{m}{m+1}} \times \left(\frac{C}{\varepsilon}\right)^{\frac{m}{m+1}} \times q^{\frac{m-1}{m+1}} \times \left(\frac{J}{\mu}\right)^{\frac{m}{m+1}} \times \frac{m+1}{2m+1} \times L^{\frac{2m+1}{m+1}} \quad (2.20)$$

From the above expression, the current density can be expressed as

$$J = N_c \mu \left(\frac{2m+1}{m+1}\right)^{m+1} \left(\frac{\varepsilon m}{(m+1)H_n}\right)^m q^{m-1} \frac{V^{m+1}}{L^{2m+1}} \quad (2.21)$$

This is limited trap charge conduction technique.

The most notable aspect of the equation is the power law dependence $J \approx V^{m+1}$. This specific I-V connection forms as a result of the exponentially distributed traps between the LUMO and HOMO. The findings of our experiments analysis the current-voltage (I-V) relation [39–40] are most appropriate by this model.

There are several charge transport models as well, such as the hopping, dispersive, and multiple trapping and release (MTR) models. In the present investigation, we will use the SCLC model and also study the effect of nanoparticles or SWCNTs on this specific charge transport mechanism.

2.11 Different methods to determine series resistance (R_s) from dark I-V characteristics

Fig. 2.13 below shows the Current Voltage characteristics and ln I Vs. V characteristics of organic solar cell in dark mode. It is observed that the ln I Vs. V plot is linear at low bias voltage and deviates from linearity at high bias voltage [41-42].

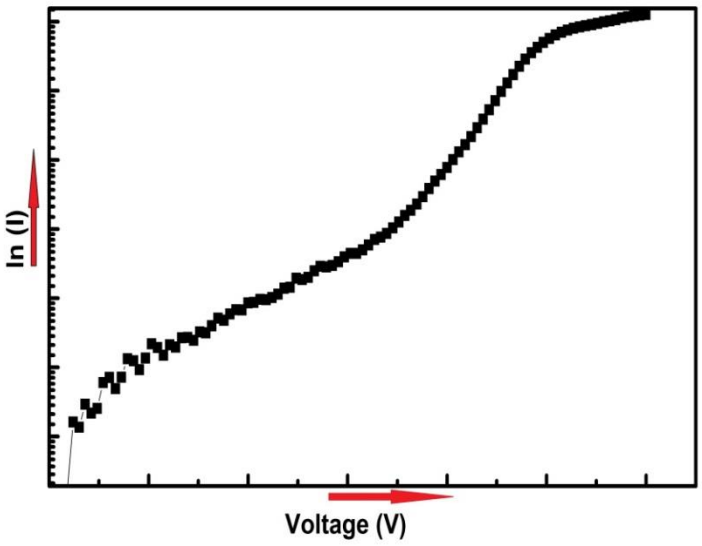

Fig. 2.13 lnI Vs. Voltage curve of organic devices

2.11.1 $\frac{dV}{dI}$ Vs. I Method

This deviation of the I-V characteristics is due to the presence of series resistance. To measure the series resistance we can simplify the Eqn. 2.22, shown below,

$$I = I_0\left[\exp\left(\frac{q(V-IR_s)}{nkT}\right)-1\right] \tag{2.22}$$

$$\frac{dI}{dI} = \frac{d}{dI}\left[I_0\left[\exp\left(\frac{q(V-IR_s)}{nkT}\right)-1\right]\right] \tag{2.23}$$

$$1 = I_0\frac{q}{nkT}\left(\frac{dV}{dI}-R_s\right)\exp\left(\frac{q(V-IR_s)}{nkT}\right) \tag{2.24}$$

$$1 = \frac{q}{nkT}\left(\frac{dV}{dI}-R_s\right)\times I \tag{2.25}$$

$$\frac{qI}{nkT}\frac{dV}{dI} = 1 + IR_s\frac{q}{nkT} \tag{2.26}$$

$$\frac{dV}{dI} = \frac{nkT}{qI} + R_s \tag{2.27}$$

The first term of this Eqn. 2.27 can be negligible at high voltage, since the value of the current is high at high bias voltage. So this Eqn. 2.27 can be written as

$$\frac{dV}{dI} \approx R_s \tag{2.28}$$

2.11.2 Cheung Cheung Method, ($\frac{dV}{dlnI}$Vs. I Method and H(I) Vs. I Method)

There are also various methods to determine R_s from the dark I-V characteristics. One of the important method is Cheung Cheung method which we have used to extract the device R_s [43]. According to this method we can simplify the Eqn. 2.22 as,

$$I = I_0\left[\exp\left(\frac{q(V - IR_s)}{nkT}\right) - 1\right]$$

$$\frac{dI}{dlnI} = \frac{d}{dlnI}\left[I_0\left[\exp\left(\frac{q(V-IR_s)}{nkT}\right) - 1\right]\right] \tag{2.29}$$

$$\frac{dI}{dlnI} = \left[I_0\frac{q}{nkT}\exp\left(\frac{q(V-IR_s)}{nkT}\right)\left[\frac{dV}{dlnI} - \frac{dIR_s}{dlnI}\right]\right] \tag{2.30}$$

$$I = \left[\frac{q}{nkT}\left[\frac{dV}{dlnI} - \frac{dIR_s}{dlnI}\right]I\right] \tag{2.31}$$

$$\frac{nkT}{q} = \frac{dV}{dlnI} - IR_s \tag{2.32}$$

$$\frac{dV}{dlnI} = \frac{nkT}{q} + IR_s \tag{2.33}$$

So from this Eqn. 2.33 it is seen that the plot of $\frac{dV}{dlnI}$ Vs. I provide the value of ideality factor (n) from the intercept at the Y axis and the slope of the curve gives the value of R_s.

Apart from that we can verify the value of R_s extracted from $\frac{dV}{dlnI}$ Vs. I plot by simplifying the Eqn. 2.22 in another way shown below,

$$I = I_0\left[\exp\left(\frac{q(V-IR_s)}{nkT}\right)\right] \tag{2.34}$$

$$\ln\frac{I}{I_0} = \left(\frac{q(V-IR_s)}{nkT}\right) \tag{2.35}$$

$$\ln I - \ln I_0 = \frac{qV}{nkT} - \frac{qIR_s}{nkT} \tag{2.36}$$

$$V = \frac{nkT}{q}\ln I - \frac{nkT}{q}\ln I_0 + IR_s \tag{2.37}$$

Putting the equation of I_0 the equation will be,

$$V = \frac{nkT}{q}\ln I - \frac{nkT}{q}\ln\left[AA^*T^2\exp\left(-\frac{q\phi_b}{kT}\right)\right] + IR_s \tag{2.38}$$

$$V = \frac{nkT}{q}\left[\ln\frac{I}{AA^{*}T^{2}}\right] + n\phi_b + IR_s \quad (2.39)$$

$$V - \frac{nkT}{q}\left[\ln\frac{I}{AA^{*}T^{2}}\right] = n\phi_b + IR_s \quad (2.40)$$

Now by considering,

$$H(I) = V - \frac{nkT}{q}\left[\ln\frac{I}{AA^{*}T^{2}}\right] \quad (2.41)$$

$$H(I) = n\phi_b + IR_s \quad (2.42)$$

By putting the value of n extracted from Eqn. 2.33 [44-45] we can extract the value of R_s. The plot of this equation gives a straight-line where the slope gives the value of R_s and the intercept at the Y axis gives the value of barrier height (ϕ_b). So according to this Cheung Cheung method we can determine the value of R_s in two ways and can show the consistency of two methods with each other.

2.12 Light I-V characteristics

The study of light I-V characteristics is very essential to measure various photovoltaic parameters and efficiency of the organic photovoltaic devices. Fig. 2.14 shows a typical current voltage characteristic under steady state light condition. Fig. 2.14 illustrates the typical power curve of a photovoltaic device.

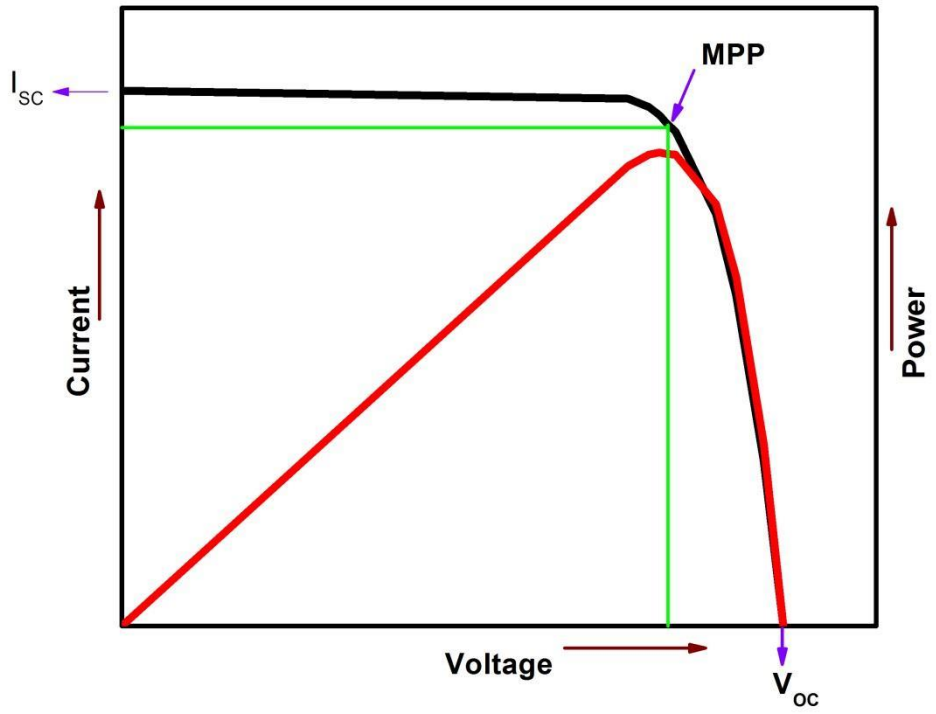

Fig. 2.14 I-V and Power curve of organic photovoltaic devices

We can study or extract various photovoltaic parameters from this light I-V curve. Such as, Open circuit voltage (V_{OC}) which is the maximum voltage across the cell when the cell is not connected to any load and current will be at its minimum value (zero). When the cell is short circuited the voltage across the cell will be minimum (zero) and the value of the current will be at its maximum value, which defined as the short circuit current (I_{SC}). At open circuit the voltage will be maximum. The maximum power of the must be point somewhere in between, shown in the Fig. 2.15. It has shown that the power will be maximum in one particular combination of current and voltage. This is called maximum power point. The power conversion efficiency of the cell is given by [46],

$$\mathrm{PCE} = \frac{P_{out}}{P_{in}} \tag{2.43}$$

Where P_{out} is the electrical power generated at the output and P_{in} is the incident optical power into the device.

To measure the quality of a photovoltaic device one of the important parameters is Fill Factor (FF) which also can be determined from Fig. 2.14. Fill Factor is the ratio of the maximum power obtained to the theoretical power of the device.

$$FF = \frac{V_{mp} \times I_{mp}}{V_{oc} \times I_{sc}} \tag{2.44}$$

For analyzing the performance of the photovoltaic cell there are various models. One of the widely used models is the single diode model shown in the Fig.2.15.

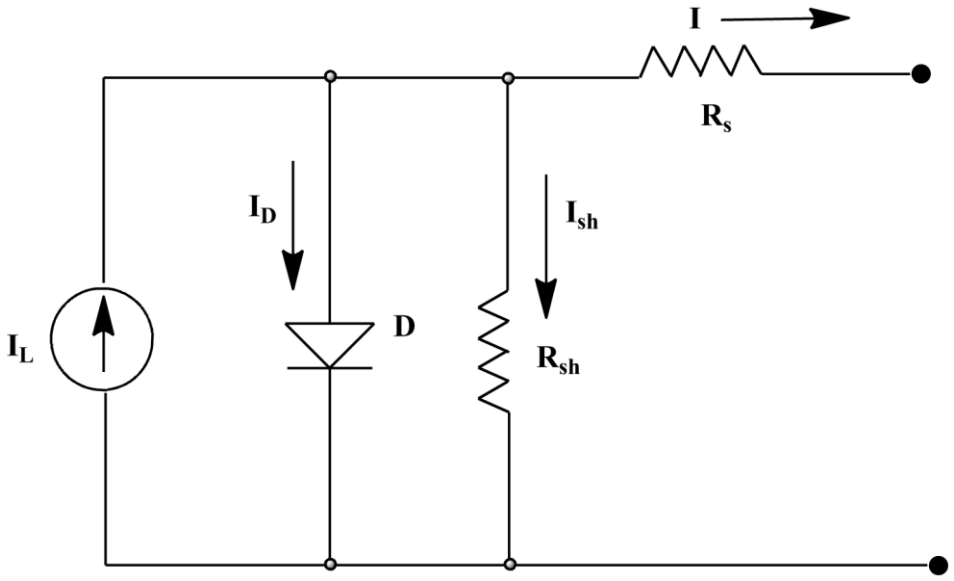

Fig. 2.15 Single diode model equivalent circuit

The current voltage equation is expressed by Shockley equation,

$$I = I_L - I_0 \left[\exp\left\{ \frac{q(V+IR_s)}{nkT} - 1 \right\} - \frac{V+IR_s}{R_{sh}} \right] \tag{2.45}$$

Where I_L is the photocurrent, k is the Boltzmann constant, I_0 is the saturation current of the diode, T is the temperature, R_s is the series resistance, R_{sh} is the shunt resistance, q is the electronic charge, and n is the ideality factor [47].

2.13 Different methods to determine series resistance (R_s) from light I-V characteristics

As discussed earlier, R_s creates a huge impact on the efficiency and the performance of the photovoltaic devices. The R_s composite of the R_s due to electrodes, various contacts and

interconnect resistance and also R_s due to active layer and interfacial resistances. To measure the R_s from the light I-V characteristics there are also various methods such as,

2.13.1 The two characteristics method

In this method two I-V characteristics are raised under two different illumination at the same temperature [48], shown in Fig. 2.16 below.

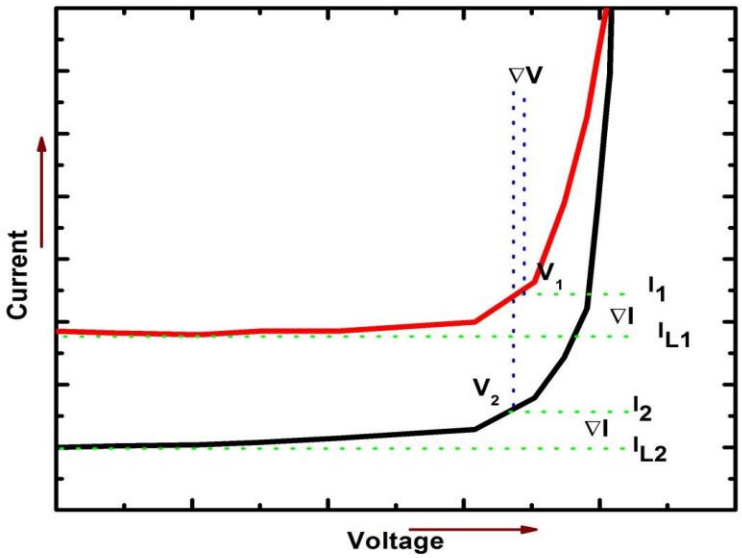

Fig. 2.16 Two I-V curves from the same solar cell at various light intensities

According to this method by considering infinite R_{sh} we can write Eqn.2.45 as,

$$I = I_L - I_0 \left[\exp\left\{\frac{q(V+IR_S)}{nkT} - 1\right\}\right] \tag{2.46}$$

Solving the equation for two different illuminations and taking the logarithms, expressed as,

$$ln\left(\frac{I_{L1}-I_1}{I_{L2}-I_2}\right) = \left(\frac{q(V_1+I_1R_S)}{nkT} - 1\right) - \left(\frac{q(V_2+I_2R_S)}{nkT} - 1\right) \tag{2.47}$$

Where I_{L1} and I_{L2} are the photo generated current under two different illumination intensity. I_{L1}-I_1 is the current difference ΔI as indicated in the Fig. 2.17. Now for these two different illumination intensity by selecting same ΔI we can null the left side of the equation. So from this the equation for R_s will be expressed as,

$$R_s = \frac{V_2 - V_1}{I_1 - I_2} \tag{2.48}$$

2.13.2 Area Method

The R_s of organic photovoltaic devices also be measured by computing the area under the illumination I-V curve [49-50]. In this area method by considering infinite R_{sh} the current voltage equation can be expressed as,

$$I = I_L - I_0 \left[\exp\left(\frac{V + IR_s}{\frac{nkT}{q}} \right) - 1 \right]$$

Where I_L is the photo current, I_0 is the reverse saturation current, R_s is the series resistance and n is ideality factor. Now we can solve this equation accordingly,

$$I = I_L - I_0 \left[\exp\left(\frac{V + IR_s}{\frac{nkT}{q}} \right) - 1 \right]$$

$$I - I_L - I_0 = -I_0 \exp\left(\frac{V + IR_s}{\frac{nkT}{q}} \right)$$

$$\ln\left(\frac{I_L + I_0 - I}{I_0} \right) = \frac{V + IR_s}{\frac{nkT}{q}}$$

$$V = \frac{nkT}{q} \ln\left(\frac{I_L + I_0 - I}{I_0} \right) - IR_s \tag{2.49}$$

The total area under the curve is,

$$A = \int_0^{I_{sc}} V(I)\, dI \tag{2.50}$$

$$= \int_0^{I_{sc}} \left[\frac{nkT}{q} \ln\left(\frac{I_L + I_0 - I}{I_0} \right) - IR_s \right] dI$$

$$= \frac{nkT}{q} \left[\ln\left(\frac{I_L + I_0 - I}{I_0} \right) \int_0^{I_{sc}} dI - \int_0^{I_{sc}} \frac{d}{dI} \left(\ln\left(\frac{I_L + I_0 - I}{I_0} \right) \int dI \right) \right] - \int_0^{I_{sc}} R_s I dI$$

$$= \frac{nkT}{q} \left[I_{sc} \ln\left(\frac{I_L + I_0 - I_{sc}}{I_0} \right) + (I_L + I_0) \ln\left(\frac{I_L + I_0}{I_L + I_0 - I_{sc}} \right) - I_{sc} \right] - \frac{R_s {I_{sc}}^2}{2} \tag{2.51}$$

Here I_{sc} is the short circuit current.

Now it is well known that $I_0 << I_L$ and also $R_s I_{sc}$ is very much smaller than $\frac{nkT}{q}$, so we can write that,

$$I_{sc} = I_L + I_0 \tag{2.52}$$

And also,

$$V_{oc} = \frac{nkT}{q} \ln \frac{I_{sc}}{I_0} \tag{2.53}$$

So the area under the curve will be,

$$A = \frac{nkT}{q}\left[I_{sc} \ln\left(\frac{I_L + I_0 - I_{sc}}{I_0}\right) + I_{sc} \ln\left(\frac{I_L + I_0}{I_L + I_0 - I_{sc}}\right) - I_{sc}\right] - \frac{R_S {I_{sc}}^2}{2} \tag{2.54}$$

$$A = \frac{nkT}{q}\left[I_{sc} \ln\left(\frac{I_L + I_0 - I_{sc}}{I_0} \times \frac{I_L + I_0}{I_L + I_0 - I_{sc}}\right) - I_{sc}\right] - \frac{R_S {I_{sc}}^2}{2}$$

$$A = \frac{nkT}{q}\left[I_{sc} \ln\left(\frac{I_L + I_0}{I_0}\right) - I_{sc}\right] - \frac{R_S {I_{sc}}^2}{2}$$

By putting,

$$A = \frac{nkT}{q} I_{sc} \ln \frac{I_{sc}}{I_0} - \frac{nkT}{q} I_{sc} - \frac{R_S {I_{sc}}^2}{2}$$

$$A = V_{oc} I_{sc} - \frac{nkT}{q} I_{sc} - \frac{R_S {I_{sc}}^2}{2} \tag{2.55}$$

So the equation of R_s under light I-V is,

$$R_s = 2\left[\frac{V_{oc}}{I_{sc}} - \frac{A}{{I_{sc}}^2} - \frac{nkT}{q}\frac{1}{I_{sc}}\right] \tag{2.56}$$

2.13.3 Maximum power point method

According to this method when the OPV device is under illumination it produces power. This approach makes the assumption that there is just one diode and keeps the solar cell under a single level of illumination. When the product of voltage and current reaches its maximum value, maximum power point may be found [51]. The series resistance may be calculated using this equation by taking infinite R_{sh} into account.

$$R_s = \frac{V_m}{I_m} - \frac{1}{B(I_L - I_m)} \tag{2.57}$$

Where,

$$B = \frac{\left[\frac{I_m}{(I_L - I_m)} + \frac{\ln(I_L - I_m)}{I_L}\right]}{2V_m - V_{oc}} \quad (2.58)$$

Where, $I_L \approx I_{sc}$

Where V_m is the voltage at the maximum power point, I_m is the current at maximum power point and V_{oc} is the open circuit voltage.

2.14 Carbon Nano tubes (CNTs) in organic device

In order to enhance the performance various kinds of guest materials are incorporated into the organic devices. As mentioned earlier the presence of traps engenders difficulties on the charge injection and transport process. Generally the trap energy in organic devices is very high, which is one of the main reasons for the high value of R_s in organic devices. In literature we have found that, the E_c is reduced by incorporation of CNTs. Incorporation of CNTs for its various characteristics reduces the trapping effect and enhances the charge transport process. So it can be said that by reducing the E_c we can also decrease the value of R_s.

The unique properties of CNTs such as high thermal and electrical conductivity, high tensile strength, high aspect ratio etc. attract the researchers to study on these materials and also investigate how these materials can be used to improve the device performance. By incorporating CNTs the charge injection process can be improved by lowering barrier height at the metal organic interface. These CNTs provide effective percolation pathways for conducting charge carriers. Apart from that CNTs are one of the deserving materials to generate photo carriers by absorbing sunlight [52-54]. Also the separation of carriers can be performed by CNTs for their formation of heterojunctions with conducting polymers.

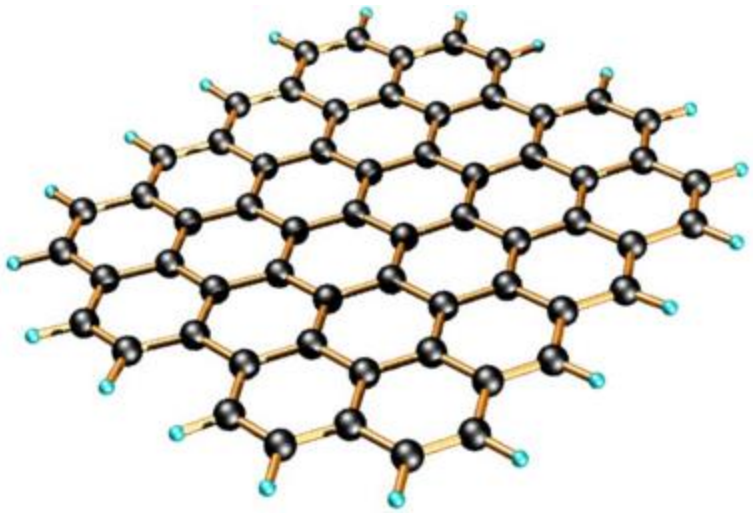

Fig.2.17 A typical structure of a Graphene sheet

Graphite and Diamond are consisting of carbon atoms where Diamond exhibits sp^3 hybridization and Graphite exhibits sp^2 hybridization [55]. In Graphite, the carbons atoms form a layered structure with a hexagonal arrangement of atoms. In 1985 Korto and co workers discovered fullerence (C_{60}), a new form of carbon. Then in the year 1991, Prof. Sumo Iijima discovered Carbon Nanotubes by an arc discharge method [56]. CNTs are one of the allotropes of carbon. CNTs are made of Graphite with tubular shape and having a nano sized diameter and micro sized length. By different types of arrangement of atoms in the cylindrical structure we can produce various types of CNTs such as SWCNTs and Muliti walled CNTs which are described below.

2.14.1 Single Walled Carbon nanotubes (SWCNTs)

SWCNT can be considered as a cylindrical shaped graphite carbon allotrope. The nanotubes are considered nearly one dimension because of their length to diameter ratio which are about 1000. Mostly SWCNTs have a diameter close to 13 nm and the length is nearly about multiple thousand times [57]. The structure of SWCNTs is shown in the Fig. 2.18.

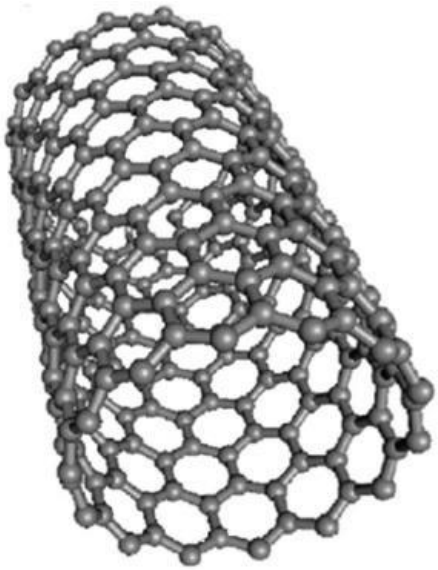

Fig.2.18 A typical structure of a SWCNT

The characteristics of SWCNTs can be either metallic or semiconducting, depending on how the graphene sheet is oriented. There is an overlap of π orbitals in each of the six member rings of a perfectly aligned SWCNT. The electrons can move in a delocalized region because to this overlap. When the six membered rings' alignment is disturbed, the π orbital overlap changes, and the conductivity can turn semiconducting. At high temperature, the electrical conductivity of SWCNT can be described by using semi classical models used with graphite, while at low temperature they reveal 2D quantum transport features [58-59].

2.14.2 Multi walled Carbon Nanotubes (MWCNTs)

MWCNTs, which Sumio Iijima discovered in 1991, are useful as nanomaterials. The study and its production are quite high because to its superior electrical and mechanical qualities. MWCNTs are made structurally up of many layers of graphite that have been rolled into a tube shape and then stacked on top of one another. MWCNTs may have lengths of the order of cm and have outer diameters in the range of 3 to 30 nm. The length to diameter ratio of MWCNTs is very high. Fig. 2.19 shows the structure of MWCNTs.

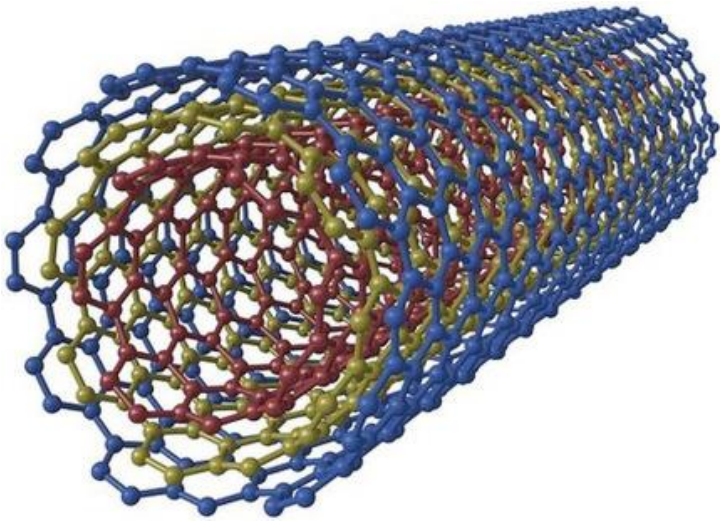

Fig. 2.19 Structure of Multiwall carbon nanotube

Because of its perfect covalent C-C bonding and unique tubular structure, MWCNTs exhibit excellent physical and chemical properties such as very good electrical and thermal conductivity, ultra high mechanical strength, high aspect ratio, large surface area, desirable environment stability, distinct optical characteristics etc. A composite of MWCNT and doped polyaniline (PANI) in its emeraldine salt was synthesized by in situ polymerization. The conductivity increases by 50–70% compared with pristine PANI. The enhancement was attributed to the presence of carboxylic acid groups on the walls of the MWCNT, which improves dispersion [60]. To determine the best MWCNT loading in the polymer matrix for efficient conductivity, a composite of PANI and MWCNT was synthesized by oxidative in situ polymerization.

2.15 Nanoparticles in organic devices

The exploration of nanoscience and nanotechnology deals with the fabrication of functional materials and devices by using various novel properties of nanomaterials. There are different preparation methods to synthesize varieties of nanostructures such as nanoparticles, nano tubes, nanowires, Nano rods etc.. The nanostructured materials exhibits two unique properties which are high surface to volume ratio and quantum confinement effect and because of these properties the characteristics get modified which include structural, electrical, optical, chemical and magnetic properties [61]. These unique properties of nanoparticles open opportunities to

fabricate devices in presence of nanoparticles in terms of improvement of the device performance.

2.15.1 Titanium Dioxide (TiO_2) Nanoparticles

Wide band gap semiconductor titanium dioxide (TiO_2) is well-known for its exceptional physical and chemical characteristics. Essentially, it can exist in four different crystalline forms: anatase, rutile, brookite, and TiO_2. In this case, rutile is the most stable phase, while anatase, brookite, and TiO_2 are metastable phases that frequently change to rutile when heated. These forms each have particular applications. Among the oxide semiconductors, TiO_2 has received considerable interest due to its unique qualities such as nontoxicity, durability against photo and chemical corrosion, strong oxidizing and reducing capacity, biocompatibility, cheap cost, good optical transmittance, photocatalyst, hydrophilicity etc.[62-63].Additionally, TiO_2 demonstrates several potential uses such as, water purification, environmental cleansing, self-cleaning, antifogging, cancer therapy, drug administration, optoelectronic devices, hydrogen generation and storage, gas sensors, dye sensitized solar cell (DSSC) and spintronic devices. The one-dimensional (1D) TiO_2 nanostructures, such as nanotubes (NTs), nano rods (NRs), nanoribbons (NRbs), and nanowires (NWs), contain a significant amount of surface area and an unique 1D shape that offers an efficient channel for electron transport with improved carrier collection. As a result, 1D TiO_2 nanostructures have drawn a lot of interest for a number of exciting and high-performance applications. Metal oxide semiconductors play a significant role in many fields of chemistry, physics, and materials science due to their suitability for a wide range of applications, including photocatalysts, sensors, waste-water and environmental cleaning, drug delivery, hydrogen production, UV photodetectors, dye sensitized solar cells, etc. [64-68]. Generally bulk TiO_2 is not very efficient for the industrial applications because of the smaller surface area and interacting media, as the above described qualities are ideal for the functioning at surface and interface or atomic level. With the size reduction in the case of nanostructured TiO_2, the ratio of surface to volume increases, resulting in a greater contact area, a reduction in surface free energy, and a variety of physical features that are considerably more evident in comparison to those of macroscopic systems.

2.15.2 Zinc Oxide (ZnO) Nanoparticles

ZnO is a II–VI compound semiconductor with a direct wide band gap (3.37 eV at room temperature), large exciton binding energy (60 meV) and excellent optoelectronic properties [69]. ZnO crystallizes in the hexagonal wurtzite structure with lattice constants, a = 3.25 Å and *c* = 5.12 Å. ZnO is an inherently n-type semiconductor but p-type conductivity can also be induced in it by appropriate doping [70]. ZnO exhibits high photoconductivity and considerable piezoelectric response [71]. The coexistence of magnetic, electric, and optical properties increases the scope for TM-doped ZnO to be a multifunctional material. Moreover ZnO is one of the potential candidates in optoelectronic applications. So, due to these unique properties of ZnO nanoparticles are used in various applications such as solar cell, bio sensor, photo detectors, gas sensors etc.

2.16 Effect of Carbon nanotubes and Nanoparticles

Carbon nanotubes (CNTs) and nanoparticles have a significant impact on organic devices due to their unique physical and chemical properties. CNTs and nanoparticles possess high electrical conductivity, enabling them to serve as conductive pathways in organic devices. Moreover the trap charges and the distribution of the traps may be significantly changed by the addition of nanoparticles or CNTs. The charge conduction mechanism is enhanced by the presence of these guest materials. In fact, the nano composites that are created when CNTs or nanoparticles are mixed with a polymer matrix can exhibit electrical characteristics that are different from those of the parent materials. This depends on whether the percolation threshold is exceeded or not by the loading or weight percentage of these guest materials. As the concentration reaches or exceeds the percolation threshold, conductivity rises rapidly. The barrier potential and threshold voltage both decrease as a result of the integration of nanoparticles or CNTs. As a result, enhanced current is produced by improved electrical conductivity, which raises the device's total efficiency. Apart from that incorporation of CNTs and nanoparticles into organic materials can improve their mechanical strength and flexibility. This property is particularly useful for developing robust and flexible devices. Several methods to add or incorporate nanoparticles or CNTs into dye-based devices are described in the literature [72-74]. Overall the use of CNTs and nanoparticles in organic devices offers a wide range of benefits, including improved electrical conductivity, optical properties, mechanical performance etc. These advancements contribute to

the development of next generation organic electronics with enhanced functionality and performance.

2.17 Conclusion

The semiconducting properties of organic semiconductors have opened up a wide field for researchers. Inspite of many advantages, devices made from these organic materials exhibit poor performance, which demands for further investigation to advance this area. Therefore, it is essential to understand the physics underlying the semiconducting characteristics of organic materials. We have provided an outline of the key ideas of organic semiconductor physics in this chapter. We have discussed how the metal-organic interface forms and how charge carriers are injected through the interface. The origin of traps has also been discussed. Trap charges have a crucial role in determining the electrical and optical behaviors as well as the device performances. The charge transport mechanism will be affected by traps in organic semiconductors, and the overall performance of the device will also change when trap energy varies. In this chapter we have discussed about the origin of R_s of organic devices. The R_s can be measured from the I-V characteristics by using different models. We have discussed various methods about how to extract the device R_s from the dark and light I-V characteristics. From literature it has been found that the value of R_s is very high. We have also discussed the role of various nanoparticles and CNTs which can be incorporated within the device as guest materials to improve the conductivity and reducing the value of R_s. In organic devices addition of these guest materials may upgrade the device performance by lowering the device R_s.

2.18 References

1. D. T. Daniel, S. F. Benjamin, et. al, Single walled carbon nanotubes network electrodes for dye solar cells, Solar Energy Materials & Solar Cells, (2010), 94 : 1665-1672
2. M. M. Stylianakis, E. Kymakis, Efficiency enhancement of organic photovoltaics by addition of carbon nanotubes into both active and hole transport layer, (2012), 100 : 093301
3. H. Shirakawa, The discovery of polyacetylene film: The dawning of an era of conducting polymers, Current Applied Physics, (20098q01) 1(1): 3-10
4. A. J. Heeger, Noble Lecture: Semiconducting and metallic polymers: The fourth generation of polymeric materials, Reviews of Modern Physics, (2001), 78 (3) : 681

5. H. Shirakawa, E. J. Louis, et al, Synthesis of electrically conducting organic polymers: halogen derivatives of polyacetylene $(CH)_X$, Journal of the Chemical Society, Chemical Communications, (1977), 16 : 578-580
6. S. Çalış, An Examination of the Achievement Levels of Acquisitions in Hybridization: High School Sample, Universal Journal of Educational Research, (2018), 6(8): 1659-1666
7. S. E. Yoon, J. Park, J. E. Kwon, S. Y. Lee, J. M. Han, C. Y. Go, etc., Improvement of Electrical Conductivity in Conjugated Polymers through Cascade Doping with Small-Molecular Dopants. Advanced Materials. (2020), 32 (49): 200512910
8. S. Wang , G. Zuo, J. Kim, H. Sirringhaus, Progress of conjugated polymers as emerging thermoelectric materials, Progress in polymer science, (2022), 129: 101548
9. M. Jaiswal, R. Menon, Polymer electronic materials: a review of charge transport, Polymer International, (2006), 55 (12): 1371-1384
10. J. L. Brédas, S. R. Marder, and J. M. André, An Introduction to the Electronic Structure of π -Conjugated Molecules and Polymers, and to the Concept of Electronic Bands, The WSPC Reference on Organic Electronics: Organic Semiconductors, (2016): 1-18
11. M. C. Scharber, N. S. Sariciftci, Low Band Gap Conjugated Semiconducting Polymers, Advanced materials technologies, (2021), 6 (4):2000857
12. S. Ahmad, Organic semiconductors for device applications: current trends and future prospects, Journal of Polymer Engineering, (2014), 34: 279-338
13. M. Eslamian, Inorganic and Organic Solution- Processed Thin Film Device Nano – Micro Letters, (2017), 9 (3): 1-23
14. Y. Shen, K. Li, N. Majumdar, J. C. Cambell and M. C. Gupta, Bulk and contact resistance in P3HT: PCBM heterojunction solar cells, Solar Energy Materials & Solar Cells, (2011), 95 (8): 2314-2317
15. O. Güllü and A. Türüt, Electronic parameters of MIS Schottky diodes with DNA biopolymer interlayer, Materials Science-Poland, (2015), 33 (3): 593-600
16. Z. Ahmad and M. H. Sayyad, Electrical characteristics of a high rectification ratio organic Schottky diode based on methyl red, Optoelectronics and Advanced Materials Rapid Communications, (2009), 3: 509-512
17. M. Shah, M. H. Sayyad and S. Kh. Karimov, Electrical characterization of the organic semiconductor Ag/CuPc/Au Schottky diode, Journal of Semiconductors, (2011), 32: 044001

18. J. A. Carr, S. Chaudhary, On the identification of deeper defect levels in organic photovoltaic devices, J.Appl.Phys., (2013), 114: 064509
19. R. Häusermann, K. Willa, B. Blülle, T. Morf, J. Lee and T. Mathis et al. Device performance and density of trap states of organic and inorganic field-effect transistors, Organic Electronics, (2016), 28: 306-313
20. K. Chakraborty, S. Chakraborty, N. B. Manik, Effect of single walled carbon nanotubes on series resistance of Rose Bengal and Methyl Red dye based organic photovoltaic device, Journal of Semiconductors, (2018), 39(9) : 0940011-0940017
21. N. Sergeeva, Investigation of Trap States in Organic Semiconductors for Organic Solar Cells Applications, Technische Universit at Dresden, (2022)
22. S. Cowan, N. Banerji, W. L. Leong, Charge formation, recombination, and sweep-out dynamics in organic solar cells, Advanced Functional Materials, (2012), 22 (6) : 1116-1128
23. H. F. Haneef , A. M. Zeidell and O. D. Jurchescu, Charge carrier traps in organic semiconductors: A review on the underlying physics and impact on electronic devices, Journal of Materials Chemistry C, (2020), 8(3): 759-787
24. S. A. Moiz, I. A. Khan, W. A. Younis, K. S. Karimov, Space Charge–Limited Current Model for Polymers Provisional chapter Space Charge–Limited Current Model for Polymers, (2016), ISBN: 978-953-51-2691
25. V. Coropceanu, et. al, Charge transport in organic semiconductors, Chemical Reviews, (2007), 107(4) : 926-952
26. M. Quintena, T. Edvinsson, A. Hagfeldt, G. Boschloo, Comparison of dye-sensitized ZnO and TiO_2 solar cells: studies on charge transport and carrier lifetime, Journal of Physical Chemistry, (2007), 111 : 1035-1041
27. F. Ana, N. U. Hakim, An analytical modeling approach to the electrical behavior of the bottom-contact organic thin-film transistors in presence of the trap states. Journal of Computational Electronics, (2019), 18(9): 543-552
28. A. Gusain, R. M. Faria, P. B. Miranda, Polymer Solar Cells—Interfacial Processes Related to Performance Issues. Frontiers in Chemistry, (2019), 7
29. S.M. Sze, K. K. Ng, Physics of Semiconductor Devices, Online ISBN:9780470068328, (2007)

30. B. K. Sarker and S. I. Khondaker, Thermionic Emission and Tunneling at Carbon Nanotube–Organic Semiconductor Interface, (2012), 6 (6): 4993-4999
31. A. Sherehiy, Thermionic emission properties of novel carbon nanostructures, The University of Louisville's Institutional Repository, (2014)
32. W. Shockley , The Theory of p-n Junctions in Semiconductors and p-n Junction Transistors, The Bell System Technical Journal, (1949), 28 (3): 435–489
33. A. E. Rakhshani, Heterojunction properties of electrodeposited CdTe/CdS solar cells, J.Appl. Phys., (2001), 90: 4265-4271
34. M. Yildirim, Determination of Contact Parameters of Au/n-Ge Schottky Barrier Diode with Rubrene Interlayer, J. Polytech., (2017), 20: 165-173
35. S. Sen, N. B. Manik, Effect of Back Electrode on Trap Energy and Interfacial Barrier Height of Crystal Violet (CV) Dye based Organic Device, Bull. Mater. Sci., (2020), 43: 1-4.
36. A. Rose, Space-Charge-Limited Currents in Solids. ,Physical Review, (1955), 97(6): 1538–1544
37. Y. Li, W. Huang, et. al, Evaluation of methods to extract parameters from current-voltage characteristics of solar cells, Solar Energy, (2013), 90 : 51-57
38. N. C. Giebink, et. al, Ideal diode equation for organic heterojunctions I : Derivation and application, Physical Review B, (2010), 82 (15) : 155305
39. M. R. Islam, S. Maity, et. al, Photocurrent growth and decay behaviour of crystal violet dye-based photoelectrochemical cell in photovoltaic mode, Ionics, (2012), 18 : 209-214
40. S. Chakraborty, N.B. Manik, Effect of single walled carbon nanotubes on the threshold voltage of dye based photovoltaic devices, Physica B, (2016), 481 : 209-216
41. Z Ahmad , M H Sayyad, Electrical characteristics of a high rectification ratio organic Schottky diode based on methyl red, Optoe lectronics and Advanced Materials Rapid Communications, (2009), 3 (5): 509 - 512
42. M Shah, M H Sayyad, S Kh Karimov, Electrical characterization of the organic semiconductor Ag/CuPc/Au Schottky diode, Journal of Semiconductors, (2011), 32 (4): 044001(1-5)
43. S. K. Cheung and N. W. Cheung, Extraction of Schottky diode parameters from forward current-voltage characteristics, Appl. Phys. Letter,(1986), 49: 85-87

44. F. Yakuphnoglu, M. Shah and A. W. Farooq, Electrical and Interfacial Properties of p-Si/P3HT Organic-on-Inorganic Junction Barrier, Acta Physica Polonica A, (2011), 120: 558-562
45. O. Güllü and A. Türüt, Electronic parameters of MIS Schottky diodes with DNA biopolymer interlayer, Materials Science-Poland, (2015), 33: 593-600
46. G. Tadeson and R. G. Sabat, Enhancement of the Power Conversion Efficiency of Organic Solar Cells by Surface Patterning of Azobenzene Thin Films, ACS Omega, (2019), 4 (26): 21862-21872
47. N. Thongprong and P. M. Duxbury, Voltage dependence of equivalent circuit parameters of bilayer organic photovoltaics, Journal of Applied Physics, (2021),129: 083104(1-14)
48. J. M. Wagner, S. Rißland, A. Schuett, J. Carstensen, R. Adelung, Distributed series resistance in a one-dimensional two-diode model revisited, Energy Procedia, (2017), 124: 197-206
49. D. T. Cotfas, P. A. Cotfas, D. Ursutiu and C. Samoila, The methods to determine the series resistance and the ideality factor of diode for solar cells-review, 13th International Conference on Optimization of Electrical and Electronic Equipment (OPTIM), Brasov, Romania, (2012): 966-972, doi: 10.1109/OPTIM.2012.6231814
50. D. Pysch, A. Mette, S.W. Glunz, A review and comparison of different methods to determine the series resistance of solar cells, Solar Energy Materials and Solar Cells, (2007), 91 (18): 1698-1706
51. H. A. Koffi, A. A. Yankson, A. F. Hughes, K. Ampomah-Benefo and J. K. A. Amuzu, Determination of the series resistance of a solar cell through its maximum power point, African Journal of Science, Technology, Innovation and Development, (2020), 12(6): 1-4
52. D. T. Daniel, et.al, Single walled carbon nanotube network electrodes for dye solar cells, Solar Energy Materials & Solar Cells, (2010), 94 : 1665-1672
53. A Aqel, et. al, Carbon nanotubes, science and technology part (I) structure, synthesis and characterization, Arabian Journal of Chemistry, (2012), 5 : 1-23
54. J. A. Andres, W.J. Blau, Enhanced device performance using different carbon nanotubes types in polymer photovoltaic devices, Carbon, (2008), 46 : 2067-2075
55. R. Aversa, R. V. Petrescu, F. I. Tiberiu Petrescu, A. Apicella, Nanodiamond for Structural Biomimetic Scaffolds, Journal of Materials Science and Chemical Engineering, (2018), 06(04): 6-17

56. T. Belin, F. Epron, Characterization methods of carbon nanotubes: a review, Materials Science and Engineering B, (2005), 119 : 105-118
57. N. Saifuddin, A. Z. Raziah, A. R. Junizah, Carbon Nanotubes: A Review on Structure and Their Interaction with Proteins", Journal of Chemistry, (2013), 2013 Article ID 676815. https://doi.org/10.1155/2013/676815
58. P. McEuen, M. S. Fuhrer, H. Parket, Single-walled carbon nanotubes electronics, IEEE Transactions on Nanotechnology, (2002), 1(1) : 78-85
59. M. S. Dresselhaus, G. Dresselhaus, R Saito, Physics of carbon nanotubes, Carbon, (1995), 33(7) : 883-891
60. C. Li, Fullerene-multiwalled carbon nanotubes complexes for bulk heterojunctions photovoltaic cells, Applied Physics Letters, (2010), 96 : 143303
61. I. Khan, K. Saeed and I. Khan, Nanoparticles: Properties, applications and toxicities, Arabian Journal of Chemistry, (2019),12(7): 908-931
62. R. Li, T. Li and Q. Zhou, Impact of Titanium Dioxide (TiO2) Modification on Its Application to Pollution Treatment—A Review, Catalysts (2020), 10(7): 804
63. S. Sagadevan, etc., Investigation on Optical, Dielectric and Invitro Anti-Inflammatory Responses of Titanium Dioxide (TiO2) Nanoparticles. Digest Journal of Nanomaterials and Biostructures. (2018), 13(3): 641 - 652
64. B. Pal and P. K. Giri, High temperature ferromagnetism and optical properties of Co doped ZnO nanoparticles, Journal of Applied Physics, (2010), 108 (8): 084322
65. J.-G. Li, R. Büchel, M. Isobe, T. Mori and T. Ishigaki, Cobalt-Doped TiO_2 Nanocrystallites: Radio-Frequency Thermal Plasma Processing, Phase Structure, and Magnetic Properties, The Journal of Physical Chemistry C, (2009), 113 (19): 8009-8015
66. X. F. Yao, T. J. Zhou, Y. X. Gai, T. C. Chong and J. P. Wang, Binding state and microstructure analyses of Co-doped TiO_2 thin film, Journal of Applied Physics, (2004), 95: 7375-7377
67. Y. B. Lin, Y. M. Yang, B. Zhuang, S. L. Huang, L. P. Wu, Z. G. Huang, F. M. Zhang and Y. W. Du, Ferromagnetism of Co-doped TiO_2 films prepared by plasma enhanced chemical vapour deposition (PECVD) method, Journal of Physics D: Applied Physics, (2008), 41: 195007

68. B. Santara, B. Pal and P. K. Giri, Signature of strong ferromagnetism and optical properties of Co doped TiO_2 nanoparticles, Journal of Applied Physics, (2011), 110: 114322
69. C. F. Klingshirn, ZnO: Material, Physics and Applications. Chemphyschem : a European journal of chemical physics and physical chemistry, (2007), 8(6): 782-803
70. L. Liu, J. Xu, etc., p-Type conductivity in N-doped ZnO: the role of the N(Zn)-V(O) complex. Physical Review Letters, (2012), 108(21): 215501
71. S. K. Mishra, Rajneesh Srivastava and Subramanian Prakash, ZnO nanoparticles: Structural, optical and photoconductivity characteristics. Journal of Alloys and Compounds, (2012), 539: 1-6
72. E. Kymakis, G.A.J Amaratunga, Single-wall carbon nanotube/ conjugated polymer photovoltaic devices, Applied Physics Letters, (2002), 80 : 112
73. E. Kymakis, et. al, Spin coated carbon nanotubes as hole transport layer in organic photovoltaics, Solar Energy Materials & Solar Cells, (2012), 96 : 298-301
74. E. Kymakis, et. al, Post-fabrication annealing effects in polymer- nanotube photovoltaic cells, Journal of Physics D: Applied Physics, (2006), 39 : 1058-1062

Chapter 3

Effect of dye concentration on Series resistance (R_s) of Thionin dye based electrochemical cell (PEC)

3.1 Introduction

In the previous chapters, we have discussed the basics of organic semiconductors and devices prepared by this material. We have discussed the formation of interfaces between metal and organic semiconductor, the charge transport theories and also the advantages, limitations of the devices. We have also discussed and compared the main proposition of the various existing charge transport models. There are various parameters which affect the device performance. One of the important parameters is the high value of series resistance of organic devices. We have discussed various methods to determine the value of R_s. One of the main reasons for the high value of R_s is the presence of traps in organic devices. To extract the trap energy we have selected SCLC model with exponential distribution of traps for our present work. These parameters are very much crucial to understand the charge transport mechanism and the nature of traps. In this chapter, we have prepared a cell based on Thionin dye. After preparation of device, the dark current – voltage (I-V) characteristics of these cells at different dye concentration have been studied. The data has been fitted with Cheung Cheung method which is modification of Thermionic emission process by including series resistance and from these fitting series resistance (R_s) and ideality factor (n) have been estimated [7].

3.2 Selection of the dye

3.2.1 Materials used

Thionin is a strongly metachromic cationic histology dye. The chemical formula of Thionin dye is $C_{12}H_9N_3S$-$C_2H_4O_2$. It is very useful for the staining of acid mucopolysaccharides. It is also a common nuclear stain and can be used for the demonstration of Nissl substance in nerve cells of the CNS. The plant peptide family of Thionin normally consists of 45-48 amino acids of which 6-8 are cysteine [8]. These create three to four disulfide bridges that stabilise an L-shape with two small antiparallel beta strands acting as the short axis and two long antiparallel alpha helices acting as the long axis. As an inert binder, poly vinyl alcohol (PVA) from S.D. Fine Chem. Ltd., Boisar, India, and polyethylene oxide (PEO) from BDH, England, UK, were utilized in this study. We purchased (99.5%) pure $LiClO_4$, EC, and PC from Fluka. We have employed Aluminum (Al) as the back electrode and indium tin oxide (ITO) coated glass as the front electrode. Fig. 3.1 shows the dye's structural layout.

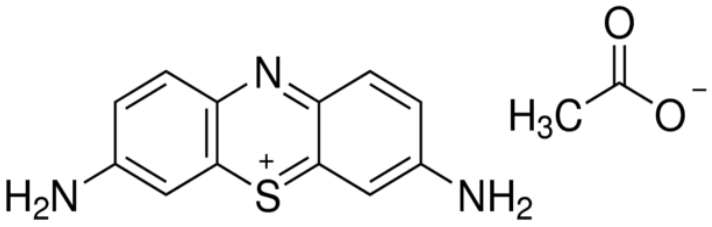

Fig.3.1 Structure of Thionin dye

3.3 Experimental details

3.3.1 Sample and cell preparation

In a cleaned test tube 5 mg of Polyvinyl Alcohol (PVA) was mixed with 30 ml of distilled water, warmed gently and stirred to make a transparent viscous solution of PVA [9-10]. Then This PVA solution was separately kept in four pre-cleaned test tubes. Then at different concentration of 2 mg, 4 mg, 6 mg and 8 mg Thionin dye were mixed in these four solutions. A solid electrolyte was prepared in another cleaned beaker by mixing Polyethylene Oxide (PEO), Lithium per Chlorate ($LiClO_4$), and Ethylene Carbonate (EC) Propylene Carbonate (PC). The mixture of PEO-$LiClO_4$ – EC – PC was mixed in the percentage weight ratio of 30.60%–3.60%–19.60%–46.20% by weight. Fig.3.2 shows different chemicals in our laboratory.

Fig.3.2 Chemicals in our laboratory

Then this electrolyte was heated at around 60°C and stirred well in a magnetic stirrer for about 5 hours. Then the electrolyte was mixed with the previously prepared four solutions of different dye concentration to form the ionic blends. These blends were then heated and stirred properly to mix them well. To prepare the cells, these viscous gel solutions of different concentration of Thionin dye were spin coated separately on four pre-cleaned ITO coated glass at a speed of 2500 rpm and the films were semi-dried in vacuum. The same blends were dropped on a spin coater and the four separate Al electrodes which was placed on the spin coater. When the electrodes are in semi-dry state, according to the dye concentration they are sandwiched together to form the Thionin dye based electrochemical cells at different concentration. Fig.3.3 (a) shows the spin coater and Fig. 3.3 (b) weighing machine which have been used in our experiment.

(a) Spin Coater

(b) Weighing Machine

Fig.3.3 (a) Spin Coater and (b) Weighing Machine

In the cell these two plates act as the two contact electrodes. Two electrical leads are then taken out of the two ends of the electrodes. All the cells have an area of 1.5cm^2. The cells were kept in vacuum for 12 hours before characterization. To make the system cost effective we have used all the components including the Thionin dye and the electrodes in commercial grade and also the measurements are carried out in the open atmosphere of the laboratory. Fig. 3.4 (a) shows the schematic diagram of a typical electrochemical cell and Fig. 3.4 (b) shows the image of a cell prepared in our laboratory.

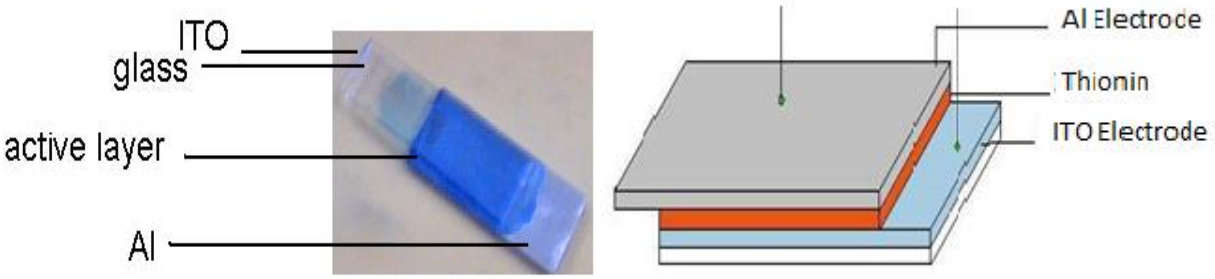

(a) **(b)**

Fig. 3.4 (a) Structure of the prepared cell, (b) Schematic diagram of the prepared ITO/Thionin/Al cell

3.3.2 Measurement

Using a Keithley 2400 source measure device, dark current-voltage (I-V) properties of the cells were measured. Fig. 3.5 shows the Keithley 2400 source measure unit. With a 1500 ms delay, the bias voltage is changed from 0 to 6 volts in 0.5 volt increments during the measurement. At a temperature of 22°C, the experiments were conducted in the laboratory's clean open environment.

Fig. 3.5 Keithley 2400 source measure unit

3.4 Results and discussion

In Fig.3.6, the dark I-V characteristics of the electrochemical cell based on Thionin dye for various concentrations are shown. With reference to any inorganic device, it can be seen from this figure that the current is extremely low.

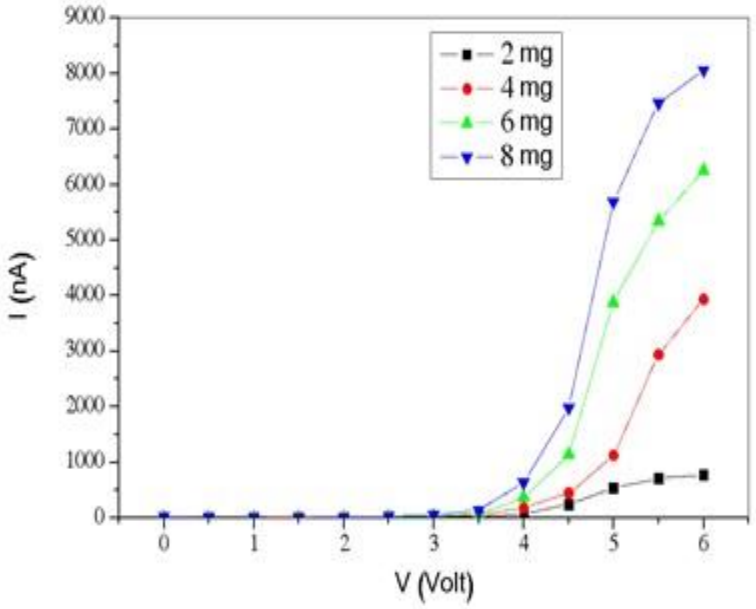

Fig. 3.6 Forward dark I-V characteristics

Current-voltage (I-V) measurements were made. The forward bias I-V properties of a diode contact for qV>3kT may be explained as, in accordance with the thermionic emission (TE) theory [11].

$$I = I_0 \left[\exp\left(\frac{qV}{nkT}\right) - 1\right] \tag{3.1}$$

Where I_0 is the reverse saturation current can be described as,

$$I_0 = AA^* T^2 \exp\left(-\frac{q\phi_b}{kT}\right) \tag{3.2}$$

Here A is contact area, A^* is the Richardson constant, T is the absolute temperature and ϕ_b is barrier height.

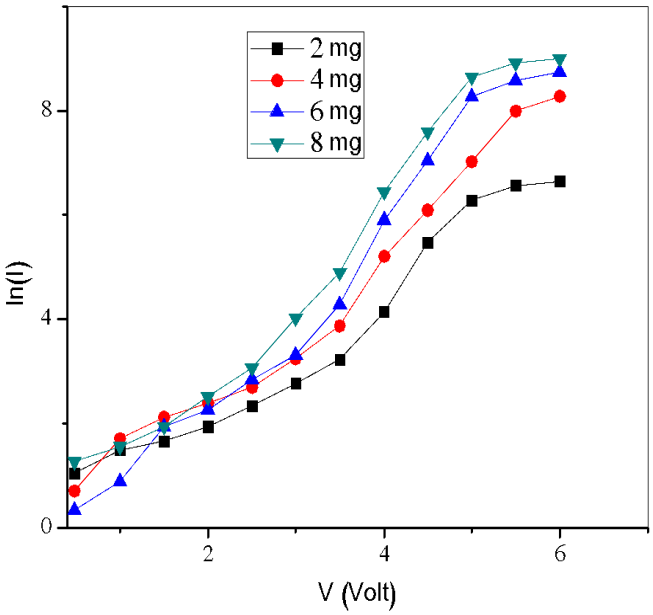

Fig. 3.7 lnI Vs. V characteristics of ITO/Thionin\Al system for different dye concentration

The ideality factor can be determined from the slope of the curve in the lnI Vs. V plot. The logarithmic values of the current versus voltage characteristics of the cells at various dye concentrations are shown in Fig.3.7. Using Eqn. 3.3, the ideality factor n was calculated from the slope of the I-V characteristic.

$$n = \frac{q}{kT}\frac{dV}{d\ln I} \tag{3.3}$$

As is well known, the quality to which the diode reflects pure thermionic emission depends on the ideality factor (n). In our ITO/Thionin/Al system, n has a relatively high value. Numerous reasons [12–13] could be responsible for the larger value of n. The extracted values of n are shown in the Table 3.1 below for various dye concentrations.

Table 3.1 Extracted values of ideality factor (n) of Thionin dye based organic devices at different dye concentration

System	Dye concentration (mg)	Extracted values of n
ITO/ Thionin/ Al	2.0	13.07
	4.0	11.96
	6.0	9.90
	8.0	9.20

These devices basically consist of an active layer made of various organic/polymer materials placed between two electrodes. The electrical characteristics, which depend on the junction behaviours, which depend on the active layer and electrode materials, are the primary determinants of how a device will operate. The operation of the devices is altered by the use of various electrodes with various work functions. In addition, organic materials lack a regular lattice structure and are disordered amorphous solids. The quantity of current is therefore very low because of structural variations and other restrictions. Additionally, it has been shown that any organic diode's dark I-V characteristics deviate from linearity on logarithmic scale due to the influence of R_s [14–15].The interface and the trapping of charge carriers at the bulk as well as at the barrier potential at the interface are the key causes of the usual value of R_s in any organic device to be quite high. The Cheung and Cheung approach has been used for determining the R_s[16–17]. The forward bias I-V characteristics caused by thermionic emission (TE) in the presence of series resistance may be represented as, according to Cheung & Cheung.

$$I = I_0 \left[\exp\left(\frac{q(V - IR_s)}{nkT}\right) - 1\right] \tag{3.4}$$

By solving the Cheung Cheung method we can extract the device R_s and n by using the following equations,

$$\frac{dV}{d\ln I} = \frac{nKT}{q} + IR_s \tag{3.5}$$

$$H(I) = n\phi_b + IR_s \tag{3.6}$$

Where,

$$H(I) = V - \left(\frac{nkT}{q}\right)\ln\frac{I}{AA^{*}T^{2}} \qquad (3.7)$$

A plot of dV/d(lnI) Vs. I will be linear and gives R_s as the slope and nkT/q as the y-axis intercept from Eqn. (3.5). Plots of dV/d(lnI) Vs. I and H(I) Vs. I at room temperature have shown in Fig. 3.8(a) to(h).

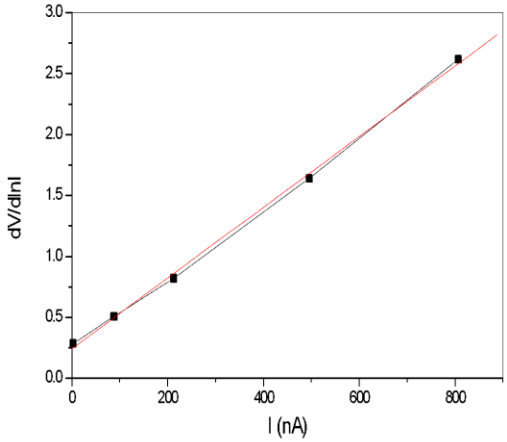

(a)

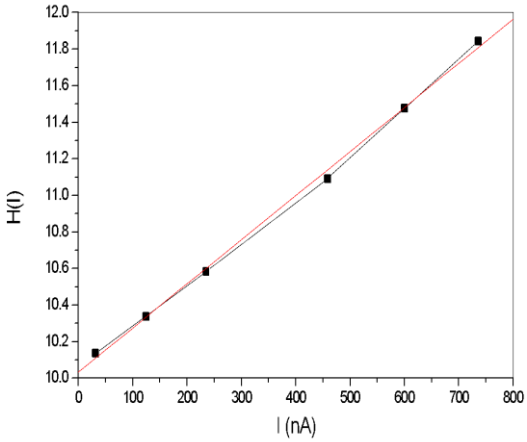

(b)

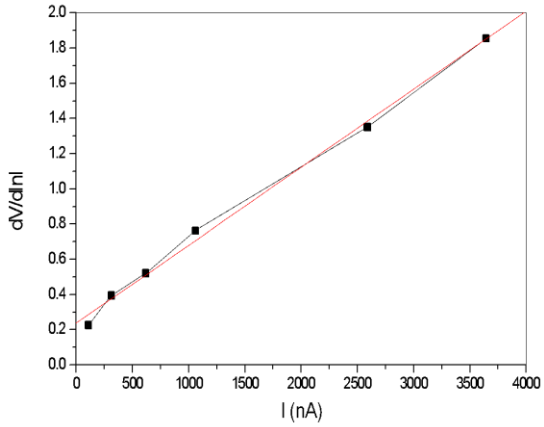

(c)

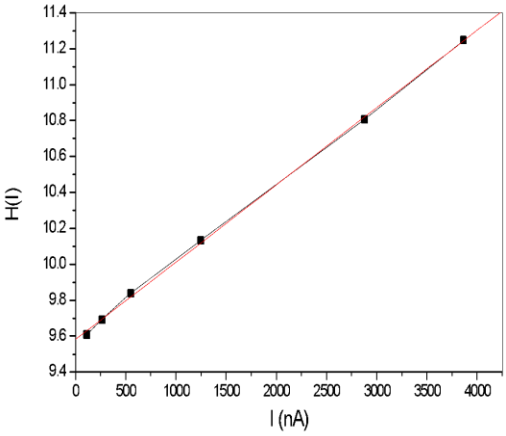

(d)

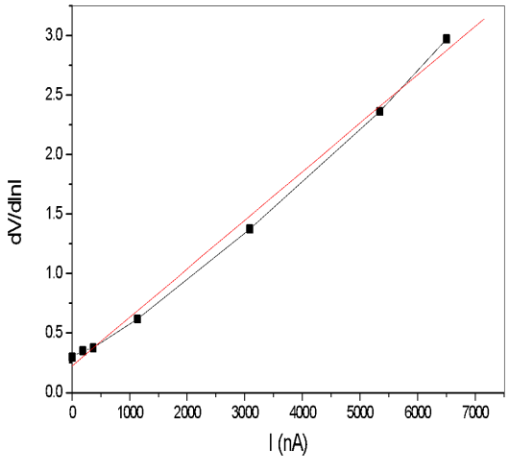

(e)

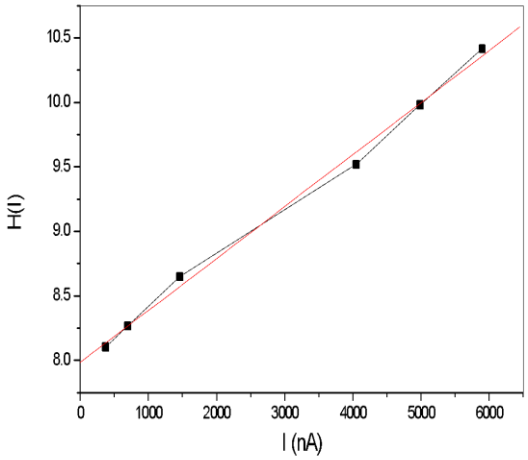

(f)

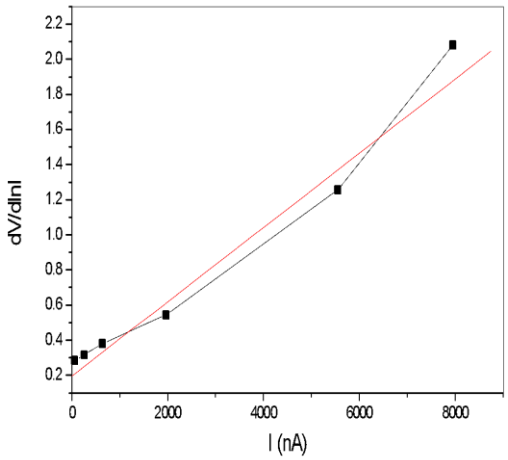

(g)

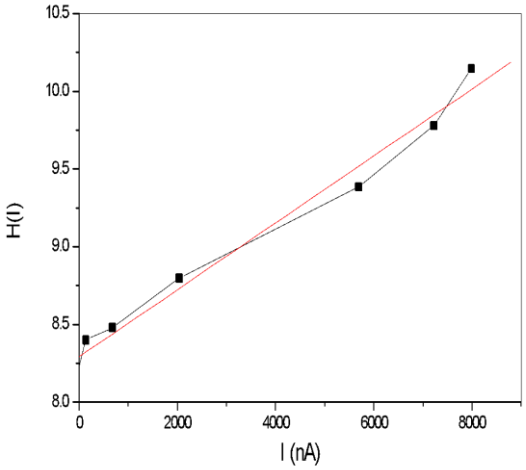

(h)

Fig 3.8 Plots of dV/dlnI Vs. current (I) and H(I) Vs. current (I) for various dye concentrations are shown in (a) and (b) for 2 mg dye concentration, (c) and (d) for 4 mg dye concentration, (e) and (f) for 6 mg dye concentration, and (g) and (h) for 8 mg dye concentration

According to Eqn. 3.5 we have plotted the $\frac{dV}{dlnI}$ Vs. I plot. A straight-line curve will be obtained from the plot with an intercept of $\frac{nKT}{q}$. We have extracted the device $R_s$from the slope of the straight line. We have also measure the R_s from Eqn. 3.6. According to the equation we have plotted H(I) Vs. I curves for different dye concentration shown in Fig. 3.8. The H(I) Vs. I plot

also gives a straight line with intercept of $n\phi_b$ at y axis. The value of R_s measured from H(I) Vs. I and from $\frac{dV}{dlnI}$ Vs. I at different dye concentration show good compatibility with each other. The extracted values of n and R_s by using the Cheung Cheung method are shown in the Table 3.2 below.

Table 3.2 Extracted values of Ideality factor (n) and Series Resistance (R_s) by using Cheung Cheung method

Dye concentration (mg)	Value of n	Value of R_s(MΩ)
2.0	9.3	2.90
4.0	8.9	0.45
6.0	7.9	0.40
8.0	7.2	0.20

So from these results it has been observed that the value of R_s is very high and with increasing dye concentration, the value is reduced. Also it has been observed that the values of n extracted from lnI Vs. V plot and $\frac{dV}{dlnI}$ Vs. I plot are slightly different from each other. This may be attributed due to the existence of R_s, interface states and voltage drop across the interface layer. Since molecules in organic materials are bound together by the weak Van der Waals force and organic semiconductors are disordered in nature, they do not have a well-defined band structure, as was already mentioned. These organic materials introduce traps between HOMO and LUMO due to weak molecular bonding and structural instability, which is how the energy bands are defined in terms of HOMO and LUMO [5]. The ITO/Thionin/Al electrochemical cell's performance is therefore influenced by traps at the device's interface states and bulk area. The applied voltage must be greater than the potential barrier of the contact for carriers to flow. However, due to the disordered structure of organic semiconductors and their high sensitivity to traps, a significant percentage of the charge carriers injected from the electrode become trapped in these trap energy states at the interface. Both the current and the mobility of the charge carriers are significantly decreased as a result of the carriers' incapacity to get away from the electrode. The trapped carriers in the zone between HOMO and LUMO may be released or recombined with the opposing charge carriers at greater voltage, which increases the device's current. Despite this, the device's current is incredibly low due to the organic material's disorder,

the presence of traps, and the recombination of carriers at the metal semiconductor interface. The electrical parameters n and R_s of this organic devices result in having very high values as a result. The charge trapping in the metal organic dye interaction is another anticipated factor contributing to this high value of R_s. As dye concentration rises, more charge carriers are produced, which enhances the efficiency of the device.

3.5 Conclusions

In this chapter, we have examined the I-V characteristics of an organic ITO/Thionin/Al diode. To create the diode the viscous solution of the dye has been sandwiched between two electrodes, namely indium tin oxide (ITO) and aluminum (Al). The dark I-V data has been measured. Both the thermionic emission theory and the Cheung Cheung method, which is essentially a variation of the thermionic emission theory by introducing the impact of series resistance function have been used to fit the data. It has been shown that raising the dye concentration can minimize the R_s, which greatly influence how well a device works. The extracted values of R_s are about 2.9 MΩ, 0.45MΩ 0.40 MΩ and 0.20 MΩ respectively for the dye concentration of 2 mg, 4 mg, 6 mg and 8 mg. Moreover from the Thermionic Emission theory the ideality factor is calculated from the linear portion of the lnI Vs. V plot and by using Cheung-Cheung function n of the device has been estimated from the Y-axis of the dV/d(lnI) Vs. I plot. It is found that in both the cases n is quite high but by considering series resistance effect this value decreases and with reduction of series resistance the ideality factor (n) also been reduced.

3.6 References

1. M. Grätzel, Photoelectrochemical cells, Nature, (2001), 414: 338-344
2. J. Kahovec, R. B. Fox, K. Hatada, Nomenclature of regular single stranded organic polymers, Pure and Applied Chemistry, (2002), 74 (10) : 1921-1956
3. A. Haldar, S. Maity, N..B. Manik, Electrical and photovoltaic characterizations of methyl red dye doped solid-state photoelectrochemical cell, Ionics, (2009), 15 : 79-83
4. M. R. Islam, S. Maity, A. Haldar, N. B. Manik, A N Basu, Photocurrent growth and decay behaviour of crystal violet dye-based photoelectrochemical cell in photovoltaic mode, Ionics, (2012), 18 : 209-214

5. M. R. Islam, S. Saha, N. B. Manik, A. N. Basu, Transient current study in Safranine-T dye based organic photo-electrochemical cell using exponentially distributed trap assisted charge transport model, Indian Journal of Physics, (2012), 86 (12) : 1101-1106
6. S. Maity, A. Haldar, N. B. Manik , Effect of plasticizer on safranine-T-dye-based solid-state photo electrochemical cell, Ionics, (2008), 14 : 549-554
7. M. Benhaliliba, Extracted electronic parameters of a novel Ag/Sno_2: In/Si/Au Schottky diode for Solar cell application, Journal of Nano- and Electronic Physics, (2015), 7: 02029 (1-4)
8. K. Hong, T. Austerlitz, Kh. T. Bohlmann, H. Bohlmann, The thionin family of antimicrobial peptides, PLOS one, (2021), 16: 1-23
9. A. Haldar, S. Maity, N. B. Manik, Effect of back electrode on photovoltaic properties of crystal-violet-dye-doped solid-state thin film, Ionics, (2008), 14 : 427-432
10. M. E. Colclough, H. Desai, R.W. Millar, N.C. Paul, M. J. Stewart, P. Golding, Energetic polymers as binders in composite propellants and explosives, Polymers for Advanced Technologies, 1994, 5 : 54–560
11. E.H. Rhoderick, Metal-Semiconductor Contacts, Oxford University Press, (1978)
12. S. Aydoğan, Ü. İncekara, A. R. Deniz, A. Türüt. Extraction of electronic parameters of Schottky diode based on an organic Indigo tin disulfonate Sodium (IS). Solid State Communications, 2010, 150:1592-1596
13. Z. Ahmad , M. H.Sayyad. Extraction of electronic parameters of Schottky diode based on an organic semiconductor methyl-red.Physica E, 2009, 41:631–634
14. Z. Ahmad , M. H.Sayyad. Electrical characteristics of a high rectification ratio organic Schottky diode based on methyl red. Optoelectronics and Advanced Materials Rapid Communications, (2009), 3: 509 – 512
15. M. Shah, M. H. Sayyad, Kh. S. Karimov, Electrical characterization of the organic semiconductor Ag/CuPc/Au Schottky diode. Journal of Semiconductors, (2011), 32:044001(1-5)
16. S. K. Cheung, N. W. Cheung, Extraction of Schottky diode parameters from forward current-voltage characteristics. Applied Physics Letters, (1986), 49:85-87
17. L. Paoli, P.A. Barnes, Saturation of the junction voltage in stripe-geometry (AlGa)As double -heterostructure junction lasers. Applied Physics Letters, (1976), 28:714-71

Chapter 4

Effect of nanoparticles on Series resistance of Phenosafranine (PSF) and Methyl Red (MR) dye based organic devices

4.1 Introduction

In the previous chapter, we have estimated the series resistance (R_s) and ideality factor (n) of the Thionin dye based electrochemical cell by varying the dye concentration. In this chapter, we have fabricated Phenosafranine (PSF) dye based organic devices in presence of TiO_2 and ZnO nanoparticles and studied R_s. The effects of addition of nanoparticles on the trap energy and R_s have also been studied. We have also fabricated Methyl Red (MR) based organic devices in absence and presence of ZnO nanoparticles and studied the variation of electronic parameters in terms of trap energy.

4.2 Selection of the dye

4.2.1 Materials used

Phenosafranine (PSF): PSF is one among the significant cationic dyes belonging to the phenazinium group of substances. PSF has the chemical formula $C_{18}H_{15}N_4Cl$ and a molecular weight of 322.79 g/mole. It has a planar conjugated rigid structure, and for our project, we bought PSF from Sigma-Aldrich in Germany. It has been employed in several semiconductor applications, as energy sensitizers, in examining micro heterogeneous environments, and in numerous biological photochemical applications [1-2]. Fig. 4.1 depicts the PSF's structure.

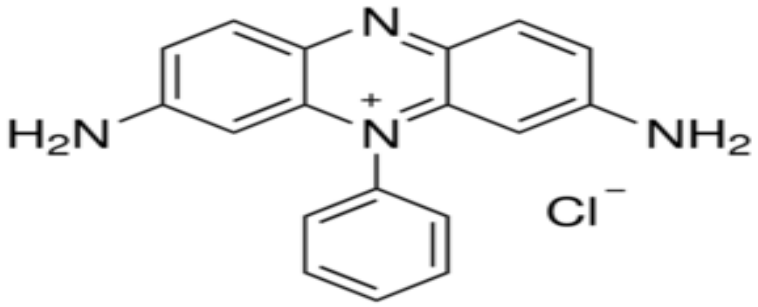

Fig. 4.1 Structure of Phenosafranine (PSF) dye

Methyl Red (MR): The chemical formula for MR dye is $C_{15}H_{15}N_3O_2$ (2-[4-(dimethylamino) phenylazo] benzoic acid) [3]. It is an aromatic azo compound. We purchased MR dye for our job from Finar Chemicals in Ahmedabad, India.MR has a molecular weight of 269.31 g/mol. This

MR dye is water soluble, and the absorption in the visible spectrum is what gives it its colour. In the following Fig. 4.2, the structure of the MR dye is depicted.

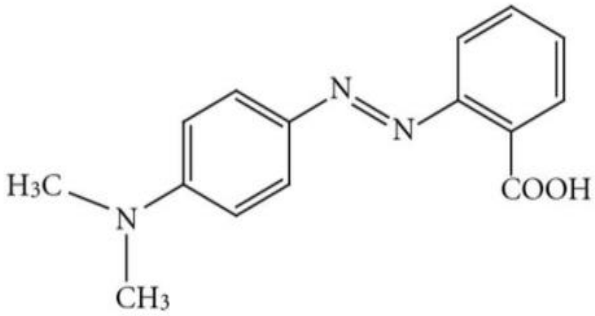

Fig.4.2 Structure of an aromatic azo group-attached Methyl Red (MR) dye

TiO_2 and ZnO nanoparticles have been utilised to explore the impact of nanoparticles. These nanoparticles were brought from Sigma-Aldrich in Germany. Figure 4.3 below depicts the structure of TiO_2 and ZnO. In this study, we explored the impact of nanoparticles on organic devices by including TiO_2 and ZnO particles on PSF dye. In order to investigate the same phenomenon, we also made MR dye-based organic devices both with and without ZnO nanoparticles. Due to its high work function of 4.8 eV, indium tin oxide (ITO) was employed as the front electrode to build the cell, while Aluminum (Al), with a work function of around 4.2 eV, was used as the rear electrode.

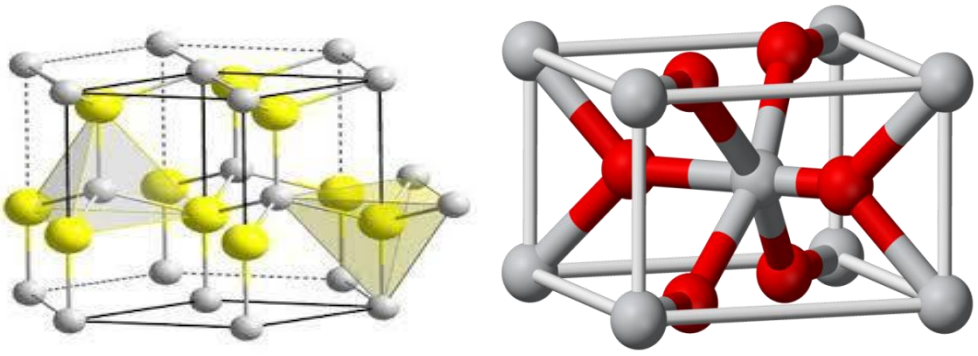

(a) (b)

Fig. 4.3 Structure of (a) ZnO nanoparticle and (b) TiO_2 nanoparticles [4-5]

4.3 Experimental details

4.3.1 Sample and cell preparation

4.3.1 (a) PSF dye based organic devices

5 mg of PVA was added to 30 ml of distilled water in a clean beaker to make the PSF solution. The mixture was then stirred with a magnetic stirrer for 30 minutes at 80˚C to make a clear PVA solution. 2 mg of PSF dye were added to this PVA solution and thoroughly mixed further for ten minutes. Three portions of this solution were placed in three test tubes that had already been cleaned. The first test tube was set aside. To create PSF solutions with TiO_2 and ZnO nanoparticles in the other two test tubes, 2 mg of TiO_2 and 2 mg of ZnO nanoparticles were combined individually. The prepared PSF solution was spin coated at 1,500 revolutions per minute (rpm) onto an ITO coated glass that had already been cleaned, and the film was then dried at 3,500 revolutions per minute (rpm). The same solution was also spin coated on an Al electrode. For the creation of the PSF cell, both of these electrodes were sandwiched together. 12 hours were used for drying the cell under vacuum. Similarly, TiO_2 and ZnO cells were prepared by spin coating PSF solution containing a mixture of nanoparticles of TiO_2 and ZnO. 12 hours were used for keeping the prepared cells under vacuum. After proper drying, these cells have been examined. Scanning electron microscopy (SEM) images were taken for both TiO_2 and ZnO cells in a JEOL field emission scanning electron microscope (JSM-6700F) operating at an accelerating voltage of 5 kV.

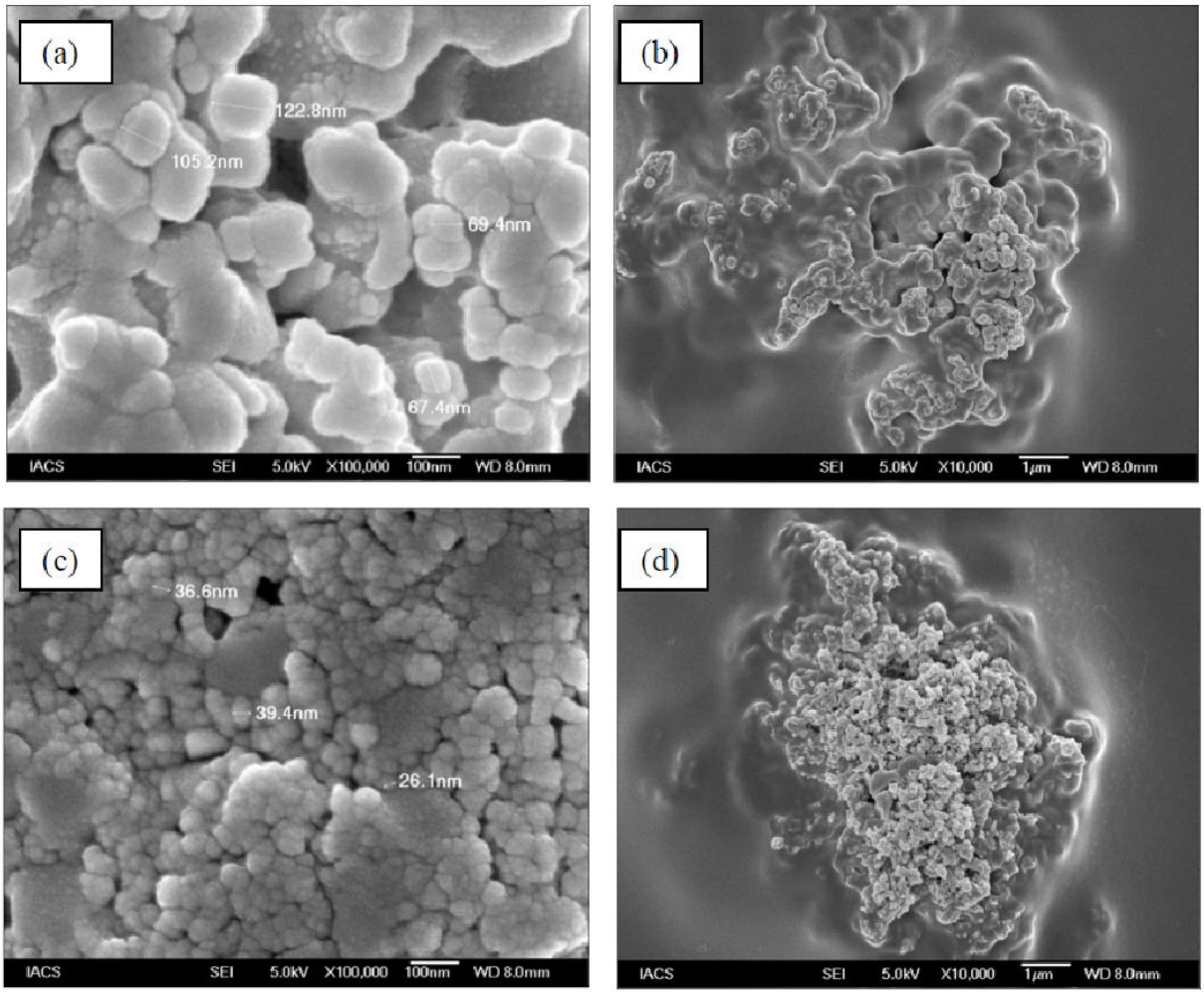

Fig. 4.4 SEM images of the PSF + TiO_2 cell in (a), (b), and the PSF + ZnO cell in (c), (d), respectively, at higher and lower magnifications

The scanning electron microscopy (SEM) pictures for PSF + TiO_2 and PSF + ZnO are obtained with the JEOL's scanning electron microscopy using JMS 6360 model. The PSF + TiO_2 and PSF + ZnO cells in Fig. 4.4 (a) and (c) demonstrate the sizes of the TiO_2 and ZnO nanoparticles. Additionally, it can be shown in Fig. 4.4(b) and (d) that the addition of PVA, which slows the flow of charge particles, causes the nanoparticles to coagulate. Thus, it is best to use the least amount of PVA possible when preparing the cell.

4.3.1 (b) MR dye based organic devices

To prepare the PVA solution at first, we combined 4 mg of PVA with 20 ml of distilled water. We then stirred the mixture for 30 minutes at 80°C with a magnetic stirrer. The PVA was supplied by S. D. Fine Chem. Ltd., Boisar, India; M.W. 125,000. The PVA solution was then thoroughly stirred for a further 30 minutes while 2 mg of MR dye was added. The MR dye solution was then divided in two and maintained in two test tubes that had already been cleaned. In one of the test tubes, 2 mg of ZnO nanopartcles were now individually combined. The other test tube was left just as it was. Thus, we had two test tubes. There was MR solution in one test tube and MR with ZnO nanoparticle solution in the other. The MR dye solution was then spin coated over ITO coated glass at a speed of 1500 rpm, and dried at a speed of 2500 rpm. The same solution was spin coated on Al electrodes in a similar manner and at the same speed. Then, these two electrodes were sandwiched to create MR dye-based organic devices. In a similar manner, the solution of MR with ZnO was spin coated on ITO and Al electrode and developed MR dye based organic device in presence of ZnO nanoparticles. After preparing, the devices were kept under vacuum for 12 h. The schematic diagram of sandwich-type MR dye-based organic device and MR dye in the presence of ZnO nanoparticles have shown in Fig. 4.5.

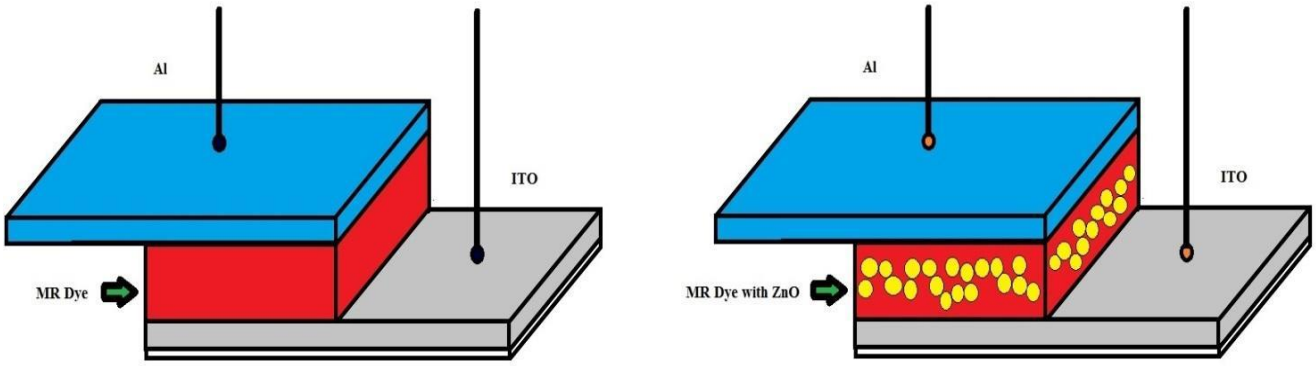

(a) (b)

Fig. 4.5 Diagrams of two different types of organic devices using MR dye (a) devices based on MR dye, and (b) devices using MR dye with ZnO nanoparticles

4.3.2 Measurements

After proper drying, these cells were examined. Keithley's 2400 source measuring unit was used to measure steady state I-V characteristics. ITO electrode is connected to the positive terminal of the bias voltage, while Al electrode is connected to the negative terminal.

The bias voltage was adjusted for the PSF dye-based cells from 0 to 6 Volt in 0.5 V increments with a 500 ms delay. For the MR dye-based cells, the voltage was changed from 0 to 5 V in increments of 0.5 V with a 1000 ms delay. The experiment was carried out at 26°C, which is the average room temperature [6].

4.4 Results and discussion

The dark I-V characteristics of the PSF and the MR dye based organic devices in absence and presences of nanoparticles are shown in the Fig. 4.6 and 4.7 below. From these figures it is observed that the amount of the current gets enhanced with subsuming of the nanoparticles.

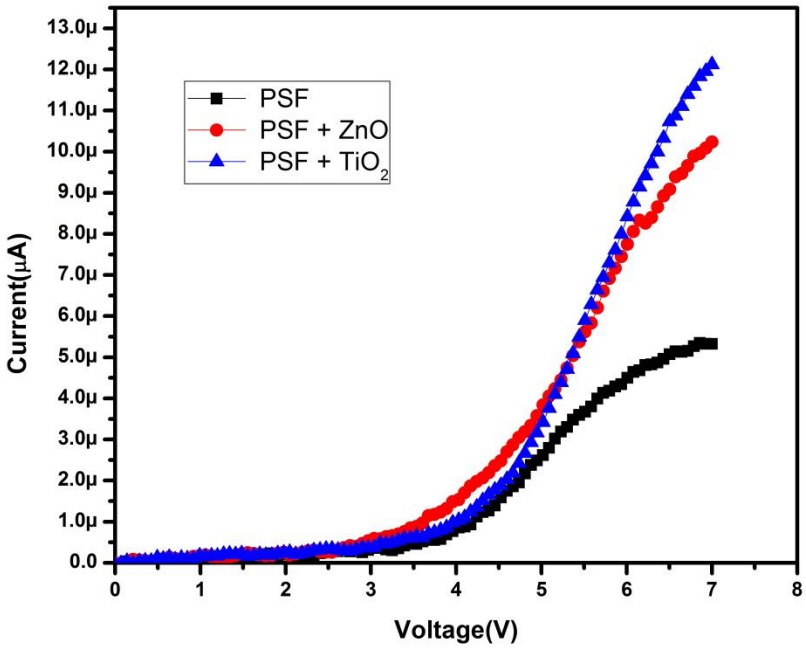

Fig. 4.6 The dark I-V characteristics in forward biased of ITO/PSF/Al, ITO/PSF+TiO_2/Al, ITO/PSF+ZnO/Al

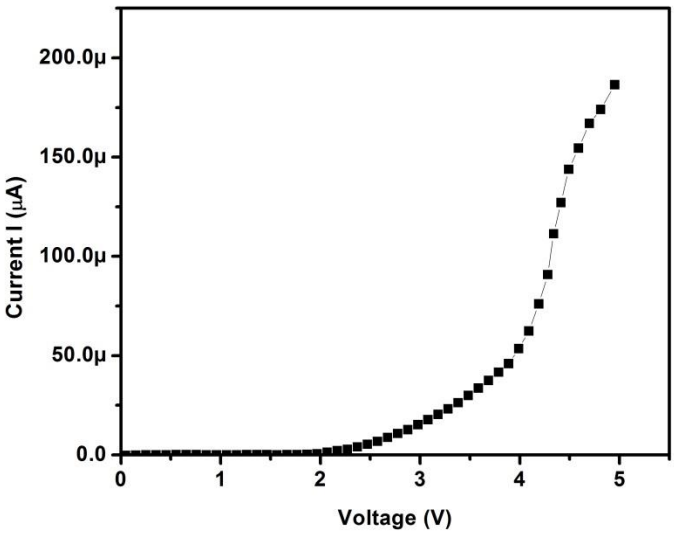

(a)

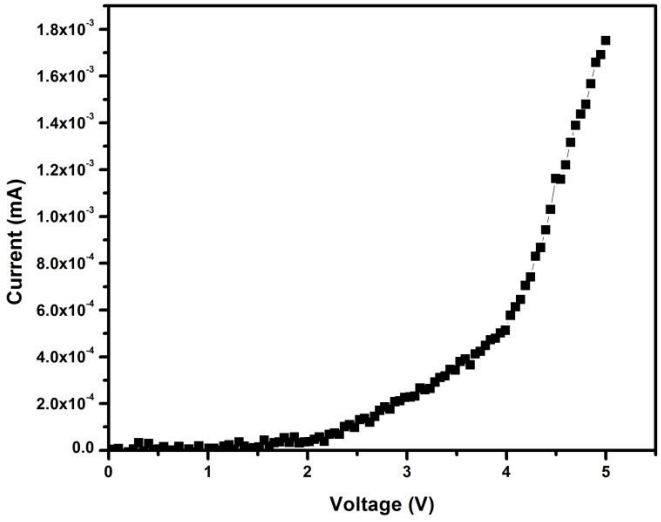

(b)

Fig. 4.7 The dark I-V characteristics in forward biased of (a) ITO/MR/Al and (b) ITO/MR+ZnO/Al

The I-V characteristics exhibit nonlinear behavior and therefore we have analyzed the I-V characteristics by using Shockley equation[7-9],

$$I = I_0 \exp\left(\frac{q(V - IRs)}{nkT}\right) \tag{4.1}$$

Where I_0 is the reverse saturation current which is given by,

$$I_0 = AA^* T^2 \exp\left(-\frac{q\phi_b}{kT}\right) \tag{4.2}$$

Where I_0 is the reverse saturation current, q is the electronic charge, k is the Boltzmann constant, T is the temperature, V is the applied voltage, n is the ideality factor and R_s is the series resistance [10-11].

The slope of the linear section of the lnI Vs. V plot can be utilised to calculate the ideality factor, which indicates how closely a device follows with the diode equation or the Thermionic emission process.

$$n = \frac{q}{kT}\frac{dV}{d\ln I} \tag{4.3}$$

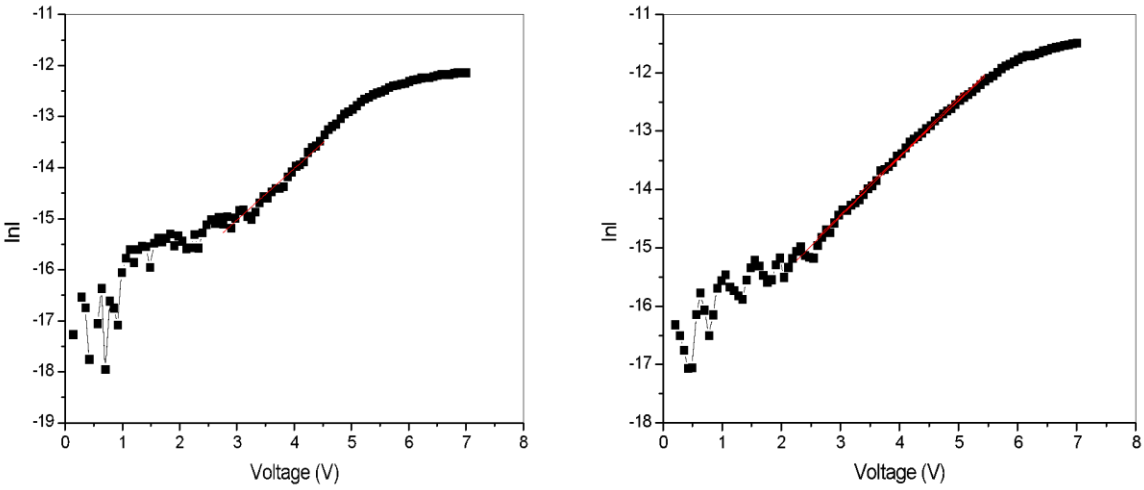

(a) (b)

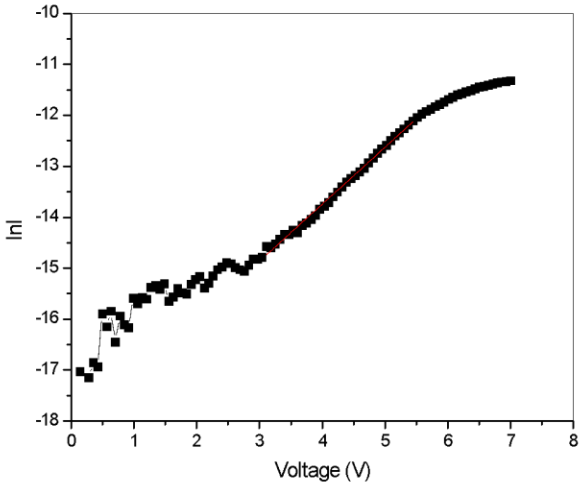

(c)

Fig. 4.8 lnI Vs. V characteristics of ITO/PSF/Al system (a): for Without nanoparticle, (b): for ZnO, (c): for TiO_2 nanoparticle

It is observed from the lnI Vs. V plot that the devices gives a linear region at low voltage and deviates from its linearity and gives a rise of curvature at high voltage as shown in Fig 4.8. The value of n is very high and with incorporation of nanoparticles the value gets reduced.

Table 4.1 Extracted value of n from lnI Vs. V plot of PSF dye based cells without and with TiO_2 and Zno nanoparticles

Organic Dye	Sample	Value of ideality factor (n)
PSF	PSF	38.17
	PSF+ ZnO	37.5
	PSF+TiO_2	34.59

Table 4.2 Extracted value of n from lnI Vs. V plot of MR dye based cells without and with ZnO nanoparticles

Organic Dye	Sample	Value of ideality factor (n)
MR	MR	16.9
	MR+ZnO	13.8

Now according to the Cheung Cheung method [12-13] the value of R_s has been measured from the $\frac{dV}{dlnI}$Vs. I plot by using the below equation,

$$\frac{dV}{dlnI}=\frac{nkT}{q}+IR_s \tag{4.4}$$

As explained earlier in the $\frac{dV}{dlnI}$Vs. I plot the values of series resistance and ideality factor are obtained from the slope and intercept of the graph. The $\frac{dV}{dlnI}$Vs. I plot of the PSF and MR dye based cells in absence and presence of nanoparticles are shown in the Fig 4.9 below.

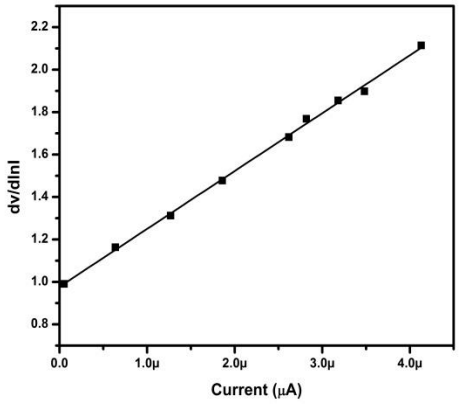

(a)

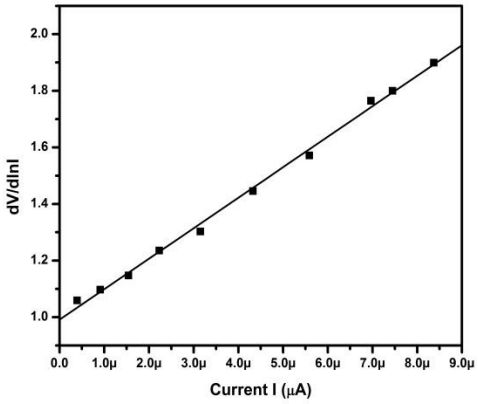

(b)

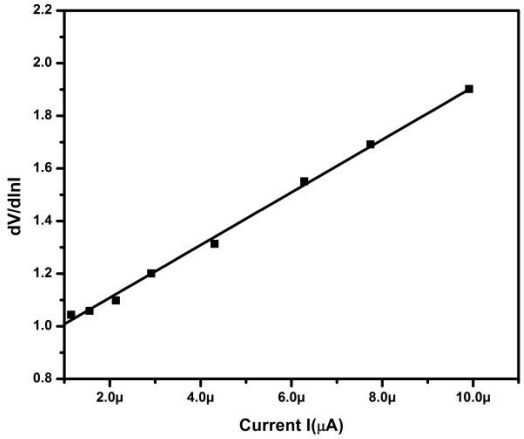

(c)

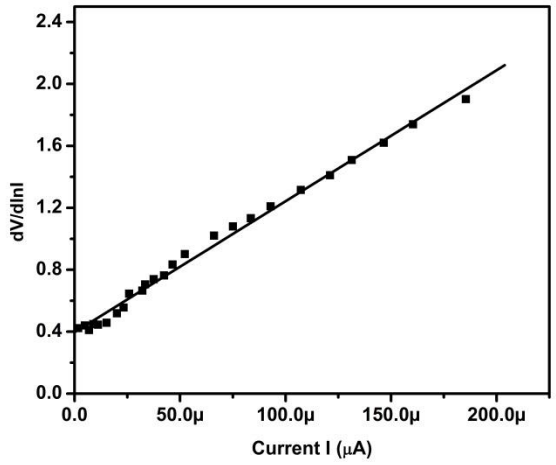

(d)

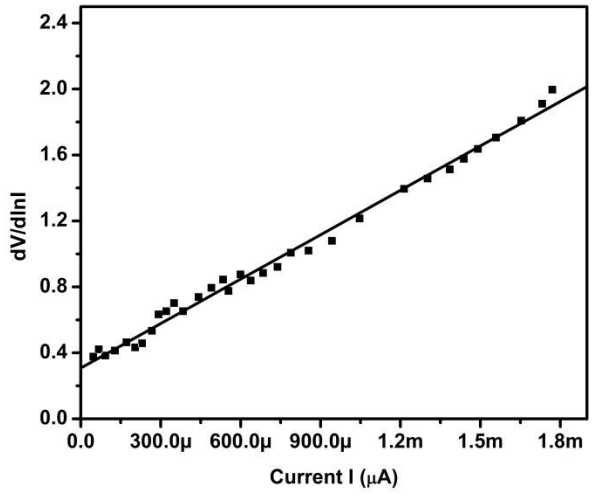

(e)

Fig. 4.9 dV/dlnI Vs. Current (I) of (a) only PSF, (b)PSF with ZnO, (c) PSF with TiO_2 nanoparticles,(d) Only MR and (e) MR with ZnO nanoparticles

We have also measured R_s from the H(I) Vs. I plot by using the below equation,

$$H(I) = n\phi_b + IR_s \qquad (4.5)$$

Where, $H(I) = V - (\frac{nkT}{q})\ln\frac{I}{AA^*T^2}$ (4.6)

The barrier height (ϕ_b)is determined by the intercept of the H(I) vs. I plot, and the slope of the curve gives the value of R_s. In Fig. 4.10 below, the H(I) Vs. I plot of the PSF and MR dye-based cells in the presence and absence of nanoparticles is displayed.

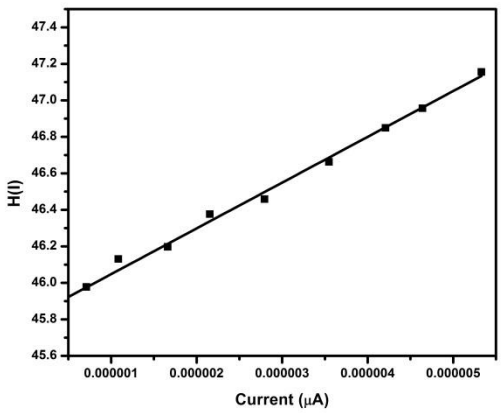

(a)

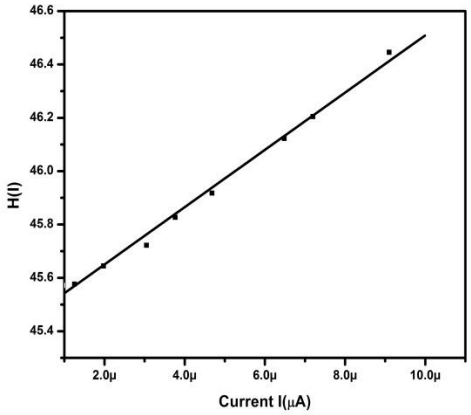

(b)

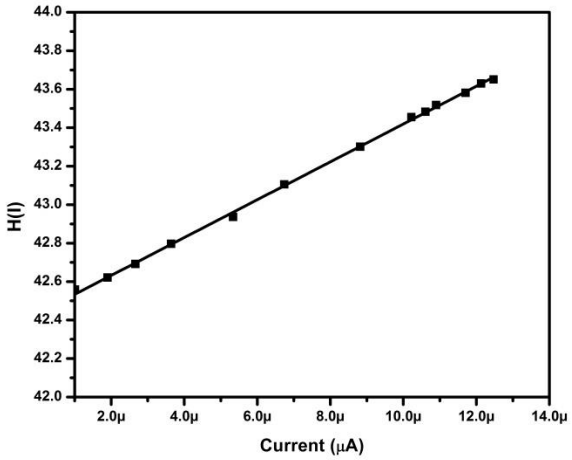

(c)

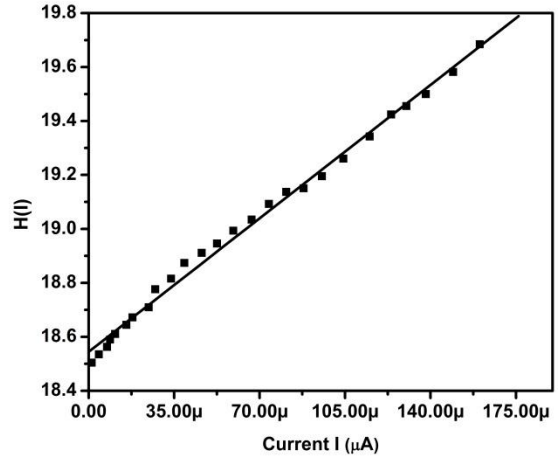

(d)

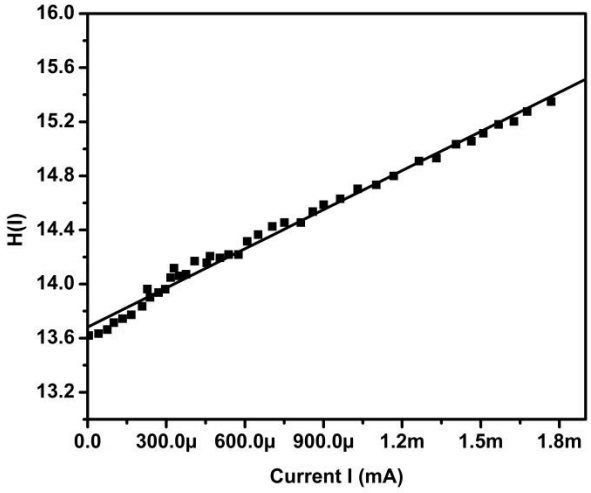

(e)

Fig. 4.10 H (I) Vs. Current (I) plot;of (a) only PSF, (b)PSF with ZnO, (c) PSF with TiO_2 nanoparticles,(d) Only MR and (e) MR with ZnO nanoparticles

Table 4.3 n and R_s of PSF dye based cells without and with TiO_2 and ZnO nanoparticles

Sample	Value of n	R_s from dV/dlnI Vs I plot (KΩ)	$R_s$from H(I) Vs. I plot (KΩ)
PSF	37.47	272.70	250.80
PSF+ ZnO	36.90	112.10	108.30
PSF+TiO_2	34.80	100.10	98.30

Table 4.4 n and R_s of MR dye based cells without and with TiO_2 and ZnO nanoparticles

Sample	Value of n	R_s from dV/dlnI Vs I plot (KΩ)	$R_s$from H(I) Vs. I plot (KΩ)
MR	15	8456	7065
MR+ZnO	11.9	923	964

As a result, it has been found that every organic device has a very high value of R_s, and with addition of nanoparticles this value decreases. In general, there are several causes behind the high value of R_s. One of the key factors is the effect of trap energy on the device.

In any organic device the interface formation in between organic semiconductor and electrode creates a vital role in the device performance [12-13].The schematic diagram of the metal-organic dye interface of the ITO/Organic dye/Al is shown in Fig. 4.11.

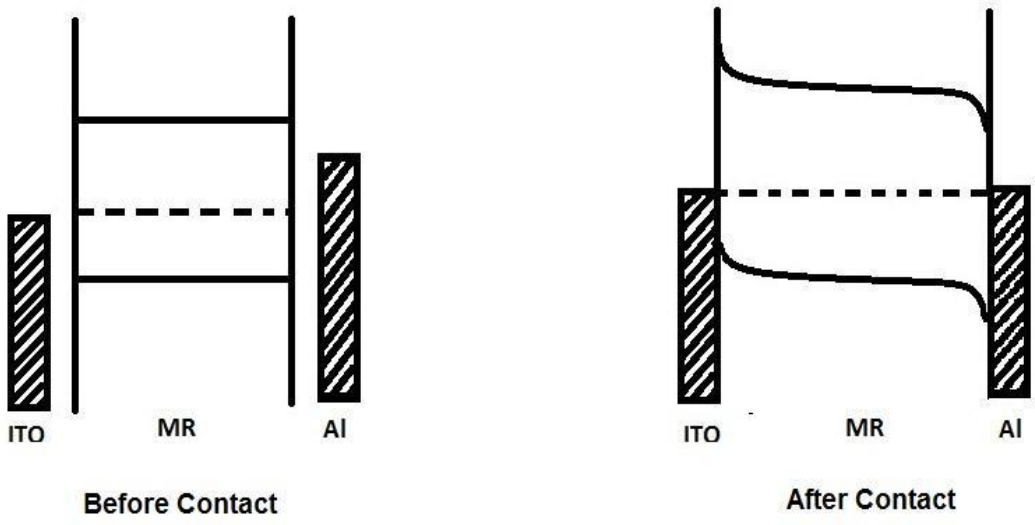

Fig. 4.11 ITO/Organic Dye/Al interface schematic energy band diagram showing Schottky contact between Al and Organic Dye and ohmic contact between ITO and Organic Dye

As shown from Fig. 4.11, Al is employed as a low work function material in this study, while ITO is used as a high work function material. The transfer of free charge carriers causes the interfaces to change when the organic dye is placed between these two electrodes, and this effect continues for until the Fermi level is aligned. Therefore a Schottky barrier is established at the Al/Organic dye interface, and an ohmic contact is created at the ITO/Organic dye interface. A potential barrier is produced close to the rectifying contact as a result of the band bending effect caused by the transfer of free charge carriers. At equilibrium, there is no flow of charge carriers because of this barrier. Now as organic semiconductors are disordered solids, they do not have proper band structure and introduce trap states in the energy region between HOMO and LUMO. In any organic device, these trap states make charge injection and charge transport phenomena challenging [14–15]. For a given distribution, the injected charges are dependent on the trap energy (E_c) and trap charge density. Additionally, localised energy states are introduced at the interface when an organic dye and a metal come into contact, raising the barrier potential of the device. Due to the decreased charge injection and carrier flow caused by the higher barrier potential, organic device R_s is affected. So it can be said that one of the main reasons for organic devices having high R_s is because of the presence of trap charges and high trap energies. Apart from that it can also be affirmed that with reduction of trap energy we can significantly reduce the device R_s. By assuming the trap energy distribution as exponential the trap charge concentration may be expressed as [16]

$$n_t = H_n \exp\left(\frac{F_n}{kT_c}\right) \quad (4.7)$$

Where H_n is the trap density, F_n is the electron Fermi level, k is the Boltzmann constant and T_c is the characteristic temperature of the exponential trap distribution ($T_c = \frac{E_c}{k}$, Where E_c is the characteristic trap energy.

Now solving the Poisson's equation with this exponential trap distribution the current voltage equation can be expressed by the following form,

$$I = AN_c\mu q^{1-m}\left(\frac{m\varepsilon}{H_n\,(m+1)}\right)^m\left(\frac{2m+1}{m+1}\right)^{m+1}\left(\frac{V^{m+1}}{L^{2m+1}}\right) \quad (4.8)$$

Where N_c is the effective density of states, μ is the mobility, ε is the product of the permittivity of the vacuum (ε_0) and the dielectric constant (ε_r), V is the applied voltage, L is the thickness of the active layer and m is the ratio of the characteristic temperature T_c with absolute temperature T.

$$\left(m = \frac{T_c}{T}\right)$$

From equation 4.8, it is clearly seen that the equation follows the power law dependence of,

$I \approx V^{m+1}$

To observe the conduction mechanism we have studied the lnI Vs. lnV plot of the cells. Fig. 4.12 below shows the lnI Vs. lnV plot of the PSF and MR dye based cells in absence and presence of nanoparticles.

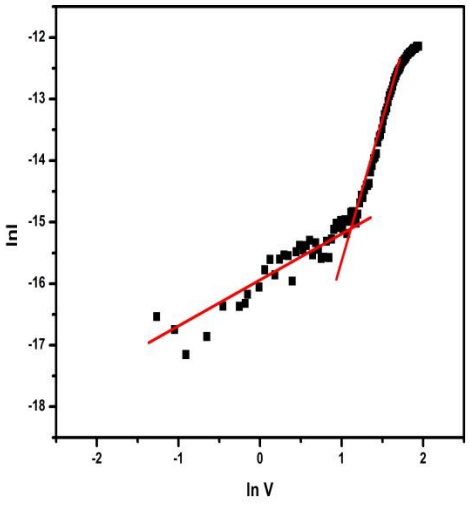
-12
-13
-14
-15
-16
-17
-18
InI
-2
-1
0
1
2
ln V

(a)

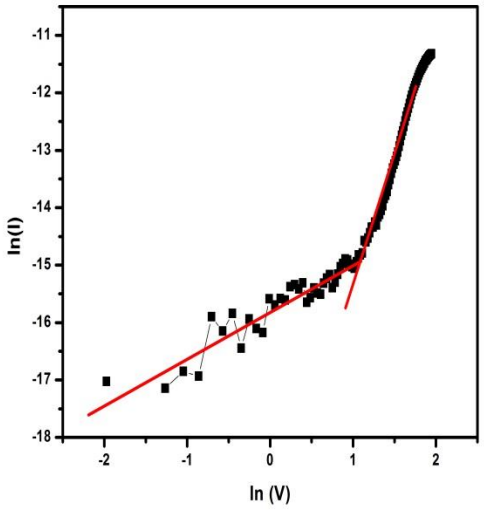
-11
-12
-13
-14
-15
-16
-17
-18
ln(I)
-2
-1
0
1
2
ln (V)

(b)

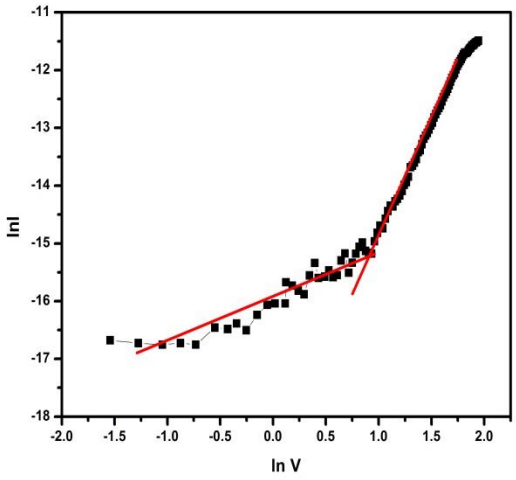
-11
-12
-13
-14
-15
-16
-17
-18
InI
-2.0
-1.5
-1.0
-0.5
0.0
0.5
1.0
1.5
2.0
ln V

(c)

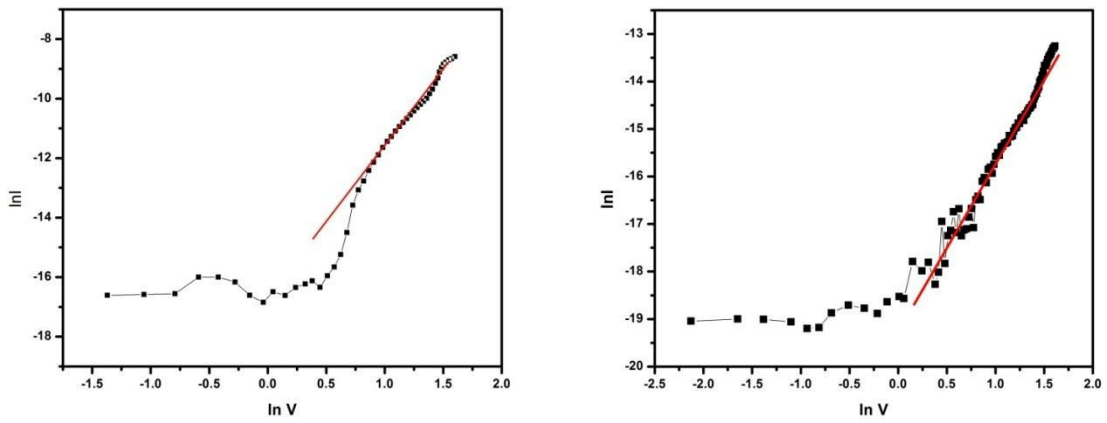

(d) (e)

Fig. 4.12 lnI Vs. lnV plot (a) for only PSF dye based device, (b) for PSF dye with TiO_2, (c) for PSF dye with ZnO nanoparticle, (d) for only MR dye based device and (e) for MR dye with ZnO nanoparticle organic device

As seen in Fig. 4.12, it may be said, the plots are separated into two regions. Below transition voltage is one region. Injection limitation and ohmic nature characterise the conduction process in this region. The charge carriers are basically injected from the electrode to the bulk region in this region once voltage is applied. The value of m is less than 1 in this region. As the voltage increased the current increased along with it, but because there are traps, these injected charge carriers are trapped and fewer free charge carriers are allowed into the device. So in another region which is above the transition voltage, the value of m is greater than 1. The trapped charge carriers in this region may be released or recombined when the voltage increases, enhancing the device's overall free charge. The conduction process is therefore controlled by the SCLC conduction process as this region is above transition voltage. The extracted value of trap energies of the MR dye based organic device in absence and presence of ZnO are shown in the Table 4.5 and Table 4.6 below.

Table 4.5 Trap energy values that were extracted for three distinct systems in absence and presence of TiO_2 and ZnO nanoparticles separately for PSF dye

System	Extracted value of m	Extracted value of E_c in (eV)
Only PSF	3.38	0.087
PSF+ ZnO	2.92	0.075
PSF+TiO_2	2.90	0.074

Table 4.6 Trap energy values that were extracted for two distinct systems in absence and presence of ZnO nanoparticles separately for MR dye

System	Extracted value of m	Extracted value of E_c in (eV)
Only MR	3.8	0.098
MR+ ZnO	2.2	0.056

From the Table 4.5 and Table 4.6 it is observed that with incorporation of nanoparticles, trap energy is reduced. And with reduction of E_c the R_s of the MR dye based organic device is also reduced. Now evaluation of the experimental outcome shown in the comparison table clearly supports that lowering of trapping energy in turn reduces the series resistance which is the reason for increment of conductivity as well as efficiency of the device. So this leads to a proportional dependency of R_s on E_c. The reduction percentage of both R_s and E_c in presence of nanoparticles has been shown in Table.4.7 and Table 4.8.

Table 4.7 Estimated Percentage of reduced R_s and E_c in presence of TiO_2 and ZnO nanoparticles for PSF dye

Nanoparticles used with PSF dye	Reduction percentage (%) of series resistance $R_s$using Nanoparticles	Reduction percentage (%) of trap energy E_c using Nanoparticles
PSF+ ZnO	58.82	13.8
PSF+ TiO_2	63.29	14.96

Table 4.8 Estimated Percentage of reduced R_s and E_c for MR dye in presence of ZnO nanoparticles

Nanoparticles used in MR dye based organic device	Reduction percentage (%) of series resistance R_s using Nanoparticles	Reduction percentage (%) of trap energy $E_c$using Nanoparticles
ZnO	89.08	42.85

4.5 Conclusions

The impact of nanoparticles on R_s has been seen in this work. To create the organic device, phenosafranine (PSF) and methyl red (MR) dyes have used. In the case of PSF, we have created three different devices, one of which has only PSF while the other two contained PSF in combination with TiO_2 and ZnO nanoparticles. We have also investigated organic devices based on MR dye in both the absence and presence of ZnO nanoparticles. Measurements and analysis have been done on the dark I-V characteristics. Thermionic emission theory and the Cheung Cheung function, which is essentially a modification of the Thermionic emission theory by including the influence of R_s, have been used to describe the data. The value of R_s has been shown to be quite high without the addition of nanoparticles. One of the primary causes of this high value of R_s is trapping of charge carriers at the interface and in the bulk area of the devices. By taking into account the exponential trap distribution, we determined the value of E_c. The extracted E_c values have examined with the calculated R_s values. It has been observed that the trap energy is reduced when nanoparticles are included, which lowers the value of R_s.

4.6 References

1. A. Y. Khan, B. Saha, G. S. Kumar, Phenazinium dyes safranine O and phenosafranine induce self-structure in single stranded polyadenylic acid: Structural and thermodynamic studies, Journal of Photochemistry and Photobiology B: Biology, (2014), 132: 17-26
2. A. K. Jana, Solar cells based on dyes, Journal of Photochemistry and Photobiology A: Chemistry, (2000), 132: 1-17

3. S. Chakraborty, and N. B. Manik, Improvement of electrical and photovoltaic properties of methyl red dye based photoelectrochemical cells in presence of single walled carbon nanotubes, Frontiers of Optoelectronics, (2015), 8: 289-297
4. Dr. M. Nasr, Dr. C. Eid, Prof. R. Habchi, Prof. Dr. P. Miele, Dr. M. Bechelany, Recent Progress on Titanium Dioxide Nanomaterials for Photocatalytic Applications, Chem sus Chem, (2018), 11: 3023-3047
5. R. Escudero, R. Escamilla, Ferromagnetic behavior of high-purity ZnO nanoparticles, Solid state communications, (2011), 151: 97-101
6. S Sen, and N. B. Manik, Study on the Effect of 8 nm Size Multi Walled Carbon Nanotubes (MWCNT) on the Barrier Height of Malachite Green (MG) Dye Based Organic Device', International Journal of Advanced Science and Engineering, (2020), 6: 23-27
7. M. Shah, Kh.S. Karimov, Z. Ahmad, M.H. Sayyad, Electrical characteristics of Al/CNT/NiPc/PEPC/Ag surface-type cell, Chinese Physics Letter, (2010), 27: 106102
8. S. Okur, F. Yakuphanoglu, M. Ozsoz, P. Kara Kadayifcilar, Electrical and interface properties of Au/DNA/n-si organic-on-inorganic structures, Microelectron, (2009), 86: 2305-2311
9. M. Shah, M. H. Sayyad, Kh.S Karimov, F. Wahab, Electrical characterization of the ITO/NiPc/PEDOT : PSS junction diode, J. Appl. Phys., (2010), 43: 405104 (1-5)
10. F. Yakuphanoglu, Controlling of silicon–insulator–metal junction by organic semiconductor polymer thin film, Synthetic Metals., (2010), 160: 1551-1555
11. F. Yakuphanoglu, M. Kandaz, B. F. Senkal, Inorganic–organic photodiodes based on polyaniline doped boric acid and polyaniline doped boric acid:nickel(II) phthalocyanine composite, Sensors & Actuators: A. Physical, (2009), 153: 191-196
12. S. K. Cheung, N. W. Cheung, Extraction of Schottky diode parameters from forward current-voltage characteristics, Applied Physics Letters, (1986), 49: 85-87
13. M. Benhaliliba, Extracted electronic parameters of a novel Ag/Sno_2: In/Si/Au Schottky diode for Solar cell application, Journal of Nano- and Electronic Physics, (2015), 7: 02029 (1-4)
14. A. J. Carr, and S. Chaudhary, On the identification of deeper defect levels in organic photovoltaic devices, Journal of Applied Physics, (2013), 114: 064509 (1-7)

15. S. K. Dey, Md. R. Islam, N. B. Manik, and A. N. Basu, Non-exponential photocurrent growth and decay in safranine-T dye doped solid state polymer photo electrochemical cell, Journal of Material Science, (2003), 38 (1): 93–99
16. A. Haldar, S. Maity, and N. B. Manik, Electrical and photovoltaic characterisations of methyl red dye doped solid-state photoelectrochemical cell, Ionics, (2009), 15: 79–83

Chapter 5

Effect of temperature on Series resistance and trap energy of Methyl Red (MR) dye based organic device

5.1 Introduction

In our previous chapter, we have studied the effect of trap energy on device R_s on PSF and MR dye based device. As we know that, in any electronic device temperature plays an important role on the device performance [1-2]. With changing of temperature, the characteristics of the devices get affected due to the variance of different parameters. In this context, study of the physics behind the high value R_s and also the effect of variation of temperature on organic device R_s are very crucial for the proper understanding of the organic devices behavior. So in this work we have studied the device R_s at different temperatures. We have also observed the device ideality factor (n) with variation of temperature. However, many works have reported on how to reduce the device trap energy [3-4] but the change of trap energy with variation of temperature has not been studied yet. So it will also be a very important study if we observe how trap energy gets affected with variation of temperature. Therefore in this work the relation of trap energy with temperature have also been studied.

5.2 Selection of the dye

5.2.1 Materials used

MR is an azo dye with molecular formula of $C_{15}H_{15}N_3O_2$ (2-[4-(dimethylamino) phenylazo] benzoic acid). The property of this dye has mentioned previously in section 4.2.1. This MR dye is easily available and we had procured it from Finar Chemicals, Ahmedabad, India. The molecular weight of MR is 269.3 g/mol. This dye is inexpensive. The structure of the MR is shown in Fig.5.1. Its color originates from the absorbance in the visible region of the spectrum as electrons are delocalized in the benzene [5].

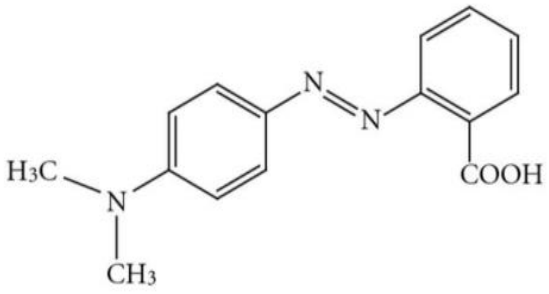

Fig. 5.1 Structure of MR dye with an aromatic azo group attached

5.3 Experimental details

5.3.1 Sample preparation

For the cell preparation at first in a cleaned beaker we had taken 20 ml distilled water and added 4 mg of Poly Vinyl Alcohol (PVA) into the distilled water. Then this solution was stirred for 30 minutes with a magnetic stirrer at 80˚C. Now in this prepared PVA solution we mixed 2 mg of MR dye and stirred the solution again for another 30 minutes. Then this MR dye solution was kept in a pre-cleaned test-tube. Now to prepare the cell we have taken two electrodes, Indium Tin Oxide (ITO) as front electrode and Aluminum (Al) as back electrode. At first, we placed the MR dye solution on ITO and spin coated the solution at a speed of 1500 rpm then again dried at a speed of 2500 rpm. After that we spin coated the MR dye solution on Al electrode in the similar manner discussed above. Then these two electrodes were sandwiched together and formed the MR dye based organic device. After preparing the device, it was kept under vacuum for 12 h [6].

5.3.2 Measurements

The prepared cell was characterized after proper drying. For the I-V measurement at first the MR dye based organic device was placed inside a cryostat which was designed in our laboratory. Then liquid nitrogen was poured inside the liquid chamber of the cryostat which was pre evacuated to a pressure of 10^{-4} Torr by using a high vacuum pumping unit (Model No. PU-2 Ch-8, manufactured by Vacuum Product & Consultant) [7]. The temperature measurement was performed in the range of 253 K-315 K. To measure the temperature we used a Chormel - Alumel thermocouple (TC) and the TC output was recorded by using Kethly 2000 multi meter. The dark Current - Voltage measurement in the temperature range of 253 K - 315 K was performed by using Keithley 2400 source measure unit.

5.4 Results and Discussions

The forward dark I-V characteristics of the MR dye based organic device at different temperatures in the range of 253K - 315 K are shown in the Fig. 5.2 below. It is observed that the current of the MR dye based organic device is very low in a few microamperes range and the current of this device is increased with rising of the temperature as shown in the Fig. 5.2.

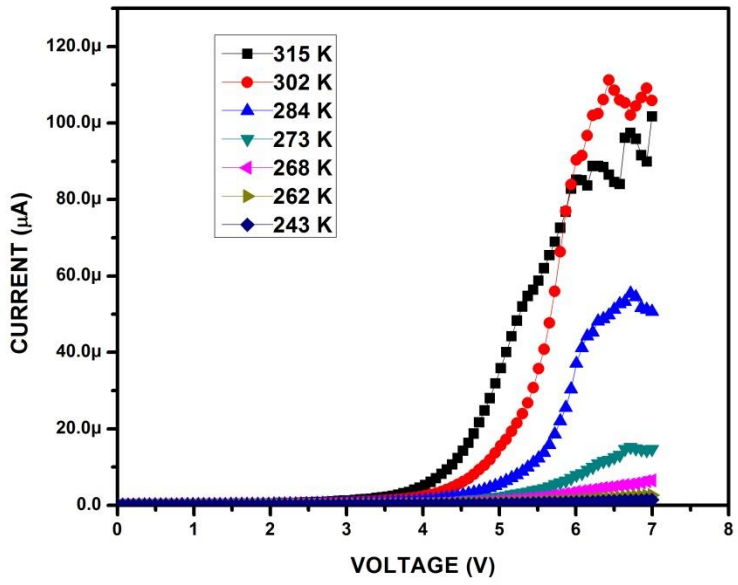

Fig. 5.2 An investigation of the forward dark I-V characteristics of ITO/ MR/ Al at 253 K to 315 K

To extract the value of R_s and n we have analyzed the dark I-V characteristics by using the equation described Cheung- Cheung method [8-10],

$$I = I_0[\exp(\frac{q(V-IR_s)}{nkT}) - 1] \quad (5.1)$$

and,

$$I_0 = AA^* T^2 \exp(-\frac{q\phi_b}{KT}) \quad (5.2)$$

Where q is the electronic charge, k is the Boltzmann constant, T is the temperature, V is the applied voltage, n is the ideality factor, R_s is the series resistance and I_0 is the reverse saturation current, A is the contact area, A* is the Richardson constant, T is the temperature in Kelvin scale, ϕ_b is the barrier height [11].

By solving the Cheung Cheung method we can extract the device R_s and n by using the following equations,

$$\frac{dV}{d\ln I} = \frac{nkT}{q} + IR_s \quad (5.3)$$

$$H(I) = n\phi_b + IR_s \tag{5.4}$$

Where,

$$H(I) = V - \left(\frac{nkT}{q}\right)\ln\frac{I}{AA^*T^2} \tag{5.5}$$

According to Eqn. 5.3 we have plotted the $\frac{dV}{d\ln I}$ Vs. I plot. A straight-line curve will be obtained from the plot with an intercept of $\frac{nkT}{q}$ as shown in Fig. 5.3. We have extracted the device R_s from the slope of the straight line.

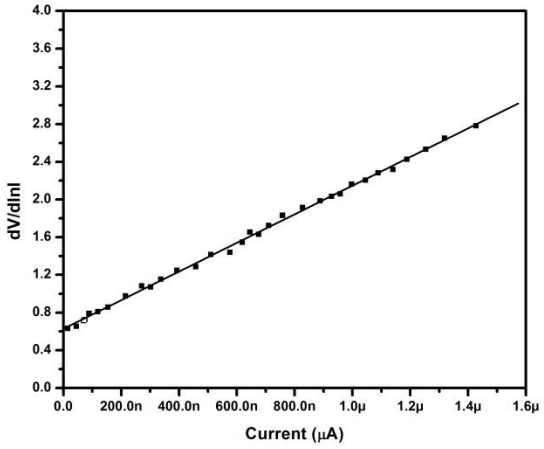

(a)

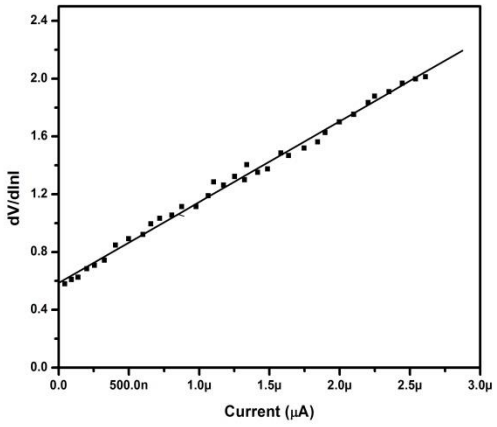

(b)

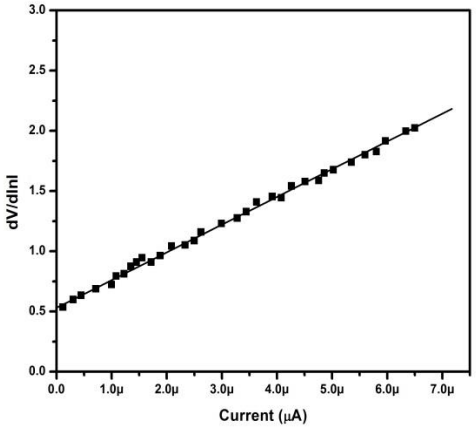

(c)

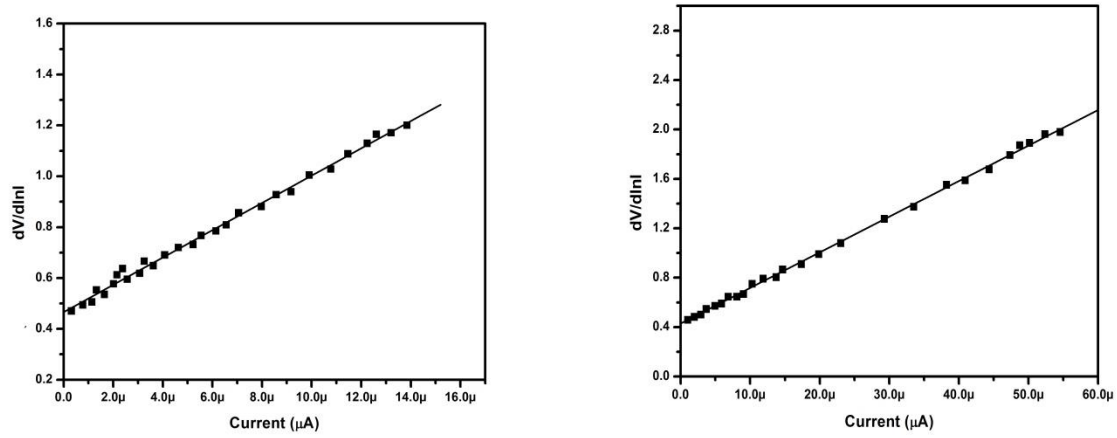

(d) (e)

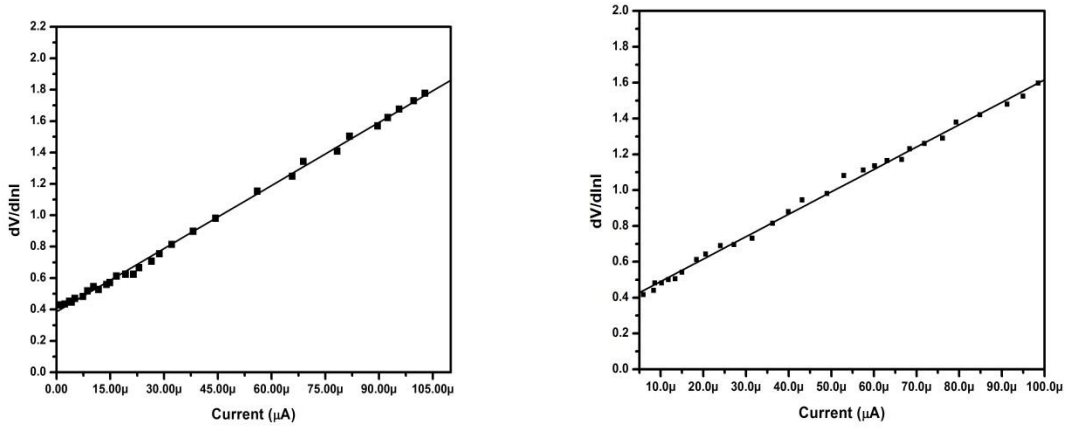

(f) (g)

Fig. 5.3 $\frac{dV}{dlnI}$ Vs. Current (I) of MR dye based organic device within the range of temperatures from 253 K to 315 K. Where (a) in temperature 253 K, (b) in temperature 262 K, (c) in temperature 268 K, (d) in temperature 273 K, (e) in temperature 284 K, (f) in temperature 302 K, (g) in temperature 315 K

It is observed that the extracted value of R_s and n of the MR dye based organic device is very high and with increasing of the temperature, the values of the parameters get reduced. We have also measured the R_s from Eqn. 5.5. According to the equation we have plotted H(I) Vs. I curves for different temperatures shown in Fig. 5.4. The H(I) Vs. I plot also gives a straight line with

intercept of $n\phi_b$ at y axis. The value of R_s measured from H(I) Vs. I and from $\frac{dV}{dlnI}$ Vs. I at different temperatures shows good compatibility with each other.

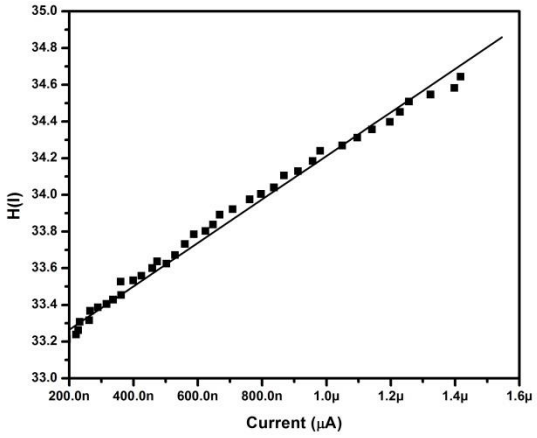

(a)

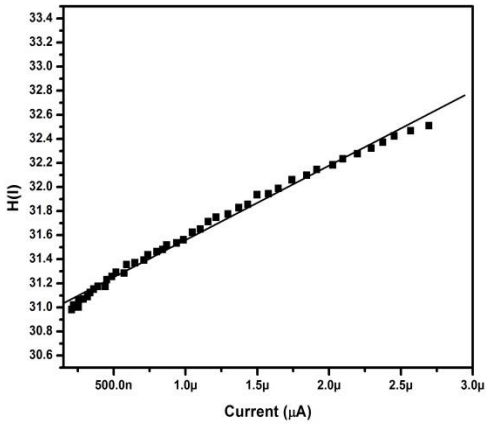

(b)

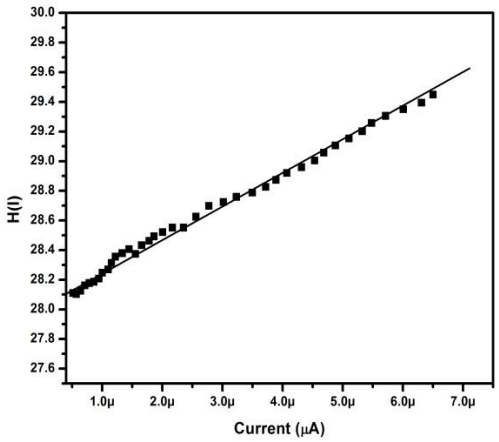

(c)

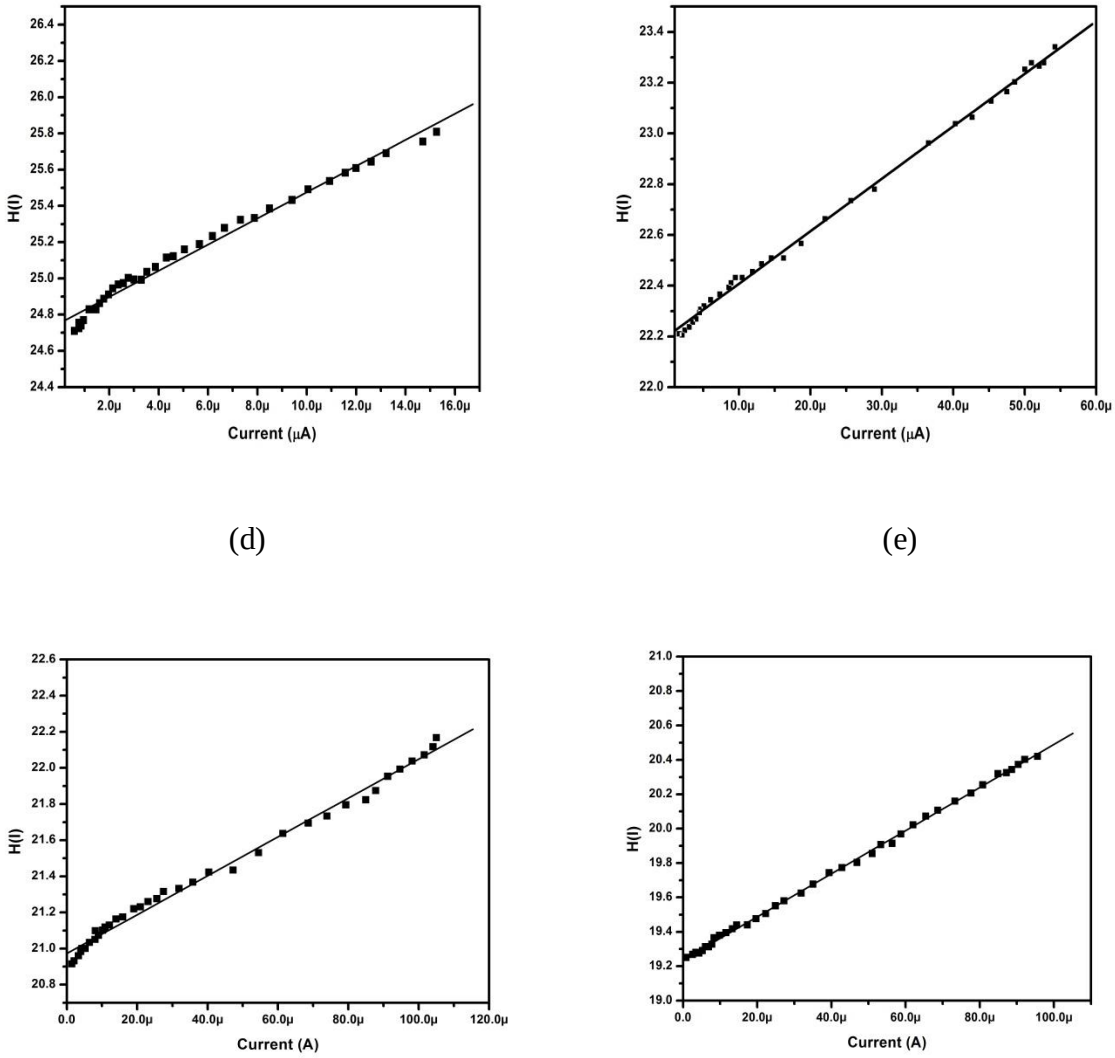

Fig. 5.4 H(I) Vs. Current (I) of MR dye based organic device within the range of temperatures from 253 K to 315 K. Where (a) in temperature 253 K, (b) in temperature 262 K, (c) in temperature 268 K, (d) in temperature 273 K, (e) in temperature 284 K, (f) in temperature 302 K, (g) in temperature 315 K

The extracted values of R_s and n at temperature from 253 K to 315 K by using these two methods are shown in the Table 5.1 below.

Table 5.1 The n and R_s values extracted from the MR dye based organic device in temperature range of 253 K to 315 K

Temperature (K)	Value of Ideality factor (n)	Values of R_s from $\frac{dV}{dlnI}$ Vs. I in (MΩ)	Values of R_s from H(I) Vs. I in (MΩ)
253	24.23	1.51	1.20
262	22.30	0.559	0.618
268	20.1	0.230	0.226
273	17.69	0.053	0.072
284	16.01	0.028	0.020
302	14.67	0.013	0.010
315	13.80	0.012	0.012

From the Table 5.1, it can be clearly seen that the both R_s and n decrease with increasing temperature. In this MR dye based organic device the R_s become very high due to the interface states in between electrodes and the organic dye. As organic semiconductors are disordered in nature, they include energy states in the band structure [12-13]. These additional energy states, called traps introduced structural defects at the interface and throughout the structure of the organic device. So due to these energy states the interface gets affected and enhances the overall barrier potential which results in less numbers of free charge carriers in MR dye based organic devices. Moreover, presence of traps capture some of these carriers which further recombine or release from the traps with increasing potential and govern the charge conduction process. Therefore the value of R_s and n of the MR dye based organic device is very high at low temperature. Now at high temperature, the thermally generated carriers are enhanced and in this condition with increasing of the bias voltage, the numbers of free charge carriers are enhanced. This increment of the free charge carriers upgrades the overall conductivity of the device, which reduces these parameters. The plot of n with temperature and the plot of R_s with temperature are shown in Fig. 5.5 and Fig. 5.6. The figures suggest that, both the values of R_s and n reduce with increasing of temperature.

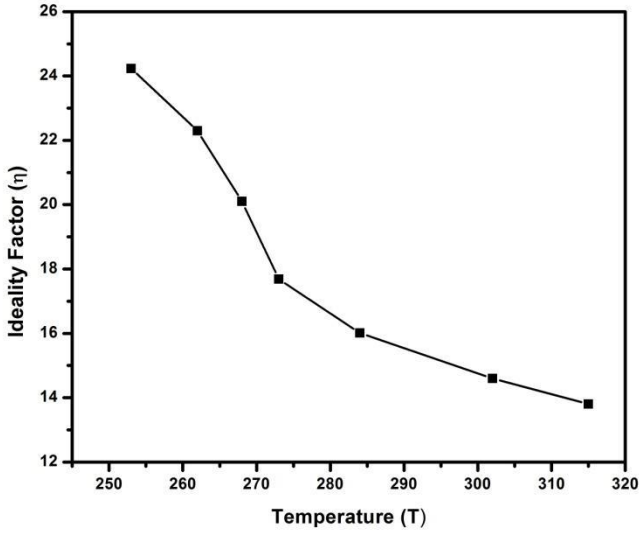

Fig. 5.5 Decreasing nature of ideality factor (n) of ITO/MR/Al organic device with rising of temperature from 253 K to 315 K

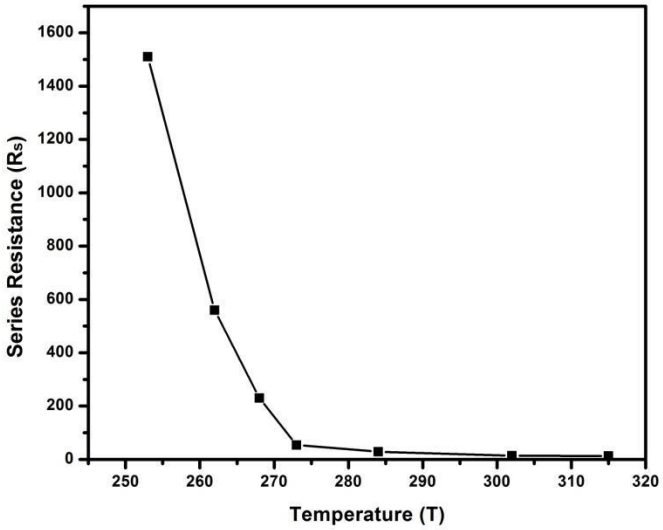

Fig. 5.6 Decreasing nature of Series resistance (R_s) of ITO/MR/Al organic devices with rising of temperature from 253 K to 315 K

In this present chapter, we have also studied the trap energy, which plays an important role in charge injection and charge transport process in any organic device. To measure the E_c we have considered the distribution of trap energy level as exponential energy distribution [14].

$$n_t = H_n \exp\left(\frac{F_n}{kT_c}\right) \tag{5.6}$$

Where H_n is the trap density, F_n is the electron Fermi level, k is the Boltzmann constant and T_c is the characteristic temperature of the exponential trap distribution ($T_c = \frac{E_c}{K}$, Where E_c is the characteristic trap energy.

Now solving the Poisson's equation with this form of exponential trap distribution, the IV equation can be written as [15],

$$I = An_c\mu q^{1-m}\left(\frac{m\varepsilon}{H_n\,(m+1)}\right)^m\left(\frac{2m+1}{m+1}\right)^{m+1}\left(\frac{V^{m+1}}{L^{2m+1}}\right) \tag{5.7}$$

Where N_c is the effective density of states, μ is the mobility, ε is the product of the permittivity of the vacuum (ε_0) and the dielectric constant (ε_r), V is the applied voltage, L is the thickness of the active layer and m is the ratio of the characteristic temperature T_c with absolute temperature T.

$\left(m = \frac{T_c}{T}\right)$.

From Eqn.5.7 it is cleared that the equation follows the power law dependence of,

$$I \approx V^{m+1} \tag{5.8}$$

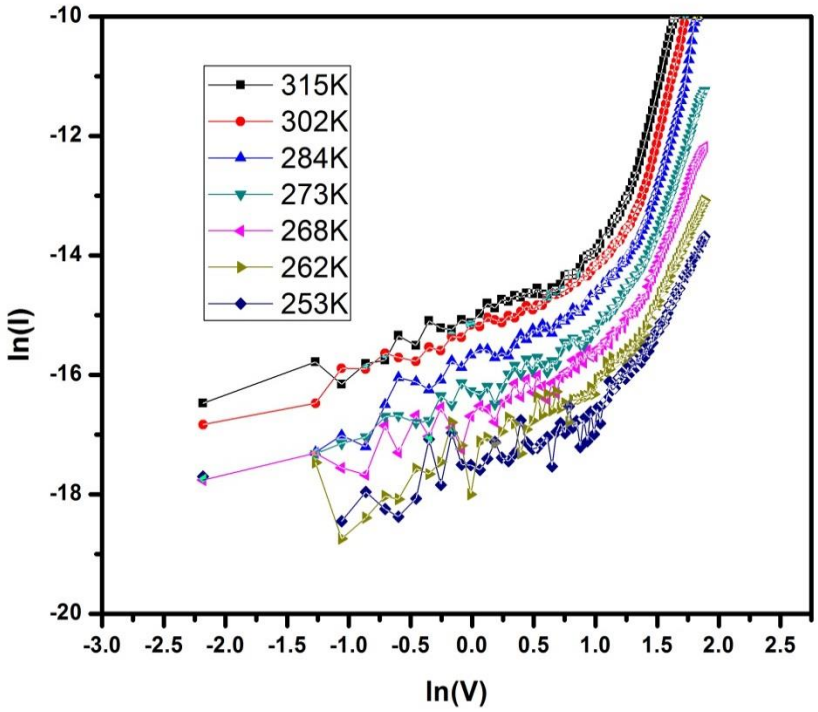

Fig 5.7 lnI Vs. lnV plot of ITO/MR/Al in the temperature range of 253 K to 315 K

Now we have observed the logarithm plots of the dark I- V characteristics to estimate the E_c at different temperatures. The lnI Vs. lnV plot of the MR dye based organic device at different temperatures 253 K - 315 K is shown in Fig. 5.7. From the Figure the values of m+1 at different temperatures have been calculated by using Eqn. 5.7. We have analyzed the variation of m with changing of temperature. The extracted values of m at different temperatures are shown in the Table 5.2.

Table 5.2 Extracted trap energy values for an MR dye-based organic device in 253 K- 315K temperature ranges

Temperature (K)	Extracted value of m from region II	Value of trap energy (E_c) (eV)
253	2.9	.063
262	3.3	.074
268	3.9	.090

273	4.3	.101
284	5.1	.124
302	5.6	.145
315	5.9	.160

Basically in any organic device, traps create localized energy states and are distributed energetically. Due to this, during conduction, one part of the injected charge carriers is trapped and which results in restriction in the charge conduction process. So total injected charges can be divided into two parts, one part contains free charges and another part is the trapped charge at different trap centers of the organic materials. Now the number of trap charges depends on trap density (H_n) and trap energy (E_c). In this context, by considering exponential trap distribution, we have studied the log-log plot of dark I-V characteristics of the MR dye-based organic device at different temperatures. From the ln I Vs. ln V plot and the above result it has been noticed that the I- V characteristics are divided into two regions. In region I which is at low bias voltage, the conduction mechanism is governed by the ohmic conduction mechanism. In this region, the amount of injected charge carriers is very low so that the relation between current and voltage is linear. Whereas in region II which is at high bias voltage the amount of injected charge carriers is increased. But due to the presence of localized energy states and low mobility of the charge carriers in the organic film, the charge carriers are trapped and the conduction mechanism is governed by Space charge limited current (SCLC) mechanism where nonlinear relation between current and voltage with power law is observed [16]. In the ohmic conduction mechanism, the value of m is low nearly to 1 or less than 1, and in the SCLC conduction mechanism where exponential trap energy distribution is considered the value of m is greater than 2. The trap energy that plays a vital role in the charge conduction process of the organic device has been measured from region II. It is discerned that at low temperature the value of E_c of the MR dye based organic device is low and with increasing temperature, the value is increased. But we have also noticed that with rising temperatures the overall current is increased. So it can be said that trapping of charge carriers is increased with rising temperatures. These increased trapped charges, restrict the charge conduction process and reduce the current through the device. But at high temperature the thermally generated carriers are also increased which enhances the free carriers. Now in these circumstances with increasing of the bias voltage, the amount of injected

charge carriers and thermally generated carriers are abruptly enhanced by the free charge carriers, which compensate the reduced current caused by trapped charge carriers. This indemnification of charge carriers enhanced the overall current of the organic device. Therefore, from the results it can be concluded that temperature plays an important role on the various parameters of the organic devices and affect the charge conduction process of the devices.

5.5 Conclusion

In this work we have studied the dark current voltage characteristics of the MR dye based organic device at different temperatures. The I-V measurements have performed at 253 K, 262 K, 268 K, 273 K, 284 K, 302 K and 315 K. We have analyzed the I-V characteristics by using the Cheung- Cheung method and extracted devices R_s and n. It has been observed that with rising temperature the value of R_s and n get reduced. Basically with rising temperatures the number of free charge carriers are increased which reduces the device R_s. The value of R_s also measured from H(I) Vs. I plot at different temperature and it is observed that the values of R_s show compatibility with the values measured from $\frac{dV}{dlnI}$ Vs. I plot. Apart from that, we have also studied the trap energy (E_c) of the device at different temperatures. It is observed that the value of E_c get increased with the rise of temperature. From this result it can be concluded that with rising temperatures the amount of trapped charge carriers are enhanced and the current reduced. Nevertheless, with rising of temperature escalated the trapping of charge carriers, the numbers of free charge carriers in the high temperature still increased the overall current which enhanced the device conductivity. Actually at high temperature with increasing bias voltage, the injected charge carriers are abruptly increased which indemnify the decreased current with enhancement of the free charge carriers. Therefore the overall current of the MR dye based organic device is increased and reduces the device R_s.

5.6 References

1. H. Li, D. He, Q. Zhou, P. Mao, J. Cao, L. Ding, J. Wang, Temperature - dependent Schottky barrier in high - performance organic solar cell, Scientific Reports, (2017), 7: 1-10

2. N. Mendil, M. Daoudi, Z. Berkai, A. Belghachi, Temperature effect on charge carrier mobility in SubPc and C_{60} organic semiconductors for photovoltaic applications, 2eme Conférence Internationale des Energies Renouvelables (2014), (CIER'14)
3. S. Saha, N. B. Manik, Enhancement of efficiency of Phenosafranin based organic photovoltaic devices using nano particles, Indian Journal of Physics, (2012), 86: 605-611
4. 16. A. Haldar, S. Maity, N. B. Manik, Electrical and photovoltaic characterisations of methyl red dye doped solid-state photo electrochemical cell, Ionics, (2009), 15: 79–83
5. S. Saha, N. B. Manik, Study of solvent dependence of Methyl Red and C_{60} based organic photovoltaic devices, Thin Solid Films, (2012), 520: 6274-6281
6. S. Chakraborty, N. B. Manik, Improvement of electrical and photovoltaic properties of methyl red dye based photo electrochemical cells in presence of single walled carbon nanotubes, Frontiers, (2015), 8: 289-297
7. S. Maity, P. Dalapati, N. B. Manik, Temperature dependent dark current-voltage study of Thionine dye doped solid state photo electrochemical cell (PEC), Journal of Optoelectronics and advanced materials,(2013), 15: 1417-1422
8. S. K. Cheung, N. W. Cheung, Extraction of Schottky diode parameters from forward current voltage characteristics, Applied Physics Letters, (1986), 49: 85-87
9. M. Shah, S. Kh. Karimov, Z. Ahmad, M. H. Sayyad, Electrical characteristics of Al/CNT/NiPc/PEPC/Ag surface-type cell, Chinese Physics Letters, (2010), 27: 106102 (1-4)
10. M. Shah, M. H. Sayyad, S. Kh. Karimov, Electrical characterization of the organic semiconductor Ag/CuPc/Au Schottky diode, Journal of Semiconductors, (2011), 32: 044001(1-5)
11. S. Sen, N. B. Manik, Effect of Back Electrode on Trap Energy and Interfacial Barrier Height of Crystal Violet (CV) Dye based Organic Device, Bulletin of Materials Science, (2020), 43: 60 (1- 4)
12. John A. Carr, S. Chaudhary, On the identification of deeper defect levels in organic photovoltaic devices, Journal of Applied Physics (2013), 114: 064509
13. S. M. H. Rizvi, B. Mazhari, Investigation of Traps in Thin-Film Organic Semiconductors Using Differential Analysis of Steady-State Current–Voltage Characteristics, IEEE Transactions on Electron Devices, (2018), 65: 3430 - 3437

14. S. Chakraborty, N. B. Manik, Effect of COOH-functionalized SWCNT addition on the electrical and photovoltaic characteristics of Malachite Green dye based photovoltaic cells, Journal of Semiconductors, (2014), 35: 124004(1-6)
15. P. K. Das, S. Bhunia, N. B. Manik, Effect of Trap Energy on Series Resistance of Phenosafranine Dye Based Organic Diode in Presence of TiO2 and ZnO Nanoparticles, Advanced Materials Research, (2020), 1159: 112 - 123
16. S. Chakraborty, N. B. Manik, Effect of single walled carbon nanotubes on the threshold voltage of dye based photovoltaic devices, Physica B, (2016), 481: 209-216

Chapter 6

Study on the Series Resistance of Crystal Violet (CV) and Malachite Green (MG) Dye Based Organic Photovoltaic Device in Presence of Single Walled Carbon Nanotubes

6.1 Introduction

In our previous chapter we have studied the effect of temperature on the series resistance (R_s) and trap energy (E_c) of MR dye based organic device. In this present chapter we have prepared organic devices by using Crystal violet (CV) dye and Malachite Green (MG) dye in absence and presence of single walled carbon nanotubes (SWCNT) and studied the dark and light I-V characteristics. We have investigated the effect of addition of SWCNT on R_s and E_c. The Cheung Cheung method has been used to extract R_s from the dark current voltage (I-V). We have also studied the light I-V characteristics to find out the R_s under illumination. As we know that under illumination, the charge transport process is governed by the incident photon energy (E_m) which is absorbed by the OPV device. So we have extracted the E_m from the light I-V characteristics and estimated the R_s by using area method under light illumination in absence and presence of SWCNT.

6.2 Selection of the dye

6.2.1 Materials used

The structure of Crystal Violet (CV) dye (BDH, England, UK)is shown in Fig. 6.1.The Crystal Violet with molecular formula of [$C_{25}N_3H_{30}Cl$] is a triarylmethane dye and the molecular weight of CV is 407.986 g/mol. Moreover CV, a cationic dye, is also dissociated in aqueous solution [1]. The optical response of the CV dye is quite satisfactory, and CV dye-based OPV devices will respond well in both light and dark IV conditions.

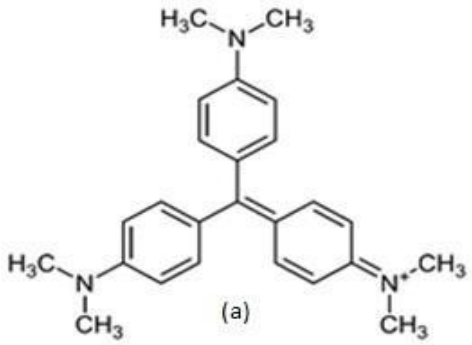

Fig. 6.1 Structure of Crystal Violet (CV) dye

Malachite Green (MG) is a water soluble cationic dye and it belongs to the triarylmethane group and has a molar mass of 364.911 g/mol (chloride) [2-3]. The structure of the MG dye is shown in Fig. 6.2.MG dye has been chosen because it has a good quantum yield. It has been procured from the Finar Chemicals, Ahmedabad.

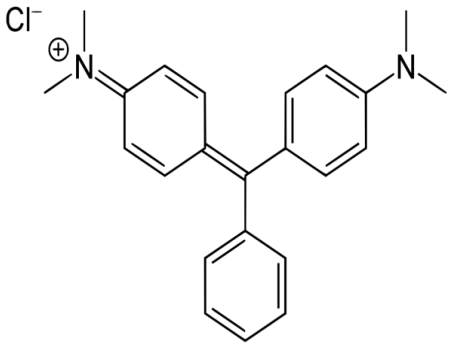

Fig. 6.2 Structure of Malachite Green (MG) dye

The structure of SWCNT is shown in Fig. 6.3. In SWCNT, the carbon atoms are hexagonally oriented and they are composed of a single graphene sheet rolled up in a tube-like structure [4]. Various promising properties such as good stability and flexibility, desirable optical properties, high carrier mobility, tunable conductivity, etc. of SWCNT exhibit that it is a potential material for organic devices. Its large surface aspect ratio is favorable for charge transfer as it reduces the recombination process. The diameter and length of SWCNT is 1 nm and 10 µm respectively. Due to its semiconducting properties, SWCNT enhances the charge transport mechanism of the device. In our work, SWCNT has been obtained from SRL, India. We have used Poly Vinyl Alcohol (PVA) as a transparent inert binder, which has been purchased from S. D. Fine Chem. Ltd., Boisar, India.

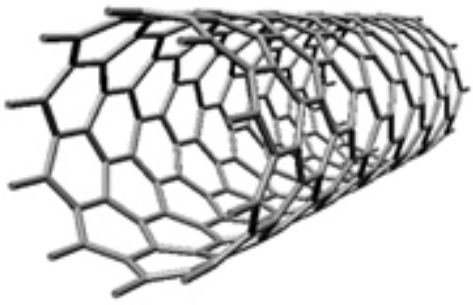

Fig. 6.3 Structure of SWCNTs

6.3 Experimental details

6.3.1 Sample Preparation

6.3.1 (a) Crystal Violet (CV) and Malachite Green(MG) dye based organic devices in absence and presence of SWCNTs

At first, we prepared two Poly Vinyl Alcohol (PVA) solutions by mixing 1 mg PVA with 10 ml of distilled water in each solution. PVA - water mixture was stirred for 30 min to make a homogeneous PVA solution. PVA has been used as an inert binder. Then 1 mg of CV dye was mixed in one PVA solution and1 mg of MG dye was mixed in another prepared PVA solution. Then the solutions were well stirred with a magnetic stirrer for another 30 minutes to prepare CV and MG dye solutions. After this to prepare the CV dye based OPV devices the CV dye solution was again separately kept in two pre-cleaned test tubes. Now in one test tube, 1 mg of SWCNT was added. So, two different solutions were prepared with and without SWCNT. Then one part of this CV dye solution was spin coated on ITO coated glass at a speed of 1500 rpm. Due to this high speed the solution was distributed uniformly on the electrode by the centrifugal force. After that the applied solution was dried at room temperature at a speed of 3500 rpm. In a similar manner, this solution was spin-coated on Aluminum electrode. Then these two electrodes were sandwiched together to form the CV dye based organic device. After preparing these two devices, they were kept under vacuum for 12 h. Similarly the solution of CV with SWCNT was spin coated on ITO and Aluminum electrode and prepared CV dye based organic device in presence of SWCNT [5]. In the similar way we have fabricated two different MG dye based OPV devices in absence and in presence of SWCNT. These two devices were also kept in vacuum for 12 hours before their characterization.

6.3.2 Measurement

Keithley 2400 source measure unit was used for the I-V measurement. ITO coated electrode was positively biased. The bias voltage was varied from 0 to 6 V with step variation of 0.2 V and with a delay of 1500 ms.. A solar simulator (Model 150 W Newport Corporation) was used for the light I - V measurement. A calibrated lux meter (Kyoritsu Electrical Instruments Works Ltd., Tokyo Model 5200) was used to measure the light intensity. Room temperature was kept at 22 °C during this measurement [6].

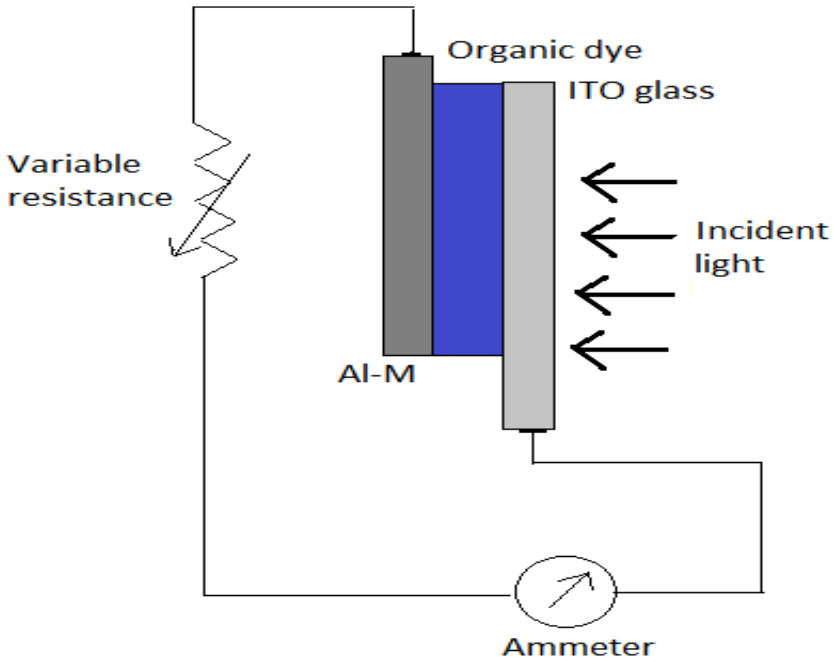

Fig. 6.4 Light strikes a transparent front electrode made of ITO, and a back electrode made of Al covered with Mylar is utilised for photovoltaic measurement

6.4 Result and Discussion

The steady state I-V characteristics of CV dye based and MG dye based organic devices in absence and presence of SWCNTs are shown in the Fig 6.5 (a), 6.5 (b) and 6..6 (a), 6.6 (b) respectively.

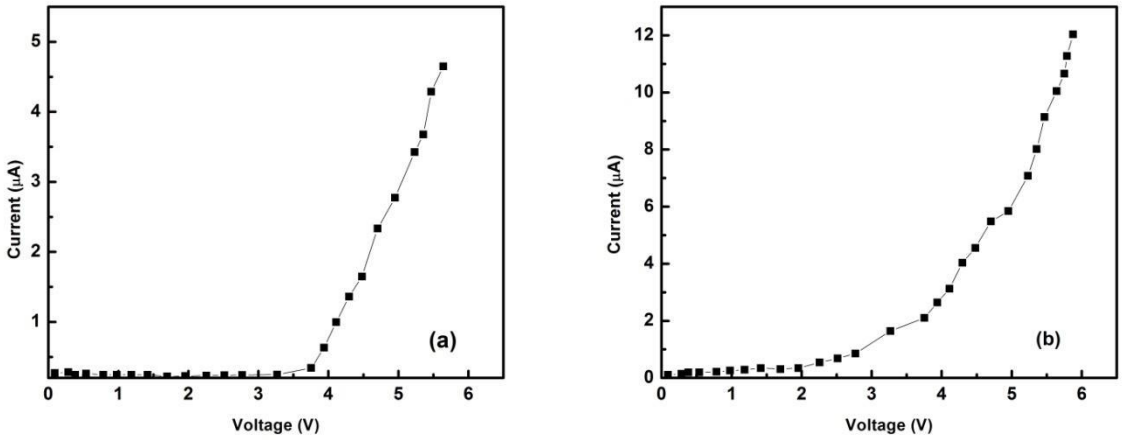

Fig. 6.5 Forward dark Current Voltage characteristics of (a) ITO/CV/Al Coated with Mylar and (b) ITO/CV+SWCNT/Al Coated with Mylar

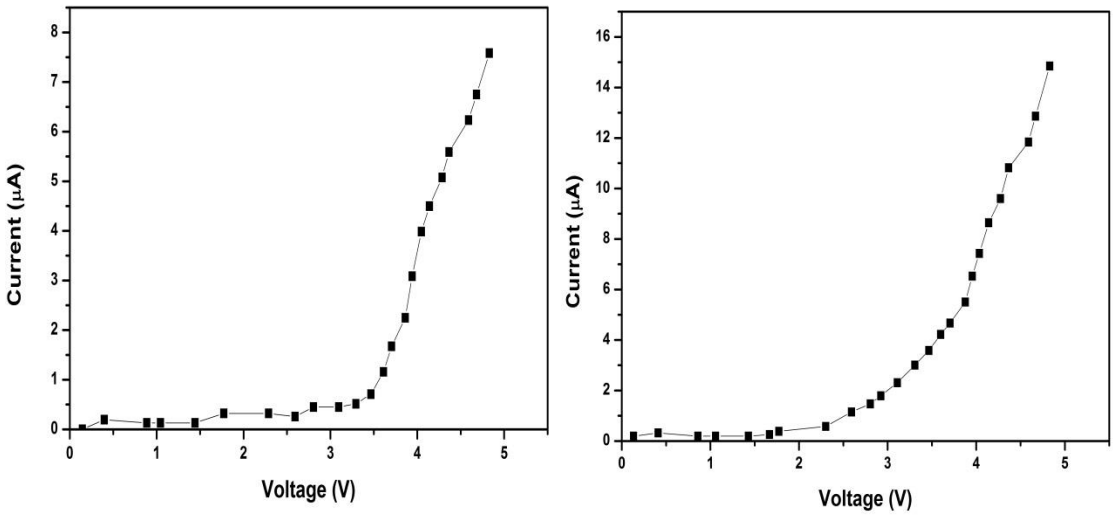

Fig. 6.6 The forward dark Current Voltage characteristics of (a) ITO/MG/Al Coated with Mylar and (b) ITO/MG+SWCNT/Al

From the dark I-V characteristics it is observed that the devices exhibit non-linear behavior. As discussed earlier, the presence of organic material in between the front and back electrode interface is one of the main reasons for non-ideal behavior. It is also observed that from the dark I-V characteristics that addition of SWCNTs enhances the amount of current significantly. Basically it can be said that the incorporation of SWCNTs reduces the process of recombination

by providing low percolation pathways for the charge carriers [6] which in turn results in improvement of the charges flow at metal organic layer interface.

The R_s from the dark I-V characteristics has been estimated by using the following equations described by Cheung Cheung method [7-9],

$$I = I_0 \left[\exp\left(\frac{q(V-IR_s)}{nkT}\right) - 1\right] \quad (6.1)$$

and,

$$I_{0=}AA^* T^2 \exp(-\frac{q\emptyset_b}{kT}) \quad (6.2)$$

Where q is the electronic charge, k is the Boltzmann constant, T is the temperature, V is the applied voltage, n is the ideality factor, R_s is the series resistance and I_0 is the saturation current, A is the contact area, A* is the Richardson constant, T is the temperature in Kelvin scale, ϕ_b is the barrier height [10].

To extract the device R_s by using Cheung Cheung method, the following equations are used.

$$\frac{dV}{dlnI} = \frac{nkT}{q} + IR_s \quad (6.3)$$

$$H(I) = n\phi_b + IR_s \quad (6.4)$$

Where,

$$H(I) = V - (\frac{nkT}{q})\ln\frac{I}{AA^*T^2} \quad (6.5)$$

The representation of dV/dlnI Vs. I plots of CV and MG dye based organic devices in absence and presence of SWCNTs shown in Fig 6.7 (a), 6.7 (b) and 6.7 (c), 6.7 (d) respectively. From the plot the linear portion gives the value of R_s.

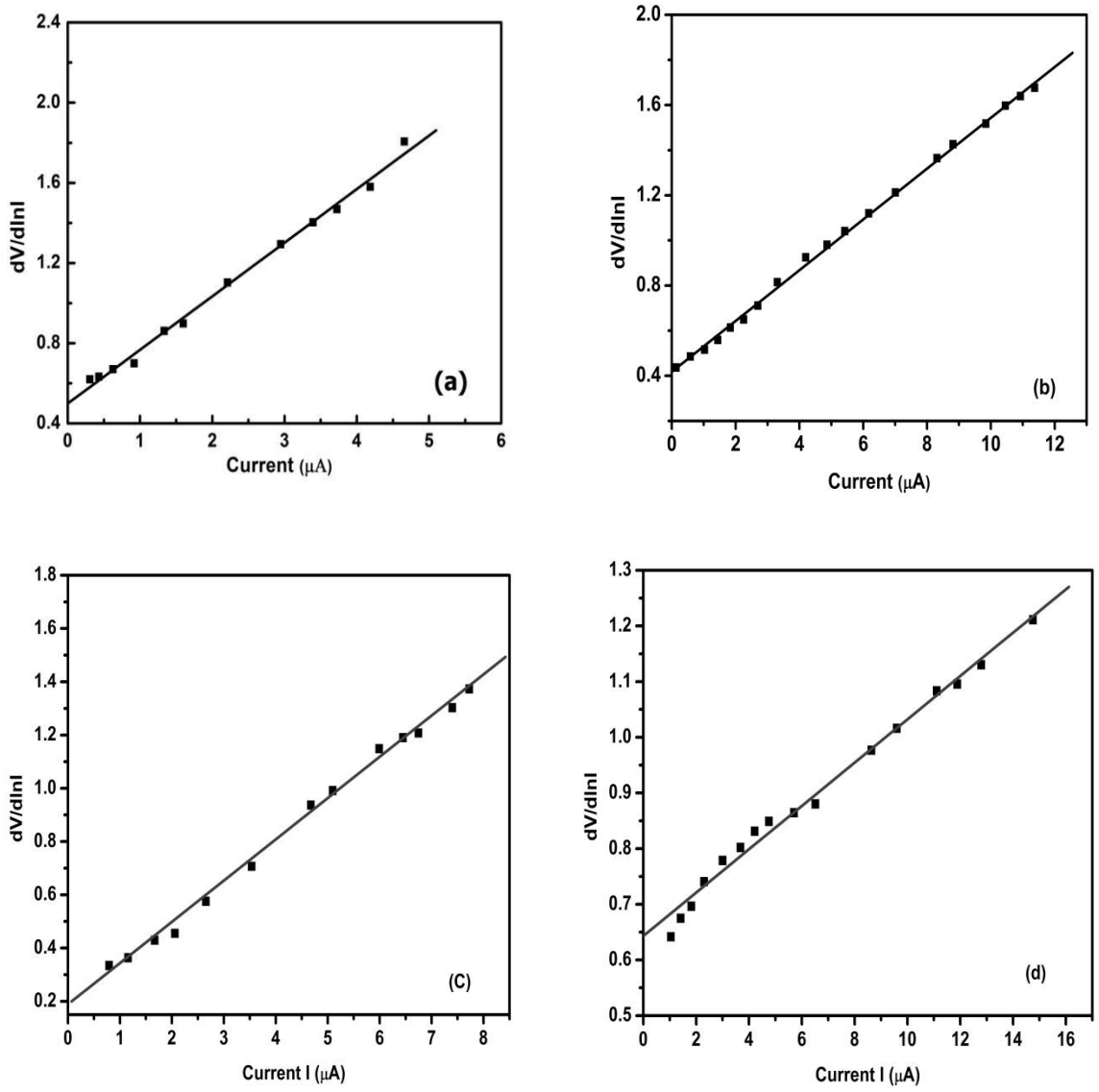

Fig. 6.7 dV/dlnI Vs. Current (I) (a) & (b): for CV dye based organic device, (c) & (d): for MG dye based organic device in absence and presence of SWCNT

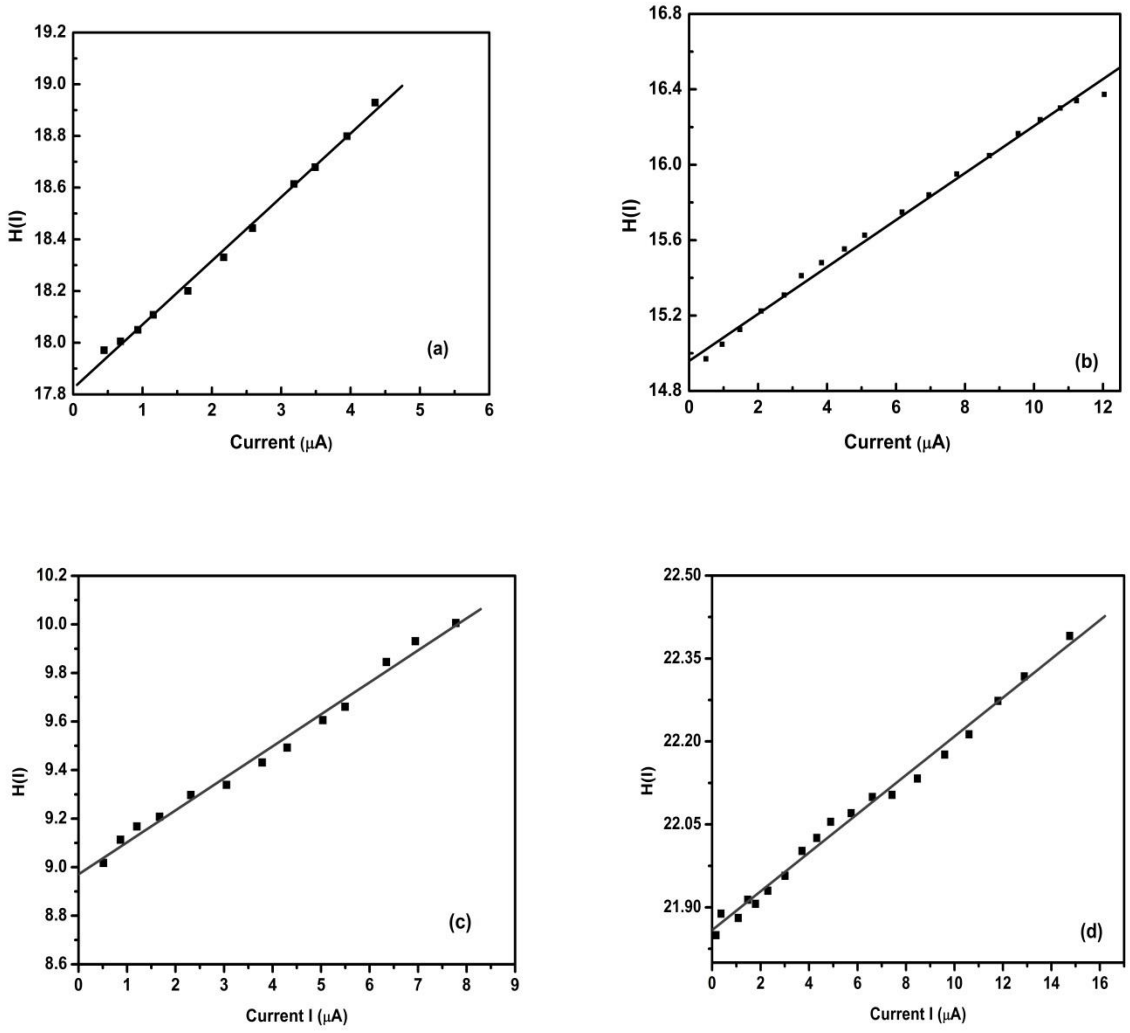

Fig. 6.8 H (I) Vs. Current (I) plot; (a) & (b): for CV dye based organic device, (c) & (d): for MG dye based organic device in absence and presence of SWCNT

The value of R_s are also estimated from H(I) Vs. I plot. Fig. 6.8 (a) and (b) represent the H(I) Vs. I plot of CV dye based organic devices whereas Fig. 6.8 (c) and (d) are the representation of MG dye based organic devices. The values of R_s extracted by using these two different methods show a good constituency with each other.

Table 6.1 Extraction of n and R_s for the organic device based on CV dye in absence and presence of SWCNT

Sample device	Ideality factor (n)	Series Resistance using dV/dlnI-I plot (MΩ)	Series Resistance using H(I) - I plot (MΩ)
ITO/CV/Al	17.30	0.276	0.246
ITO/CV+SWCNT/Al	15.76	0.112	0.124

Table 6.2Extraction of n and R_s for the organic device based on MG dye in absence and presence of SWCNT

Sample Device	Ideality factor (n)	Series Resistance using dV/dlnI-I plot (MΩ)	Series Resistance using H(I) - I plot (MΩ)
ITO/MG/Al	28.4	.154	.131
ITO/MG+SWCNT/Al	24.06	0.0389	.0350

From the result it is clearly observed that the addition of SWCNTs reduces the value of R_s. As stated earlier, the interface between organic dye and electrodes plays an important role in the device characterization which will control the value of R_s. So by considering the CV and MG dye are as p type semiconductors we have shown the band diagram. We sandwich the organic dye in between ITO and Al, where ITO is used as front electrode with work function of 4.8 eV and Al is used as back electrode with work function of 4.2 eV.

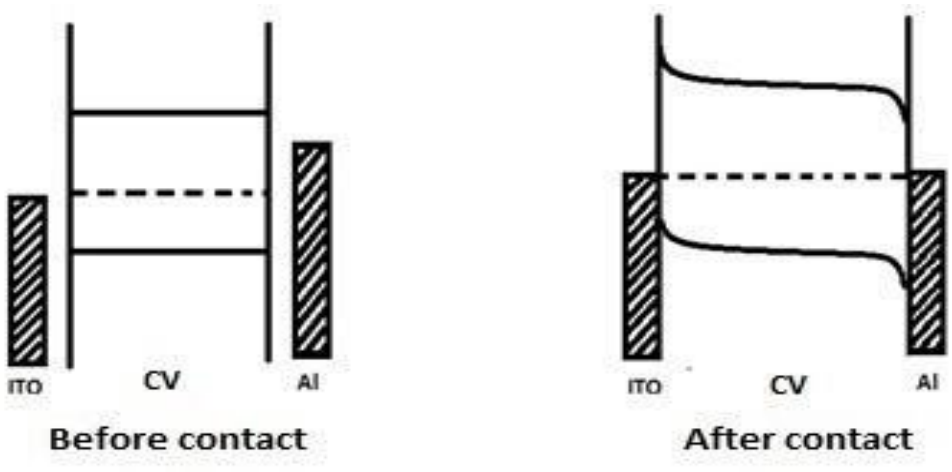

Fig. 6.9 Schematic energy band diagram of ITO/CV/Al interface where ITO/CV from ohmic contact and Al/CV form Schottky contact

A potential barrier will be created at the interface as a result of the band bending effect caused by charge carrier migration, as can be observed from Fig. 6.9. The interface of OPV devices is also affected and introduces energy states because organic semiconductors are more likely to contain electron traps. The barrier potential of the device is once again increased as a result of the enhanced energy states at the interface surface potential. As a result, some of the charge carriers that were injected are trapped during conduction, while the remaining charge carriers are free to participate in conduction. The resulting current is relatively low initially due to low carrier injection at low voltage. It is predicted that the trapping will be relatively small at low voltage as well, but it will rise significantly as voltage increases. Charge carriers recombine as a result of the excessive trap concentration. So the conductivity becomes limited and the R_s of the organic devices is very high.

The presence of traps in organic semiconductors controls the shape of the I-V characteristics. Different experiments have been performed on different systems by many researchers, to get better insight about the variation of trap distribution and its effect on the I-V characteristics. Earlier it was also reported that the trap concentration and distribution also change depending on defect states [11-12]. It is expected that the I-V characteristics can be well explained by considering exponential trap distribution in case of high trap states. In our work as we have sandwiched the organic dye in between the two electrodes the defect states at the interface are increased. So we have considered exponential trap distribution to fit our experimental data and

estimated the trap energy (E_c) in absence and presence of SWCNTs by using the Poisson's equation.

$$J_c = N_c \mu q^{(1-m)} \left(\frac{m_\epsilon}{H_n(m+1)}\right)^m \left(\frac{2m+1}{m+1}\right)^{(m+1)} \frac{V^{(m+1)}}{L^{(2m+1)}} \quad (6.6)$$

Where J_c refers to the current density in the trap controlled SCLC region, N_c is the effective density of states in LUMO and HOMO, ϵ is equal to $\epsilon_r \epsilon_0$ with ϵ_0 being the permittivity of free space and ϵ_r is dielectric constant, V is applied voltage and m can be expressed as shown in equation 6.6 [13]

$$m = T_c/T \quad (6.7)$$

Where T_c is the temperature of exponential trap distribution, can be expressed as,

$$T_c = \frac{E_c}{k} \quad (6.8)$$

So the expression of trap energy E_c is

$$E_c = mkT \quad (6.9)$$

From the lnI Vs. ln V plot we can measure the value of m and by substituting the value we can obtained the value of E_c. Fig. 6.10. Shows the lnI Vs. lnV plots of CV and MG dye based OPV devices in absence and presence of SWCNTs.

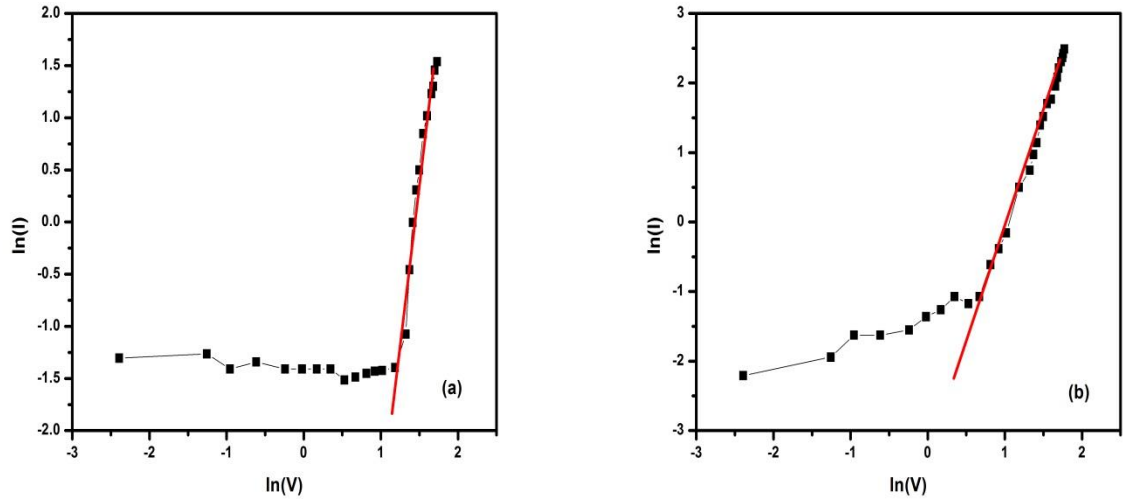

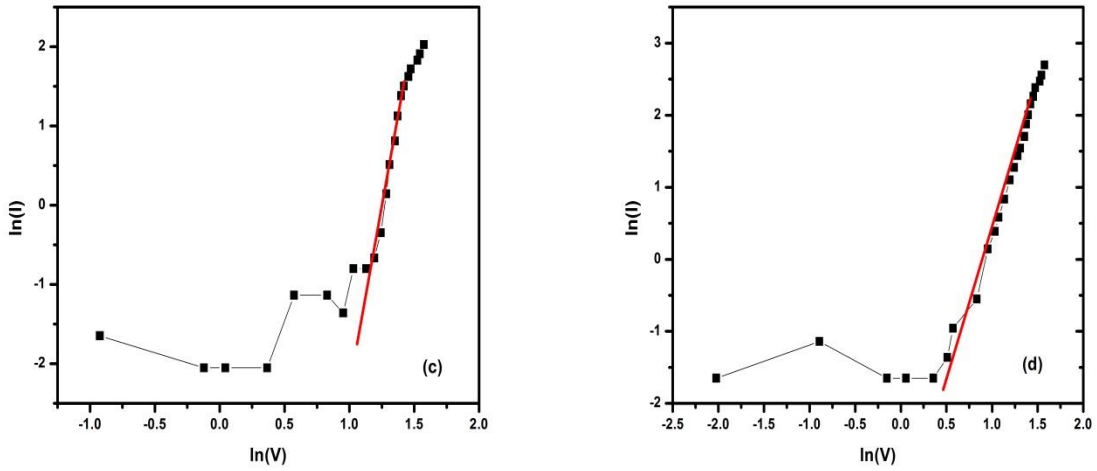

Fig. 6.10 lnI Vs. lnV characteristics of (a) ITO/CV/Al Coated with Mylar and (b) ITO/CV+SWCNT/Al Coated with Mylar (c) ITO/MG/Al Coated with Mylar and (d) ITO/MG+SWCNT/Al Coated with Mylar

Table 6.3 Values of the trap energy of the CV and MG dye based organic devices in the absence and in the presence of SWCNT

	Trap Energy in (eV) of CV dye based OPV device	**Trap Energy in (eV) of MG dye based OPV device**
Without SWCNT	0.085	0.086
With SWCNT	0.060	0.057

From the extracted value of E_c, it is observed that addition of SWCNTs reduces the value of trap energy. SWCNTs basically give trapped carriers a percolation route and enhance free charge carriers, which lowers the trap energy. The total current of the device is improved, and the device R_s is decreased, as the trap energy is reduced.

In this work the light I-V characteristics of these devices have also been studied. In the light I-V characteristics photons strike the transparent electrode of the cell. In order to control the charge conduction process, the charge carriers must first absorb the incident energy [14]. Consequently, in the OPV device, the photoconduction process is dependent on the photon energy's (E_m) absorption. In addition, it is possible to state that increasing photon energy will result in a rise in the number of free carriers, which will further enhance the charge-conduction process. As a

result, we have determined the E_m as well as how the E_m affects R_s both without and with the subsuming of SWCNTs in this study. To extract the delivered E_m we have considered the current voltage relation under light illumination as [15],

$$I = I_s\left[e^{\frac{qV}{\eta KT}} - 1\right] - I_{ph} \tag{6.10}$$

Where, $I_{ph}$is the photo current

Now considering,

$$V_c = \frac{\eta KT}{q} \tag{6.11}$$

Then

$$I = I_s\left[e^{\frac{V}{V_c}} - 1\right] - I_{ph} \tag{6.12}$$

The short circuit current (I_{sc}) will be obtained when V=0,

So,

$$I_{sc} = -I_{ph} \tag{6.13}$$

Also the open circuit voltage (V_{oc}) will be obtained when I=0,

So,

V_{oc}= V [I=0]

$$0 = I_s e^{\frac{V}{V_c}} - I_S - I_{ph} \tag{6.14}$$

$$I_s e^{\frac{V}{V_c}} = I_s + I_{ph} \tag{6.15}$$

$$\frac{V}{V_c} = \ln\left(\frac{I_s + I_{ph}}{I_s}\right) \tag{6.16}$$

$$V = V_{oc} = V_c \ln\left[\frac{I_{ph}}{I_s} + 1\right] \cong V_c \ln\left[\frac{I_{ph}}{I_s}\right] \tag{6.17}$$

The power dissipation of the device can be defined as,

$$P = V * I \tag{6.18}$$

$$p = I_s V\left[e^{\frac{V}{V_c}} - 1\right] - I_{ph} V \tag{6.19}$$

Now at Maximum power,

$$\frac{dP}{dV} = 0 \tag{6.20}$$

At maximum power, the corresponding voltage and current are V_m and I_m respectively

So,

$$\frac{dP}{dV} = 0 = I_s\left[e^{\frac{V_m}{V_c}} - 1\right] - I_{ph} + I_s\frac{V_m}{V_c}e^{\frac{V_m}{V_c}} \tag{6.21}$$

The equation can be written as,

$$I_s e^{\frac{V_m}{V_c}}\left[1 + \frac{V_m}{V_c}\right] = I_s + I_{ph} \tag{6.22}$$

$$e^{\frac{V_m}{V_c}} = \frac{I_s + I_{ph}}{I_s\left[1 + \frac{V_m}{V_c}\right]}$$

$$V_m = V_c \ln\left[\frac{I_s + I_{ph}}{I_s} * \frac{1}{1 + \frac{V_m}{V_c}}\right]$$

$$V_m = V_c \ln\left[\frac{I_s + I_{ph}}{I_s}\right] + V_c \ln\left[\frac{1}{1 + \frac{V_m}{V_c}}\right] \tag{6.23}$$

Now, $V_c \ln\left[\frac{I_s + I_{ph}}{I_s}\right] = V_{oc}$

So the voltage V_m will be,

$$V_m = V_{oc} - V_c \ln\left[1 + \frac{V_m}{V_c}\right] \tag{6.24}$$

Now we can also get the equation for I_m from the Maximum power condition

$$P = I_s V\left[e^{\frac{V}{V_c}} - 1\right] - I_{ph} V$$

$$\frac{dP}{dV} = 0 = I_s\left[e^{\frac{V_m}{V_c}} - 1\right] - I_{ph} + I_s\frac{V_m}{V_c}e^{\frac{V_m}{V_c}}$$

Now as,

$$I_m = I_s\left[e^{\frac{V_m}{V_c}} - 1\right] - I_{ph}$$

$$I_m = I_s\frac{V_m}{V_c}e^{\frac{V_m}{V_c}} \tag{6.25}$$

$$I_m \approx I_{ph}\left[1 - \frac{V_c}{V_m}\right] \tag{6.26}$$

The maximum power will be then,

$$P_m = I_m * V_m \tag{6.27}$$

$$= I_{ph}\left[1 - \frac{V_c}{V_m}\right] * \left[V_{oc} - V_c \ln\left[1 + \frac{V_m}{V_c}\right]\right]$$

$$= I_{ph}\left[V_{oc} - V_c \ln\left[1 + \frac{V_m}{V_c}\right] - \frac{V_c}{V_m}V_{oc} + \frac{V_c}{V_m}V_c \ln\left[1 + \frac{V_m}{V_c}\right]\right]$$

$$= I_{ph}\left[V_{oc} - V_c \ln\left[1 + \frac{V_m}{V_c}\right] - \frac{V_c}{V_m}\left[V_{oc} - V_c \ln\left[1 + \frac{V_m}{V_c}\right]\right]\right]$$

$$= I_{ph}\left[V_{oc} - V_c \ln\left[1 + \frac{V_m}{V_c}\right] - \frac{V_c}{V_m} V_m\right]$$

$$= I_{ph}\left[V_{oc} - V_c \ln\left[1 + \frac{V_m}{V_c}\right] - V_c\right] \quad (6.28)$$

Now we know that,

$$P_m = I_{ph} * \frac{E_m}{q} \quad (6.29)$$

Where,

$$E_m = q\left[V_{oc} - V_c \ln\left[1 + \frac{V_m}{V_c}\right] - V_c\right] \quad (6.30)$$

E_m is the energy per photon which is delivered to the active region of a photovoltaic device under illumination. We have measured the value of E_m from the light I-V characteristics. The light I-V characteristics of the CV and MG dye based OPV devices in absence and presence of SWCNTs are shown in the Fig. 6.11 below.

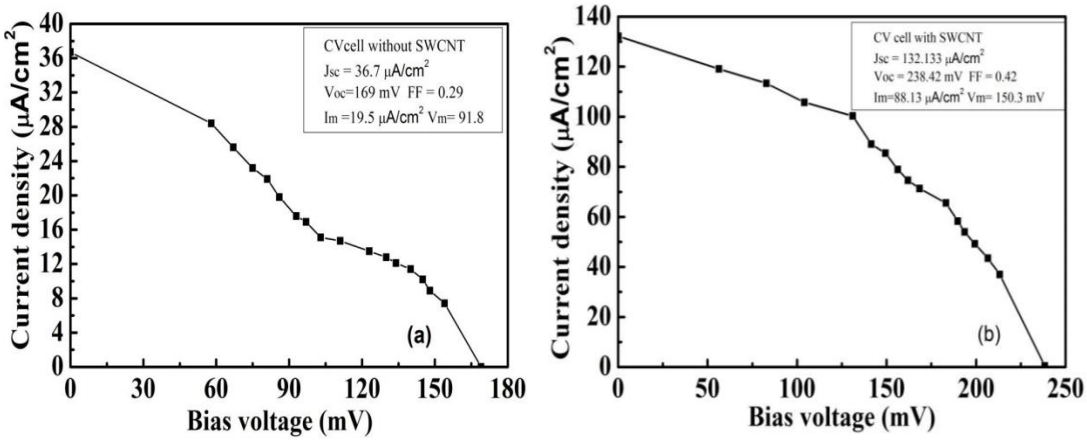

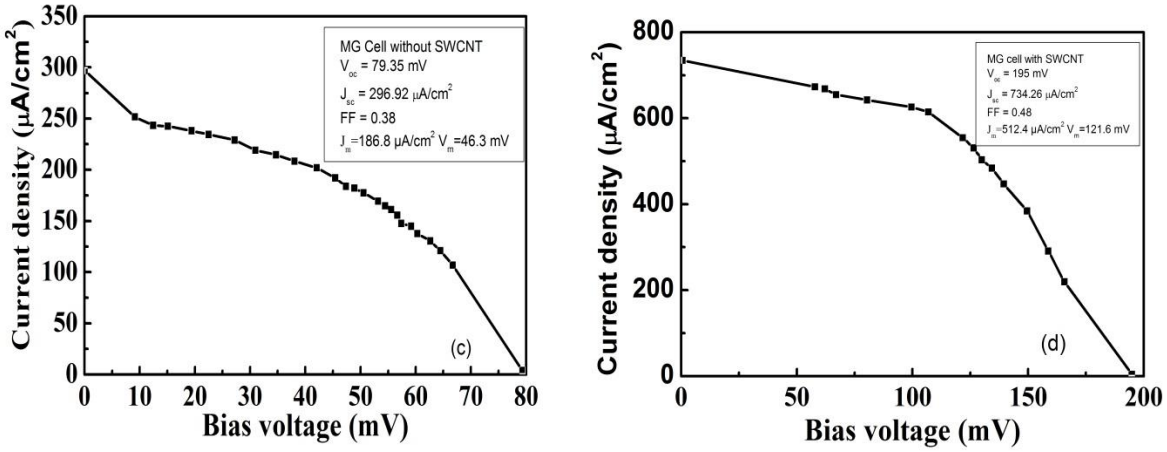

Fig. 6.11 Light I-V characteristics of (a) ITO/CV/Al Coated with Mylar and (b) ITO/CV+SWCNT/Al Coated with Mylar (c) ITO/MG/Al Coated with Mylar and (d) ITO/MG+SWCNT/Al Coated with Mylar

We have extracted the V_{OC}, I_{SC}, V_m, I_m, of the OPV devices and measured the photon energy by using the equation 6.30. The extracted values are shown in the table below.

Table 6.4 Result of extraction of photovoltaic parameters for the CV dye based organic device without and with subsuming of SWCNT

Sample Device	V_{oc} (mV)	J_{sc} ($\mu A/cm^2$)	V_m (mV)	J_m ($\mu A/cm^2$)	E_m (eV)
ITO/CV/Al coated with Mylar	169	36.7	91.8	19.5	1.65×10^{-17}
ITO/CV+SWCNT/Al coated with Mylar	238.42	132.133	150.3	88.13	2.60×10^{-17}

Table 6.5 Result of extraction of photovoltaic parameters for the MG dye based organic device without and with subsuming of SWCNT

Sample Device	V_{oc} (mV)	J_{sc} ($\mu A/cm^2$)	V_m (mV)	J_m ($\mu A/cm^2$)	E_m (eV)
ITO/MG/Al coated with Mylar	79.35	296.92	46.3	186.8	4.29×10^{-18}
ITO/MG+SWCNT/Al coated with Mylar	195.1	734.2	121.6	512.4	1.98×10^{-17}

From the result it is discerned that the value of photon energy gets increased with subsuming of SWCNTs. So with increment of the photon energy the numbers of free charge carriers are increased and enhance the overall current of the device. Therefore it can be said the value of R_s is also reduced with enhancement of the photon energy.

To measure the R_s from the light I-V characteristics we have used area method, expressed as [16-17],

$$R_{s(light)} = 2[\frac{V_{oc}}{J_{sc}} - \frac{A}{J_{sc}^2} - \frac{kT}{qJ_{sc}}] \quad (6.31)$$

The extracted values of $R_{s(light)}$ of the CV and MG dye based OPV devices in absence and presence of SWCNTs are shown in the table below.

Table 6.6 Extracted values of the Series resistance $R_{s(light)}$ from light I-V characteristics for the CV and MG dye based organic devices without and with subsuming of SWCNTs

Sample Device	$R_{s(light)}$ (kΩ)
ITO/CV/Al	7.78
ITO/CV+SWCNT/Al	3.20
ITO/MG/Al	0.475
ITO/MG+SWCNT/Al	0.352

From the above result it is clearly observed that subsuming of SWCNTs in the OPV devices reduces the value of $R_{s(light)}$. Moreover it is also discerned that the extracted values of R_s from the dark I-V characteristics are very high compared to the values of $R_{s(light)}$ under illumination.

Actually it is very well known that the R_s of an electronic or optoelectronic device based on semiconductor is given by the resistance of the neutral region of semiconductor and the contact resistance. In the case of organic semiconductor the resistance is high due to the fact that being a molecular crystal, the energy bands are very narrow. Now the nature of transportation of charge carriers through the devices is different in dark and illuminating conditions. In case of dark condition most of the charge carriers are injected from the applied voltage, whereas in case of illuminating condition along with these injected charges excess carriers are generated within the device. Now under illumination the photoconduction process of the OPV device depends on the generation of electron hole pairs upon photon absorption and separation of charge carriers at the junctions. So the amount of photon current is high compared to dark current. Therefore the value of $R_{s(light)}$ also is low in comparison to the value of R_s in dark conditions.

6.5 Conclusion

In this chapter, we looked into how SWCNTs affected the R_s of MG and CV dyes based devices. Both the electrical and photovoltaic measurements are carried out with and without the addition of SWCNTs in order to comprehend the effect. The device R_s has been extracted using the Cheung Cheung technique from the dark I-V characteristics and the area method from the light I-V characteristics. From the dark I-V measurements, the trap energy was also calculated. According to the experimental findings, E_c and R_s values are reduced in the presence of SWCNTs. So it can be said that charge carriers are easily injected when trap energy is reduced. From the light I-V characteristics we have also determined the incident photon energy that is absorbed by the OPV devices. It has been found that adding SWCNTs improves the E_m, which in turn improves the free charge carriers in the devices. Therefore, from the dark and light I-V characteristics, we have determined that the incorporation of SWCNTs reduces the R_s which must improve the device performance.

6.6 References

1. S. Sen, N. B. Manik, Modification of Trap Energy and Barrier Height in Crystal Violet (CV) Dye based Organic Device in Presence of Single Walled Carbon Nanotubes (SWCNT), International Journal of Scientific Research and Review, (2019), 7:2 (10-14)
2. S. Sen and N. B. Manik, Study on the Effect of 8 nm Size Multi Walled Carbon Nanotubes (MWCNT) on the Barrier Height of Malachite Green (MG) Dye Based Organic Device, Int. J. Adv. Sci. Eng.(2020), 6: 23-27
3. N. P. Raval, P. U. Shah and N. K. Shah, Malachite green "a cationic dye" and its removal from aqueous solution by adsorption, Applied Water Science, (2017) , 7: 3407-3445
4. H. A. Alturaif, Z. A. ALOthman, J. G. Shapter, S. M. Wabaidur, Use of Carbon Nanotubes (CNTs) with Polymers in Solar Cells. Molecules, (2014), 19: 17329-17344.
5. S. Chakraborty, N. B. Manik, Effect of COOH-functionalized SWCNT addition on the electrical and photovoltaic characteristics of Malachite Green dye based photovoltaic cells. Journal of Semiconductors, (2014) 35: 124004(1-6).

6. S. Chakraborty, N. B. Manik, Improvement of electrical and photovoltaic properties of methyl red dye based photoelectrochemical cells in presence of single walled carbon nanotubes. Frontiers of Optoelectronics, (2015), 8: 289-297.
7. S. K.Cheung, N. W. Cheung, Extraction of Schottky diode parameters from forward current-voltage characteristics. Applied Physics Letters, (1986), 49: 85-87.
8. M. Shah, S. Kh. Karimov, Z. Ahmad, M. H. Sayyad, Electrical characteristics of Al/CNT/NiPc/PEPC/Ag surface-type cell. Chinese Physics Letters, (2010), 27: 106102 (1-4).
9. M. Shah, M. H. Sayyad, S. Kh. Karimov, Electrical characterization of the organic semiconductor Ag/CuPc/Au Schottky diode. Journal of Semiconductors. (2011), 32: 044001(1-5). doi: 10.1088/1674-4926/32/4/044001
10. S. Okur, F. Yakuphanoglu, M. Ozsoz, P. K. Kadayifcilar, Electrical and interface properties of Au/DNA/n-si organic-on-inorganic structures. Micro electron, (2009), 86: 2305-2311.
11. V. Ruxaandra and S. Antohe, The effect of the electron irradiation on the electrical properties of thin polycrystalline CdS layers, Journal of Applied Physics, (1998), 84: 727
12. S. Antohe, L. Ion, N. Tomozeiu, T Stoica and E. Barna, Electrical and photovoltaic properties of photosensitised ITO/a-Si:H p–i–n/TPyP/Au cells, Solar Energy Materials and Solar Cells (2000), 62: 207
13. A. Haldar, S. Maity and N. B. Manik, Effect of back electrode on photovoltaic properties of crystal-violet-dye-doped solid- state thin film, Ionics 14 (2008) 427-432
14. K. Sharma, V. Sharma, and S. S. Sharma, Dye-Sensitized Solar Cells: Fundamentals and Current Status. *Nanoscale Res Lett* (2018), 13: 381
15. S. M. Sze, K. K. NG, Physics of Semiconductor Devices, 3rd edition, Wiley & Sóns, New Jersey, (2007), 719-736
16. D. T. Cotfas, P. A. Cotfas, D. Ursutiu, C. Samoila, The methods to determine the series resistance and the ideality factor of diode for solar cells-review, (2012), IEEE 966-972. doi: 10.1109/OPTIM.2012.6231814.
17. D. Pysch, A. Mette, S. W. Glunz, A review and comparison of different methods to determine the series resistance of solar cells. Solar Energy Materials and Solar cells, (2007),91:1698-1706.

Chapter 7

Conclusion and Future Scope of the work

7.1 Summary

In this thesis work we have studied the series resistance, as well as the effects of nanoparticles and SWCNTs on the series resistance (R_s) of organic dye based devices. The series resistance of the organic devices is quite high. One of the major reasons of this high value arises due to the presence of traps present at the interface and bulk area of the organic devices. These traps serve as recombination centers and the charges are become immobilized at these trap centers. As a result, the existence of traps limits the charge transport mechanism and lowers the total current of the device. Because of this low current the value of R_s in organic devices is very high. It has also been found that with incorporation of guest materials such as nanoparticles and SWCNTs the value of R_s is reduced. With lowering of R_s, the performance of the devices will improve .In this work we have chosen five different dyes namely, Thionin (TH), Phenosafranine (PSF), Crystal Violet (CV), Methyl Red (MR) and Malachite Green (MG). We have designed our present work into the following seven chapters.

In **Chapter 1**, we have discussed about the importance of organic semiconductors. Nowadays these organic semiconductors are currently becoming more and more popular due to their numerous unique qualities. Furthermore, conventional energy sources will be exhausted soon due to huge requirements of energy in future. So switching to renewable energy sources from conventional energy sources is really necessary. Solar energy is one of the key renewable energy sources since it can be converted into electricity because of the electrical and optical features of OSCs. However, there are also several problems with organic devices, one of which is their high R_s. So according to this problem we have formed our desired aim and objective of the present work.

In **Chapter 2**, additionally, as organic semiconductors are trap prone, we have discussed the different types of traps as well as how charges are transported when traps are present. We applied the SCLC charge transport model with an exponential trap distribution in our current work to determine the trap energy from the steady state I-V characteristics. It might be suggested that the high R_s of these organic devices is caused by this trapping of charge carriers. Additionally, we discussed several methods for obtaining the R_s. It has been predicted that adding nanoparticles or CNTs as guest materials may lower the value of R_s. As a result, in this

chapter we discussed about nanoparticle such as, ZnO and TiO_2. In addition, we also discussed SWCNTs in this work.

In order to determine the R_s, its influence, and how to decrease the value for the enhanced performance of organic devices, our experimental work with the chosen dyes has been structured in four chapters, from chapter 3 to chapter 6.

In **Chapter 3**, Thionine dye-based organic devices with various dye concentrations have been presented to examine the R_s. To get the cells prepared, the solution made with the Thionin dye was sandwiched between ITO and Al. Methods for conducting experiments as well as details on sample and cell preparation have been included. The experimental data for the various parameters have been taken. The dark I-V data was fitted using the Cheung-Cheung method to calculate the R_s. According to our findings, the value of the organic cell based on the Thionin dye has a very high R_s value and decreases as the dye concentration rises. Additionally, the cells' ideality factor, which is also quite high, was examined.

We studied at the trap energy and the impact of nanoparticles on the trap energy in **Chapter 4**. We have used MR and PSF dyes to construct the cell. We have looked at the PSF dye-based devices in the presence of ZnO and TiO_2 nanoparticles independently. We have also examined MR dye-based organic devices both with and without ZnO nanoparticles. Details on sample preparation and the experiment have been mentioned. It has been noted that performance improves with nanoparticle inclusion. The values of R_s, n, and E_c decrease when nanoparticles are present. A concise conclusion follows the discussion of the experimental findings.

We examined the R_s at various temperatures in **Chapter 5**. We produced an organic device based on MR dye and investigated its dark I-V properties at various temperatures. The sample preparation and experimental methods have been thoroughly covered. We have investigated how temperature affects R_s, n, and E_c. Our findings show that while the temperature rises, R_s and n decrease while E_c rises. The description of the results of the experiment is followed by a brief conclusion.

The dark I-V and light I-V properties of the organic devices based on the CV and MG dyes in the absence and presence of SWCNTs were examined in **Chapter 6**. The data from our experiment is presented in this chapter. In addition to compare the value of these R_s derived from dark and

light I-V characteristics, we have explored the impact of SWCNTs on R_s. In addition, we looked into how the presence of SWCNTs affected the trap energy and photon energy.

7.2 Findings of the work

The objective of the thesis was to investigate the series resistance R_s of devices fabricated using organic dyes. The impact of nanoparticles and SWCNTs on the R_s has also been studied. The features of the current and voltage have been investigated to analyze the R_s. Our work reveals that the R_s of organic devices is extremely high. There are different techniques to measure R_s. We have used three different techniques and found that the value of R_s extracted in different method has more or less same value of R_s. With incorporation of nanoparticles and SWCNTs the value of R_s gets reduced. In this study, the impact of temperature on R_s has also been looked at. Different dyes were characterized. In each chapter, the findings are discussed. In the flowing section major findings are outlined for different chapters.

7.2.1 Findings on Thionin dye based devices by varying dye concentration

Table 7.1 shows the value of R_s and n for devices based on Thionin dye as a function of dye concentration. From Table 7.1, it can be found that R_s has a very high value and that it decreases from 2.90 MΩ to 0.20 MΩ as dye concentration is increased. Organic semiconductors are disordered by nature, their molecules are kept together by a weak Van der Waals force, their band structures are not known clearly, and they are also prone to traps. Therefore, the number of free charge carriers and their mobility are both relatively small. Consequently, R_s has a very high value. An increase in free charge carriers is shown by a decrease in R_s when dye concentration is increased. The ideality factor n values obtained using the lnI Vs. V plot and by utilizing the Cheung Cheung technique are slightly different, as can be seen from Table 7.1. Additionally, it can be said that when R_s is decreased, the value of n is also decreased.

Table 7.1 Value of R_s and n from dark I-V characteristics of Thionin dye based device

Dye used	Dye concentration (mg)	Value of n	Value of R_s (MΩ)
Thionin Dye	2.0	9.3	2.90
	4.0	8.9	0.45
	6.0	7.9	0.40
	8.0	7.2	0.20

7.2.2 Findings on Methyl Red (MR) dye based devices in absence and presence of ZnO

From the Table 7.2 it is clear that, incorporating ZnO nanoparticles on MR dye causes the value of R_s to drop from 7.06 MΩ to 0.96 MΩ. When ZnO nanoparticles are present, the value of trap energy decreases as well, from 0.098 eV to 0.056 eV. The value of R_s, n and E_c are decreased due to the incorporation of ZnO.

Table 7.2 Value of R_s, n and E_c from dark I-V characteristics of MR dye based device in presence and absence of ZnO nanoparticles

Dye used		Value of n	R_s from dV/dlnI Vs. I plot (MΩ)	$R_s$from H(I) Vs. I plot (MΩ)	Extracted value of m	Extracted value of E_c (eV)
Methyl Red (MR)	Without ZnO	15	8.45	7.06	3.8	0.098
	With ZnO	11.9	0.92	0.96	2.2	0.056

7.2.3 Findings on Phenosafranine (PSF) dye based devices in absence and presence of TiO_2 and ZnO nanoparticles

Table 7.3 displays the value of R_s from the dark I-V characteristics of PSF dye-based devices in absence and presence of TiO_2 and ZnO nanoparticles. Without the addition of nanoparticles, the R_s is 0.25 MΩ, but when ZnO nanoparticles are added, the value drops to 0.10 MΩ, and when TiO_2 is added, the value drops to 0.09 MΩ. In presence of ZnO nanoparticles and TiO_2 nanoparticles, respectively, the trap energy is decreased from 0.087 eV to 0.075 eV and 0.074 eV respectively. As the trap energy decreases, the residing time or immobilized time of the charges will also decrease, which will lower R_s of the organic device.

Table 7.3 Value of R_s, n and E_c from dark I-V characteristics of Phenosafranine (PSF) dye based devices in absence and presence of TiO_2 and ZnO nanoparticles

Dye Used		Value of n	R_s from dV/dlnI Vs I plot (KΩ)	R_s from H(I) Vs I plot (KΩ)	Extracted value of m	Extracted value of E_c (eV)
Phenosafranine (PSF)	Without Nanoparticles	37.47	272.70	250.80	3.38	0.087
	With ZnO	36.90	112.10	108.30	2.92	0.075
	With TiO_2	34.80	100.10	98.30	2.90	0.074

7.2.4 Findings on Methyl Red (MR) dye based device at different temperatures

Table 7.4 shows the value of R_s for Methyl Red (MR) dye based device at various temperatures. The range of the temperature was 253 K to 315 K. It has been found that when the temperature rises, the value of R_s decreases from 1.20 MΩ to 0.012 MΩ.The value of n decrease from 24.23 to 13.80 as the temperature increases. At various temperatures, the trap energy E_c has also been observed. Table 7.4 shows that, as the temperature goes up from 253 K to 315 K, the value of E_c increase from 0.063 eV to 0.160 eV. This finding indicates that when temperature increases, the number of charge carriers that are trapped also increases. However, the presence of more free charge carriers improved the overall current in the temperature, despite the fact that charge carrier trapping increase as the temperature rises, improving the device R_s.

Table 7.4 Value of R_s, n and E_c from dark I-V characteristics of MR dye based organic device in temperature range of 253 K to 315 K

Dye used	Temperature (K)	Value of n	R_s from dV/dlnI Vs I plot (MΩ)	$R_s$from H(I) Vs I plot (MΩ)	Extracted value of m	Extracted value of E_c (eV)
Methyl Red (MR)	253	24.23	1.51	1.20	2.9	.063
	262	22.30	0.559	0.618	3.3	.074
	268	20.1	0.230	0.226	3.9	.090
	273	17.69	0.053	0.072	4.3	.101
	284	16.01	0.028	0.020	5.1	.124
	302	14.67	0.013	0.010	5.6	.145
	315	13.80	0.012	0.012	5.9	.160

7.2.5 Findings on Crystal Violet (CV) and Malachite Green (MG) dye based photovoltaic devices in presence of SWCNTs

According to Table 7.5, the dark I-V characteristics of devices based on Malachite Green (MG) and Crystal Violet (CV) dyes demonstrate that the R_s decrease in the presence of SWCNTs. The trap energy for the CV dye-based device decreases from 0.085 eV to 0.060 eV with the inclusion of SWCNTs. SWCNTs serve as charge acceptors and offer efficient percolation pathways for the conduction of charge carriers, which reduces trap energy. This decrease in trap energy improves the total current and lowers the R_s from 0.246 MΩ to 0.124 MΩ.The trap energy and R_s decrease in the case of MG dye-based devices, from 0.086 eV to 0.057 eV and 0131 MΩ to 0.035 MΩ, respectively. Moreover according to Table 7.6, the light I-V characteristics in the presence of SWCNTs, the incident photon energy and the R_s have also been detected. Addition of SWCNTs enhances the E_m, which enhances the free charge carriers in the devices. As a result, the value of R_s (light) decreases with incorporation of SWCNTs. Additionally, it can be shown that the extracted values of R_s from the dark I-V characteristics are significantly higher than the extracted values of R_s (light) under illumination.

Table 7.5 Value of R_s, n and E_c from dark I-V characteristics of CV and MG dye based device in presence and absence of SWCNTs

Dye used		Value of n	R_s from dV/dlnI Vs I plot (MΩ)	$R_s$from H(I) Vs I plot (MΩ)	Extracted value of m	Extracted value of E_c in eV
Crystal Violet (CV)	Without SWCNTs	17.30	0.276	0.246	3.33	0.085
	With SWCNTs	15.76	0.112	0.124	2.32	0.060
Malachite Green	Without SWCNTs	28.4	0.154	0.131	3.34	0.086

(MG)	With SWCNTs	24.06	0.0389	0.035	2.23	0.057

Table 7.6 Value of R_s, photon energy and different photovoltaic parameters extracted from the light I-V curves of CV and MG dye based device in presence and absence of SWCNTs

Dye used		V_{oc} (mV)	J_{sc} (μA/ cm^2)	V_m (mV)	J_m (μA/ cm^2)	Fill Factor (FF)	Value of E_m	Value of R_s (KΩ)
Crystal Violet (CV)	Without SWCNTs	169	36.7	91.8	19.5	0.29	1.65×10^{-17}	7.78
	With SWCNTs	238.4	132.133	150.3	88.13	0.45	2.60×10^{-17}	3.20
Malachite Green (MG)	Without SWCNTs	79.35	296.92	46.3	186.8	0.38	4.29×10^{-18}	0.475
	With SWCNTs	195.1	734.2	121.6	512.4	0.48	1.98×10^{-17}	0.352

The outcomes of our recent findings are extremely intriguing and informative for future study in this field. In this investigation, we discovered that organic devices have a very high value of R_s. We have explained about the physics behind this high value of R_s, and we have also applied several approaches to lower the R_s of the dye-based device in this study. We have studied the correlation between trap energy and R_s. Impact of temperature on R_s and E_c has also been investigated. Our findings will be helpful for further study in this area.

7.3 Future scope of the work

In this work, we have tried to conduct extensive study to understand the series resistance for a number of different dyes such as Thionin, Phenosafranine (PSF), Crystal violet (CV), Methyl Red (MR) etc. Effect of nanoparticles namely TiO_2, ZnO and SWCNT has been studied. It is observed that with incorporation of nanoparticles or SWCNTs, we can reduce the trap energy which again reduces the R_s and improve the overall performance of the device. However, there are still certain issues that require further discussion. For instance, it is not clear how the influence of SWCNTs or nanoparticles may affect the distribution and density of trap states. We did not think to separate the effects of shallow and deep traps in this investigation. In order to fully understand the charge transport mechanism and the impact of various nanopartilcles and SWCNTs, measurements should be made in future by incorporating TiO_2, ZnO, and SWCNTs into all such dyes by varying its weight ratio. To understand the variations in their behavior, this study should be repeated with a few other different dyes, along with various functionalized nanoparticles and CNTs. Device should also be modified to make it flexible, since flexible devices are becoming important in the coming days. To reduce the weight and to add the flexibility we can use flexible electrode where polymer materials can be used instead of ITO. To produce a flexible electrode for fabrication an organic device, different polymers are used such as Polyethylene Naphthalene (PEN) and Polyethylene Terephthalate (PET). So in the modern era more attention will be given towards the fabrication of smart and flexible organic devices which will be low cost, environmental friendly with easy fabrication process.

Publications in International/National Journals

1. **Pallab Kr. Das**, S. Bhunia, N. B. Manik"Effect of Trap Energy on Series Resistance of Phenosafranine Dye Based Organic Diode in Presence of TiO2 and ZnO Nanoparticles" Advanced Materials Research (2020) 1159, 112-123
2. S. Sen, **Pallab Kr. Das**, N. B. Manik"Study on the effect of single walled carbon nanotubes on junction properties of Safranin–T dye-based organic device", Journal of Physics Communications (2021) 5 (4), 045004
3. **Pallab Kr. Das**, S. Sen, N. B. Manik "Study on the series resistance of crystal violet dye-based organic photovoltaic device in presence of single walled carbon nanotubes", Indian Journal of Physics,(2021) 1-9
4. **Pallab Kr. Das**, S. Sen, N. B. Manik, "Effect of Single Walled Carbon Nanotubes on the Series Resistance and Trap Energy of Malachite Green Dye Based Organic Device", Journal of Nano Research (2021) 69, 43-52
5. **Pallab Kr. Das**, N. B. Manik, "Tuning of series resistance by reducing the trap energy of methyl red dye-based organic devices in the presence of ZnO nanoparticles", International Journal of Renewable Energy Technology (2021) 12 (2), 118-129
6. S. Bhunia ,**Pallab Kr. Das**, S. Basu and N. B. Manik. "Effect of titanium dioxide on solid state turmeric dye thin film" Indian Journal of Chemical Society (2020) 97 (12), 2943-2947
7. S. Bhunia, **Pallab Kr. Das** and N. B. Manik, "Effect of dye concentration on the band gap of PVA turmeric composite film" Indian Journal of Chemical Society(2020) 97 (12), 2937-2942
8. S. Bhunia**, Pallab Kr. Das,** S. Rakshit and N. B. Manik, "Estimation of Charge Carrier Density of Turmeric Dye in the Presence of Polyvinyl Alcohol (PVA) and Its Electrical Characterization as Herbal Diode"Journal of scientific Research, 14 (1), 11-25
9. S Sen, **Pallab Kr. Das**, N. B. Manik, "Modification of Interfacial Propertie of Single Walled Carbon Nanotubes" Journal of Materials Science and Surface Engineering, 9 (1), 1067-1070.

Book Chapter

1. **Pallab Kr. Das**, S. Bhunia, S. Basu, N. B. Manik, "Effect of Dye Concentration on Series Resistance of Thionin Dye-Based Organic Diode", Mathematics Applied to Engineering in Action, (2020) 119-131

List of International or National Conferences/ Seminars

1. Pallab Kr. Das, N. B. Manik, Electrical Characterisation of Crystal Violet (CV) Dye Based Organic Diode, International Seminar, IWPSD 2015, Indian Institute of Science, Bangalore, 7^{th} – 10^{th} Dec, 2015
2. Pallab Kr. Das, S. Bhunia, N. B. Manik, Effect of series resistance on ideality factor of PSF dye based organic diode, National Conference on Condensed Matter Physics (CMDAYS 2018) Bose -125 Event, University of Burdwan, 29-31^{st} August,2018
3. Pallab Kr. Das, S. Bhunia, N. B. Manik, Effect of dye concentration on the band gap of turmeric dye based herbal electronic diode, National Seminar on Emerging Frontiers in Materials Science (EFMS -2019), Behala College, 15-16^{th} February,2019
4. Pallab Kr. Das, K. Chakraborty, D. Sahoo, N. B. Manik, Charge Trapping Effect on Series Resistance (R_s) of Crystal Violet (CV) Dye Based Organic Device in Presence of Single Walled Carbon Nanotubes (SWCNT), National Seminar on Physics at Surfaces and Interfaces of Soft Materials (PSISM – 2019), Condensed Matter Physics Research Centre, Department of Physics, Jadavpur University, 26- 27^{th} September, 2019
5. Pallab Kr. Das, S. Bhunia, N. B. Manik, Electrical Characterisation of Crystal Violet (CV) Dye Based electrochemical cell, National Seminar on Chemistry for Sustainable development (CSD 2019), Sidho- Kanho Birsha University, Purulia, 26^{th} – 27^{th} November, 2019